





MicroRNA exporter HuR clears the internalized pathogens by promoting pro-inflammatory response in infected macrophages

Avijit Goswami^{1,†}, Kamalika Mukherjee^{1,†}, Anup Mazumder^{1,†,‡}, Satarupa Ganguly^{1,†}, Ishita Mukherjee² , Saikat Chakrabarti² , Syamal Roy³, Shyam Sundar⁴, Krishnananda Chattopadhyay²  & Suvendra N Bhattacharyya^{1,*} 

Abstract

HuR is a miRNA derepressor protein that can act as miRNA sponge for specific miRNAs to negate their action on target mRNAs. Here we have identified how HuR, by inducing extracellular vesicle-mediated export of miRNAs, ensures robust derepression of miRNA-repressed cytokines essential for strong pro-inflammatory response in activated mammalian macrophages. *Leishmania donovani*, the causative agent of visceral leishmaniasis, on the contrary alters immune response of the host macrophage by a variety of complex mechanisms to promote anti-inflammatory response essential for the survival of the parasite. We have found that during *Leishmania* infection, the pathogen targets HuR to promote onset of anti-inflammatory response in mammalian macrophages. In infected macrophages, *Leishmania* also upregulate protein phosphatase 2A that acts on Ago2 protein to keep it in dephosphorylated and miRNA-associated form. This causes robust repression of the miRNA-targeted pro-inflammatory cytokines to establish an anti-inflammatory response in infected macrophages. HuR has an inhibitory effect on protein phosphatase 2A expression, and mathematical modelling of macrophage activation process supports antagonistic miRNA-modulatory roles of HuR and protein phosphatase 2A which mutually balances immune response in macrophage by targeting miRNA function. Supporting this model, ectopic expression of the protein HuR and simultaneous inhibition of protein phosphatase 2A induce strong pro-inflammatory response in the host macrophage to prevent the virulent antimonial drug-sensitive or drug-resistant form of *L. donovani* infection. Thus, HuR can act as a balancing factor of immune responses to curtail the macrophage infection process by the protozoan parasite.

Keywords Ago2 dephosphorylation; drug-resistant *Leishmania*; host–parasite interaction; miRNA export; protein phosphatase 2A

Subject Categories Immunology; Microbiology, Virology & Host Pathogen Interaction

DOI 10.15252/emmm.201911011 | Received 16 June 2019 | Revised 24

December 2019 | Accepted 8 January 2020

EMBO Mol Med (2020) e11011

Introduction

Macrophages act as the first line of defence against the invading microbes in mammalian hosts which engulf the invading pathogens and kill them (Mogensen, 2009). However, the macrophages may fall prey to certain pathogens that inactivate the arsenals of the host macrophage through variety of complex mechanisms (Aderem & Underhill, 1999). The protozoan parasite *Leishmania donovani* (*Ld*), the causative agent of visceral leishmaniasis in human (Ready, 2014), can live and replicate within the host macrophages and thus can escape from the host immune system (Liu & Uzonna, 2012). Macrophage that otherwise gets activated by pathogen-derived molecules remains immunologically dormant when it is invaded by the pathogen *Leishmania* (Olivier *et al*, 2005). The parasite gets into the macrophage through host phagocytic activity and lives within the parasitophorous vacuoles, a special class of endosomal structures that get matured but do not get fused to lysosomes in infected cells through an unique mechanism induced by the internalized pathogen to prevent its own killing by host lysosomal machineries (Courret *et al*, 2002).

The inactivation of the macrophage defence machineries against invading pathogens is achieved through a selective action of pathogen-derived molecules on the host immune system (Contreras *et al*, 2010). *Leishmania* not only impairs the acquired immunity of the host by preventing processing of the pathogen-derived antigens and its presentation by infected macrophage or dendritic cells on

¹ RNA Biology Research Laboratory, Molecular Genetics Division, CSIR-Indian Institute of Chemical Biology, Kolkata, India

² Structural Biology and Bio-informatics Division, CSIR-Indian Institute of Chemical Biology, Kolkata, India

³ National Institute of Pharmaceutical Education and Research, Kolkata, India

⁴ Department of Medicine, Banaras Hindu University, Varanasi, India

*Corresponding author. Tel: +91 33 24995783; E-mails: suvendra@iicb.res.in; sb@csiriicb.in

[†]These authors contributed equally to this work

[‡]Present address: University of California Los Angeles, Los Angeles, CA, USA

their surface as part of MHC complex for antibody production (Podinovskaia & Descoteaux, 2015), but it also ensures reduction in production of nitric oxide and reactive oxygen species in invaded cells to stop killing of the internalized pathogens (Kumar *et al*, 2018). By inactivation of p38/MAPK-driven NF- κ B signalling, the transcription of the pro-inflammatory cytokine encoding mRNAs is compromised while production of anti-inflammatory cytokines like IL-10 get enhanced in *Ld* invaded macrophages (Halle *et al*, 2009; Kozicky & Sly, 2015; Kumar *et al*, 2018).

The mechanism of balanced pro- vs. anti-inflammatory cytokine production is a complex and robust process that requires intricate action and crosstalk between cellular signalling machineries and is primarily controlled by several kinases and phosphatases that regulate activation–deactivation states of cellular signalling components linked with regulation of immune response in mammalian macrophages (Kozicky & Sly, 2015; Lloberas *et al*, 2016). *Leishmania* is known to control several of these kinases and phosphatases that are involved in determining the balanced expression of both pro- and anti-inflammatory cytokines (Soulat & Bogdan, 2017).

miRNAs are tiny gene regulatory RNAs that regulate gene expression reversibly by inducing translational suppression and storage or degradation of the repressed messages (Bartel, 2018) in a contextual and candidate specific manner. The action of the miRNAs can get reversed on their targets (Bhattacharyya *et al*, 2006). Derepression of miRNA activity for target cytokine mRNAs is achieved by phosphorylation and miRNA uncoupling of the Ago2 protein in bacterial membrane lipopolysaccharide (LPS)-stimulated macrophage cells (Mazumder *et al*, 2013). This ensures a robust expression of pro-inflammatory cytokines in macrophages exposed to bacterial LPS. Interestingly, the reduction of cytokine mRNA levels after prolonged exposure of macrophage to LPS has also been noted (Mazumder *et al*, 2013) and it has been anticipated as the primary mechanism to check out excess cytokine production in activated macrophage when re-repression of the miRNA-target cytokine mRNAs has been observed. On the contrary, during infection, *Leishmania* is known to upregulate the binding of Ago2 with miRNAs (Chakrabarty & Bhattacharyya, 2017). However, there are other ways to modulate miRNP activity and levels that animal cells adopt under changed context (Patranabis & Bhattacharyya, 2016). Human ELAVL1 protein HuR is known for its anti-miRNA function. The protein, in stressed human hepatocytes, is known to act as a derepressor of miRNA function, where by binding the 3'UTR of common target messages, HuR replaces the bound miRNPs from target mRNAs and ensures uncoupling of miRNAs from the replaced miRNPs. This process is very much determined by miRNAs identity and its binding with HuR that causes accelerated extracellular export of corresponding miRNAs from human hepatocytes under stress (Mukherjee *et al*, 2016). Thus being able to induce derepression of miRNP-mediated target gene repression, HuR should supposedly favour the pro-inflammatory response in mammalian macrophage cells by accelerating expression of miRNA-targeted mRNAs that also have AU-rich elements and thus can be protected by HuR against degradation (Meisner & Filipowicz, 2011).

In this manuscript, we have identified that *Ld* has opposite effects on protein phosphatase 2A (PP2A) and HuR, and thus can eventually determine miRNA-controlled cytokine expression in mammalian macrophages. We have identified PP2A responsible for miRNP recycling in LPS-stimulated macrophage. It ensures

dampening of the pro-inflammatory cytokine production in prolonged LPS-exposed macrophages by promoting re-loading of miRNAs with Ago2 and favours repression of excess cytokine mRNAs in activated cells. PP2A favours anti-inflammatory response in *Ld*-infected macrophages and thereby essential for pathogen survival. On the contrary, HuR, that promotes the inactivation of existing miRNPs and derepresses their target genes, gets inactivated in *Ld*-infected macrophages. Restoration of HuR level, by ectopic expression of the protein in infected cells, reverses the action of the pathogen on cytokine production and clears the parasite from infected host cells or animal tissues. The antimony-resistant *Leishmania donovani* (*Ld^R*), known to induce strong anti-inflammatory response in the host, causes high PP2A expression. Thus, the infection with *Ld^R* could not be reversed by restoration of HuR level alone but through simultaneous inhibition of PP2A along with ectopic expression of HuR to negate the strong anti-inflammatory effect that the drug-resistant pathogen induces in invaded macrophages by targeting both PP2A and HuR. Finally, taken from the leads of the experimental data presented in this manuscript, the mathematical model of the macrophage activation process suggests a biphasic action of HuR and PP2A that reciprocally ensures a robust control of cytokine expression in mammalian macrophages.

Results

PP2A is necessary for Ago2 dephosphorylation

Lipopolysaccharide is an immunostimulatory molecule, derived from the outer membrane of Gram-negative bacteria that acts via TLR4 receptor to activate p38/MAPK pathway in macrophage cells (Bode *et al*, 2012). It augments the NF/ κ B signalling pathway to induce expression of pro-inflammatory cytokines (Chen *et al*, 2006). The transcriptional surge of new cytokine mRNAs is accompanied by enhanced translation and derepression of miRNP machineries during the early phase of macrophage activation by LPS when cellular miRNPs get deactivated due to phosphorylation of Ago2 and consequent unbinding of associated miRNAs. The derepression of miRNPs thus ensures the surge of pro-inflammatory cytokine production immediately after LPS stimulation (Mazumder *et al*, 2013).

However, on prolonged exposure of LPS, we documented restoration of miRNA activity, despite no major change in total cellular content of miRNA let-7a throughout the early to late stimulatory phases in LPS-treated macrophages (Fig 1A–D). With re-establishment of miRNA activity during long hours/late phase of LPS stimulation, levels of miRNA-regulated cytokine mRNAs IL-6 and TNF- α were also dropped to a much reduced level compared to high cytokine mRNAs observed in early phase of activation due to loss of miRNA activity there [Fig 1C (Mazumder *et al*, 2013)]. Cellular levels of miRNA let-7a, a miRNA known to control IL-6 mRNA, did not alter with LPS exposure but its association with Ago2 was relieved initially and then reversed over the course of LPS exposure (Fig 1D).

Reactivation of miRNPs can account for increased miRNA activity, and repression of target IL-6 mRNA was observed in prolonged LPS-treated cells. However, it should be preceded by dephosphorylation of Ago2 necessary for re-loading of Ago2 with miRNAs.

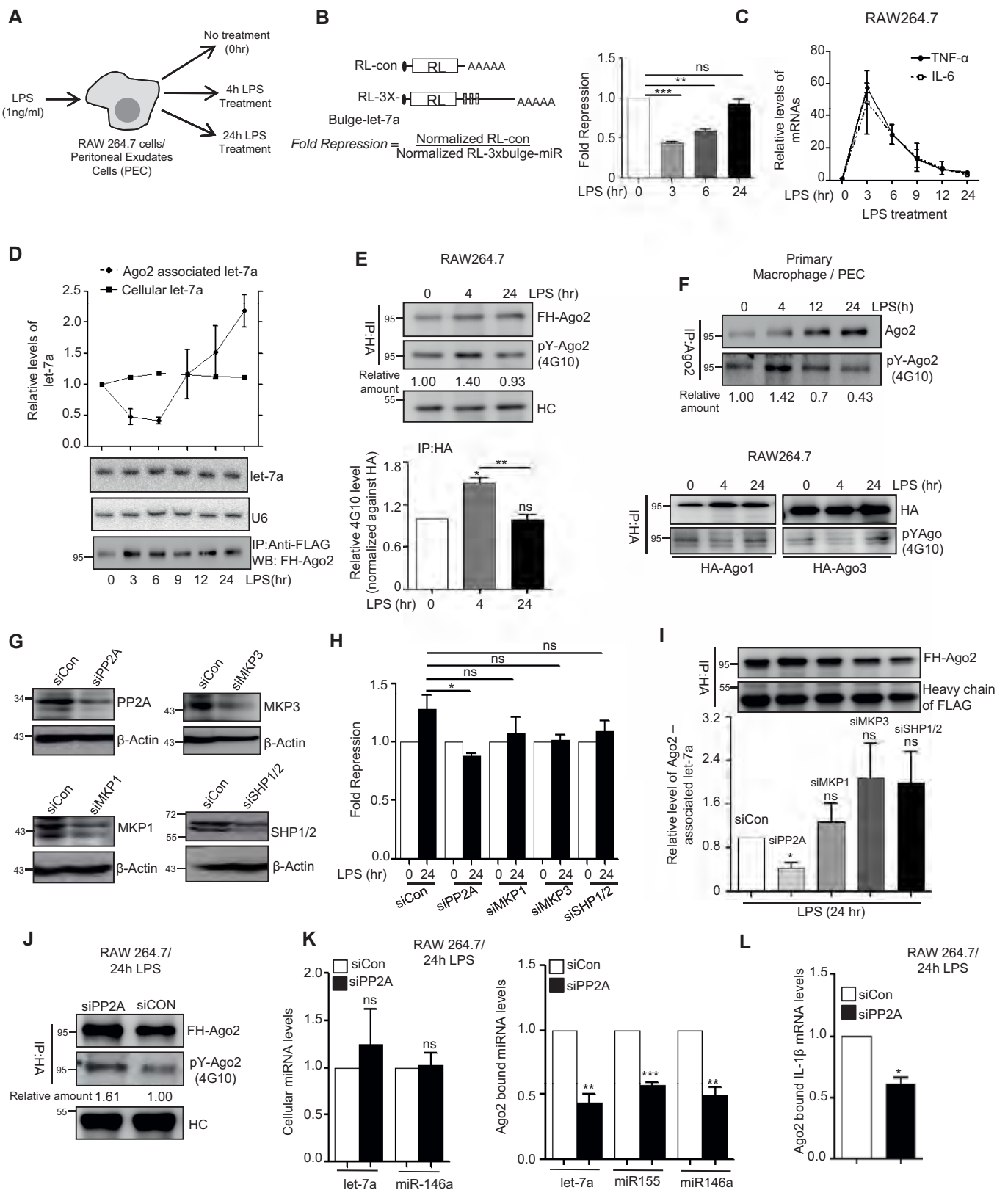


Figure 1.

Figure 1. PP2A-dependent Ago2 dephosphorylation during prolonged LPS stimulation of mammalian macrophage cells.

- A–C Reversal of miRNP activity and its restoration during the LPS treatment of RAW 264.7 cells. Schematic representation of the experiments where RAW 264.7 or PEC cells were treated with 1 ng/ml of LPS for different time points before the RNA and protein content were analysed (A). Relative fold repression for let-7a reporter in RAW 264.7 cells during LPS treatment (mean \pm s.e.m., $n = 3$) (B). The schematic representation of the constructs used for luciferase assays is shown. Relative levels of pro-inflammatory cytokines TNF- α and IL-6 mRNA, a target of let-7a miRNA, have been plotted against time of LPS stimulation, and 18S rRNA was used for normalization (mean \pm s.e.m., $n = 2$ (IL-6), $n = 3$ (TNF- α)) (C).
- D–F Time-dependent Ago2 phosphorylation and its miRNA binding in LPS-treated macrophage cells. RAW 264.7 cells were transfected with FH-Ago2 expression plasmid and treated with LPS (1 ng/ml) for different time points. Ago2 was pulled down using anti-FLAG beads, and the levels of Ago2-associated let-7a miRNA were measured by qRT–PCR. Quantity of immunoprecipitated Ago2 was detected in Western blot analysis with anti-HA antibody and used for normalization of amounts of miRNA detected by qRT–PCR. Levels of cellular let-7a were measured by Northern blot, and U6 RNA was used as loading control. Relative levels of cellular and Ago2-bound let-7a were plotted (mean \pm s.e.m., $n = 3$) (D). Phosphorylated Ago2 (pY-Ago2) level was measured using 4G10 antibody specific for phosphorylated Tyrosine. Phosphorylated Ago2 (pY-Ago2) band intensities were normalized against total Ago2 detected with HA-specific antibody that was also used for Ago2 pull down (E, upper panel). Relative 4G10 intensities were plotted from three independent experiments (mean \pm s.e.m.) (E, lower panel). Primary cells (PEC) were isolated from BALB/c mice and endogenous Ago2 was immunoprecipitated with anti-Ago2 (eIF2C2) antibody and phosphotyrosine level of Ago2 was measured using 4G10 antibody. Relative intensities of phospho-Ago2 against total amount of immunoprecipitated Ago2 were quantified and mentioned below the lanes (mean \pm s.e.m., $n = 3$) (F, upper panel). Similar experiments were done with FH-Ago1 and Ago3, and levels of phosphotyrosine in immunoprecipitated FH-Ago1 and FH-Ago3 were measured in RAW 264.7 cells (F, lower panel).
- G–I Effect of knock-down of different phosphatases on miRNA-mediated repression and miRNA association of Ago2 in 24-h LPS-treated RAW 264.7 cells. Knock-down of PP2A, MKP1, MKP3 or SHP1/2 was checked by Western blot analysis done with lysates of cells treated with respective siRNAs. β -Actin was used as loading control (G). Luciferase-based let-7a miRNA reporter assay was done in LPS-treated cells downregulated for specific phosphatases. Levels at 0-h time point were taken as units (mean \pm s.e.m., $n = 4$) (H). Ago2-associated let-7a was estimated by qRT–PCR in LPS-treated cells depleted for specific phosphatases. let-7a miRNA level was normalized against respective FH-Ago2 bands (mean \pm s.e.m., $n = 3$) (I).
- J–L Effect of PP2A knock-down on Ago2 phosphorylation and its miRNA association. Phospho Ago2 levels were measured in siCon- and siPP2A-transfected cells upon 24 h of LPS treatment using phosphotyrosine specific 4G10 antibody. HA-Ago2 was detected with anti-HA antibody (J). Cellular miRNA levels (K, left panel, mean \pm s.e.m., $n = 3$) and Ago2-associated miRNAs content in cells treated with siCon or siPP2A were measured using qRT–PCR and plotted (K, right panel, mean \pm s.e.m., $n = 3$). Ago2-associated IL-1 β mRNA level was estimated in siCon- and siPP2A-treated cells which were stimulated with LPS for 24 h (mean \pm s.e.m., $n = 3$) (L). Immunoprecipitated Ago2 content was used for normalization for both miRNA and mRNA levels in above-mentioned experiments.

Data information: In all experimental data, ns: non-significant and *, ** and *** represent P -value of < 0.05 , < 0.01 and < 0.001 , respectively, calculated by using Student's t -test. HC: heavy chain of the antibody used for immunoprecipitation. For statistical analysis, all experiments were done minimum three times. Exact P -values against each experimental set are presented in the Appendix Table S2. Positions of molecular weight markers are shown in the Western blots used in different panels. Source data are available online for this figure.

During this long exposure of LPS, we have documented reversal of Ago2 phosphorylation that had increased during early phase of LPS treatment of RAW 264.7 cells (Fig 1E). Interestingly, Ago1 and Ago3 showed an opposite effect upon LPS activation as they showed restoration of phosphorylation after 24 h of LPS exposure while a decrease in phosphorylation was noted at 4 h of LPS exposure (Fig 1F, lower panel). Cellular level of Ago2, like that of miRNA, was not altered during early or late activation phases (Figs 1E and EV1A). Similar results were also observed in primary macrophage cells (Fig 1F, upper panel).

To identify the potential candidate phosphatase that acts on phosphorylated Ago2 to reactivate it in prolonged LPS-treated cells, we first checked the expression of key phosphatases in LPS-treated cells that are known to get upregulated in LPS-activated macrophages (Kozicky & Sly, 2015). We observed an increased expression of protein phosphatase 2A (PP2A) and mitogen-activated protein kinase phosphatase 1 (MKP1) in activated macrophage (Fig EV1A and B). To specify the phosphatase that is responsible for Ago2 dephosphorylation, we targeted them individually with specific sets of siRNAs. We have noted PP2A as the effective phosphatase that acted on phosphorylated Ago2 in LPS-treated macrophage, and as observed, depletion of PP2A showed defective recovery of let-7a miRNP activity and its Ago2 association during prolonged LPS activation. Effect of siRNA-mediated depletion of two other phosphatases MKP3 and SHP1/2 showed no inhibitory effect of miRNA-activity recovery during LPS treatment (Fig 1G–I). siRNA-mediated PP2A knock-down was also effective to prevent the re-binding of the miRNAs to Ago2 but without a change in cellular miRNA content upon prolonged activation by LPS. As expected, siPP2A treatment was also associated with increased Ago2 phosphorylation

and decreased target RNA binding of Ago2 (Fig 1J–L). Interestingly, similar increase in PP2A levels were noted in RAW 264.7 cells treated with PMA or in primary macrophage treated with LPS. Increased levels of PP2A mRNAs were also noted in RAW 264.7 cells upon LPS treatment (Fig EV1C–E).

Phosphorylation–dephosphorylation cycle of Ago2 controls miRNP recycling and *de novo* miRNP formation

Like siPP2A treatment, application of okadaic acid (OA), a chemical inhibitor of PP2A (Fernandez *et al*, 2002), inhibited the Ago2 dephosphorylation and restoration of miRNA activity in prolonged LPS-treated macrophages (Fig 2A–C). Incubation of the PP2A immunoprecipitated materials with FLAG-HA-tagged Ago2 isolated from a non-immune human cell HEK293, the phosphorylated Tyrosine at 529 of Ago2 got dephosphorylated in the *in vitro* phosphatase assay. Interestingly, unlike the wild type, the Ago2-Y529F mutant that could not get phosphorylated at 529 position showed no change in its phosphorylation status upon incubation with PP2A immunoprecipitated materials. These data suggest that PP2A specifically dephosphorylates Ago2 at Y529 position and thus should be effective in controlling miRNA binding of Ago2 as phosphorylation at Y529 position of Ago2 is known to cause miRNA unbinding [Fig 2D (Rudel & Meister, 2008)]. Use of OA, the inhibitor of PP2A, increased the phosphorylated form of Ago2. OA should therefore inhibit *de novo* miRNP formation in prolonged LPS-treated cells by reducing the cellular free Ago2 pool ready for miRNA loading. As expected, inducible expression of miR-122, that got expressed in the presence of doxycycline in cells otherwise not expressing the liver-specific miR-122 but harbouring a doxycycline inducible miR-122

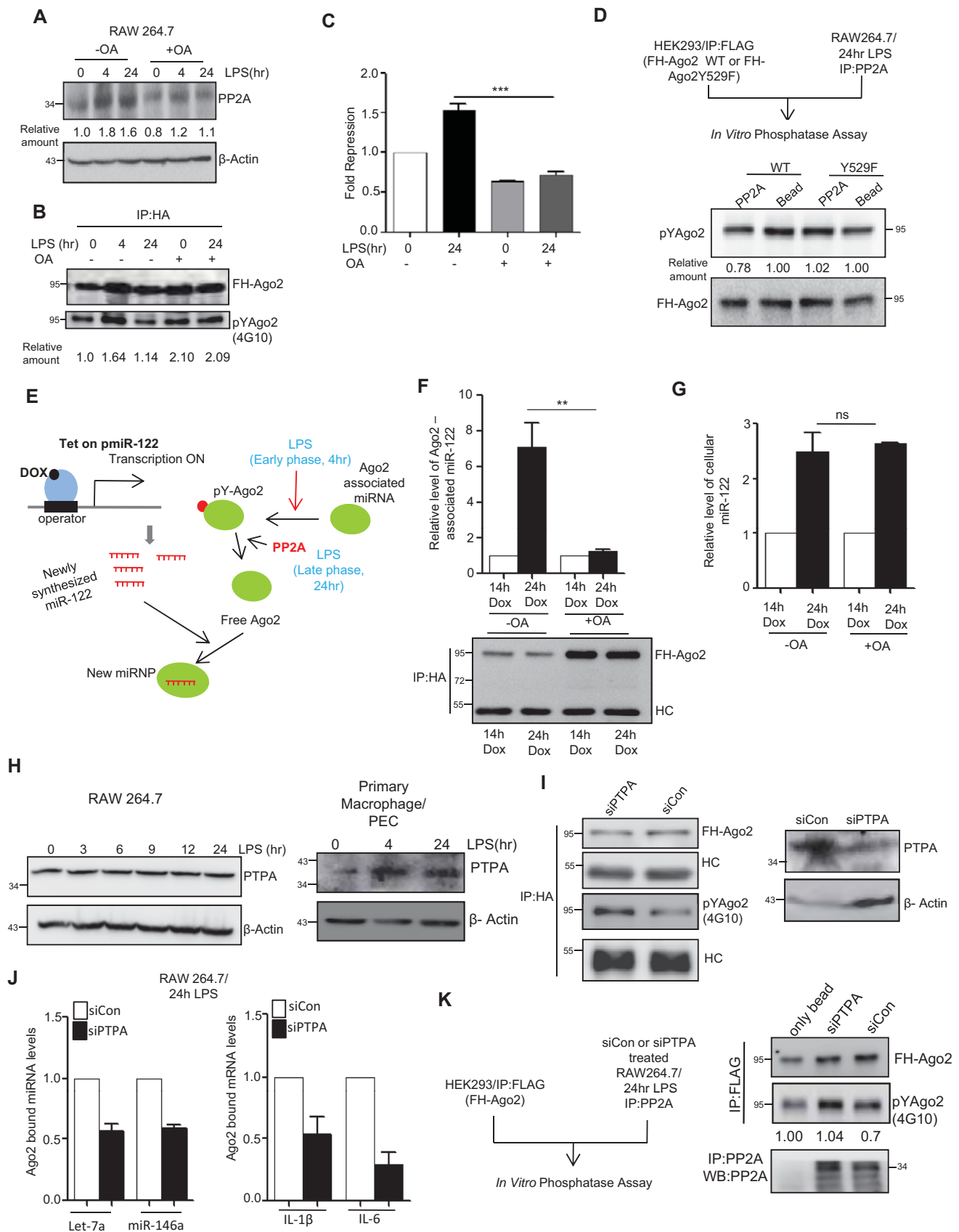


Figure 2.

Figure 2. Phosphorylation–dephosphorylation cycle of Ago2 controls miRNP recycling and *de novo* miRNP formation.

- A–C Effect of okadaic acid (OA; 100 nM), the PP2A inhibitor, on Ago2 phosphorylation and miRNA activity. Expression of PP2A was detected in Western blot done for cell extract from control and OA-treated RAW 264.7 cells after LPS stimulation (A). The amount of phosphorylated Ago2 was measured in OA-treated cells before and after LPS stimulation. The amount of Tyr phosphorylated Ago2 was measured by densitometric quantification of Western blot data upon normalization against immunoprecipitated Ago2 amount (B). Changes in fold repression for a let-7a reporter upon LPS exposure in control and OA-treated cells (mean \pm s.e.m., $n = 3$) (C).
- D Schematic representation of the *in vitro* phosphatase assay (upper panel). PP2A was immunoprecipitated from 24-h LPS-treated RAW 264.7 cells and was incubated *in vitro* with wild type or phosphorylation defective FH-Ago2 mutant (Ago2Y529F) isolated from HEK293 cells transfected with respective expression constructs. Phosphorylated Ago2 (pY-Ago2) levels were measured by Western blot analysis using anti-phosphotyrosine-specific 4G10 antibody. Relative intensities were quantified by densitometric analysis and mentioned below the respective panels. FH-Ago2 was detected by anti-HA antibody (Lower panel).
- E–G Defective *de novo* miRNP formation in cells pre-treated with PP2A inhibitor. A schematic representation of the assay done to check the *de novo* miRNP formation after doxycycline (DOX)-induced expression of miR-122, a liver-specific miRNA, in RAW 264.7 cells during LPS stimulation (E). Ago2-associated (F) and total (G) miR-122 levels were measured by qRT–PCR and normalized against immunoprecipitated FH-Ago2 content and U6 RNA, respectively. Values obtained upon 14 h of DOX treatment were considered as unit, and relative values obtained upon 24 h of DOX treatment are plotted. All samples were treated for 24 h with LPS (mean \pm s.e.m., $n = 4$).
- H–K Phosphotyrosyl phosphatase activator (PTPA) is an essential factor for PP2A-mediated dephosphorylation of Ago2. Expression of PTPA after LPS stimulation in RAW 264.7 cells as well as in PEC isolated from BALB/c mice. β -Actin was used as loading control (H). Effect of PTPA depletion on Ago2 phosphorylation level in RAW 264.7 cells (I). Phosphorylated Ago2 level was measured by Western blot in HA-immunoprecipitated materials isolated from either siCon- or siPTPA-transfected cells expressing FH-Ago2 upon 24 h of LPS treatment using a phosphotyrosine-specific 4G10 antibody (I, left panel). The PTPA was detected with anti-PTPA antibody, and β -actin was used as loading control (I, right panel). Effect of PTPA depletion on Ago2-associated miRNAs and mRNAs. Ago2-associated miRNA (J, left panel) (mean \pm s.e.m., $n = 3$) and mRNA levels (J, right panel) (mean \pm s.e.m., $n = 2$) were also quantified using qRT–PCR. Amount of FH-Ago2 in immunoprecipitated materials (shown in panel I) were used for normalization. Schematic depiction of *in vitro* phosphatase assay (K, left panel). PP2A was immunoprecipitated from siCon- or siPTPA-treated RAW 264.7 cells treated with LPS for 24 h and was incubated *in vitro* with FH-Ago2 isolated from HEK293 cells and upon the assay reaction, the phospho-Ago2 level was measured by Western blot analysis using phosphotyrosine-specific 4G10 antibody (K, right panel).

Data information: Relative quantification was done by densitometry. HC: heavy chain of respective antibodies used for immunoprecipitation. In all experimental data, ns: non-significant and ** and *** represent P -value of < 0.01 and < 0.001 , respectively, estimated by using Student's t -test. Exact P -values against each experimental set are presented in the Appendix Table S2. Positions of molecular weight markers are marked and shown in the Western blots used in different panels. Source data are available online for this figure.

expression system, failed to get incorporated to Ago2 in OA-treated cells with time. Thus, the levels of *de novo* miRNPs got reduced when PP2A was inhibited (Fig 2E–G). These results support the importance of phosphorylation–dephosphorylation cycle of existing miRNPs for *de novo* miRNP formation in mammalian cells that happens during late phase of LPS exposure of macrophages. Thus, phosphorylated Ago2 that undergoes PP2A-mediated dephosphorylation acts as substrate for subsequent *de novo* miRNA loading during late phase of LPS treatment of mammalian macrophages (Fig 2E–G).

PP2A requires Phosphotyrosyl phosphatase activator (PTPA) for dephosphorylation of Ago2

The phosphorylation of Ago2 at Tyrosine 529 was found to be downregulated in the presence of PP2A, and Tyr phosphorylation of Ago2 showed an inverse correlation with PP2A levels in macrophage cells. Interestingly, PP2A is a serine-specific phosphatase and should act on proteins with a phosphorylated serine. However, PP2A is also known to act on phosphotyrosine in the presence of an adaptor protein PTPA that could render PP2A to dephosphorylate Tyrosine (Janssens *et al*, 1998). Unlike PP2A, we detected no increase in PTPA expression in macrophage during LPS treatment (Fig 2H). However, with depletion of PTPA we detected reduced Ago2 dephosphorylation in 24 h LPS-treated RAW 264.7 cells (Fig 2I). We also checked the status of Ago2 binding of miRNA and target mRNAs in PTPA-depleted cells and have found reduced miRNA and target RNA association of Ago2 upon LPS treatment in cells depleted for PTPA (Fig 2J). We also checked the *in vitro* phosphatase activity of immune-isolated PP2A from siControl- or siPTPA-treated cells and had found reduced phosphatase activity of PP2A obtained from PTPA-depleted cells on Tyrosine phosphorylated Ago2 during the *in vitro* phosphatase assays (Fig 2K).

Protein phosphatase 2A upregulation in *Leishmania*-infected macrophages reduces phosphorylated Ago2 and ensures robust repression of pro-inflammatory cytokines

The pathogen *Ld* infects the host macrophage and evades the host immune response by inhibiting pro-inflammatory cytokine production. This can be easily achieved by sustained miRNP-mediated gene repression of target pro-inflammatory cytokine encoding mRNAs in infected cells. Retention of miRNPs with targets can be achieved by keeping the phosphorylation of Ago2 at minimal level. Ago2 phosphorylation happens primarily during LPS or PMA-mediated activation of macrophages (Mazumder *et al*, 2013). As expected, we noted a decreased pro-inflammatory cytokine production and increased anti-inflammatory IL-10 production both in RAW 264.7 and murine primary macrophages (PEC) upon *Ld* infection (Fig 3A–C). It was accompanied by a decrease in the level of Ago2 phosphorylation and increased Ago2-miRNA binding happening in infected cells (Fig 3D and E). Interestingly, the PP2A level was also increased upon *Ld* infection both in mouse primary macrophage PEC and RAW 264.7 cells (Fig 3B).

Working on the mechanism of *Ld*-induced expression of PP2A in macrophages, we did not detect any increase of PP2A mRNA or protein in RAW 264.7 cells upon treatment with heat killed *Ld* (Fig EV2A and B). Upon interaction with macrophages, *Ld* may elicit the response on PP2A expression either due to phagocytic internalization of the pathogen or due to interaction of surface ligands of *Ld* with receptors present on macrophage membrane.

We used inert latex beads that are internalized through phagocytosis in a time-dependent manner in RAW 264.7 cells (Akilbekova *et al*, 2015). However, no increase in PP2A expression was documented in cells interacting with latex beads rather a decrease in PP2A protein and mRNA level was evident (Fig EV2C–E). Lipophosphoglycan or LPG is a major surface molecule of *Leishmania* in the

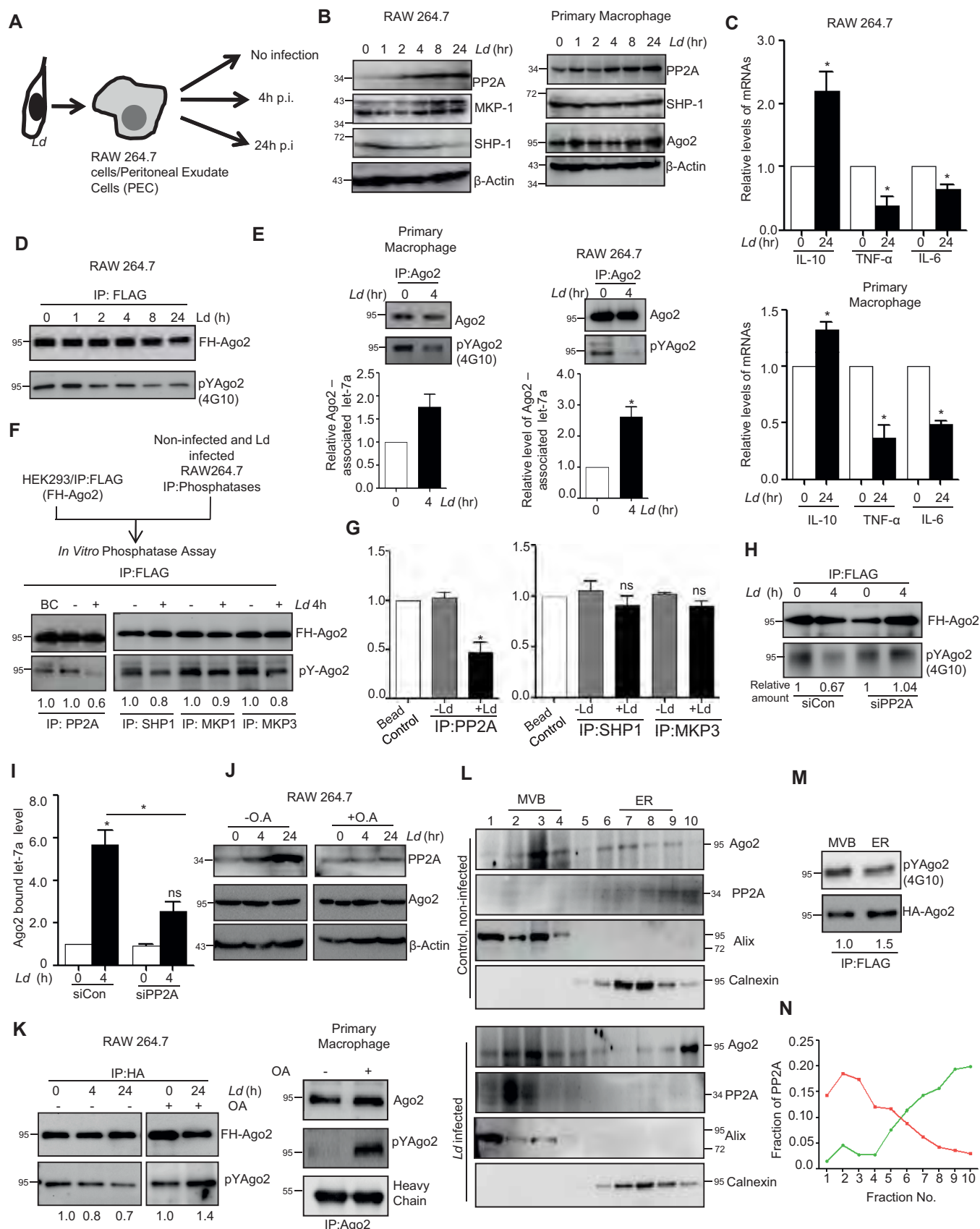


Figure 3.

Figure 3. *Leishmania donovani* upregulates PP2A to dephosphorylate Ago2 in infected macrophage cells.

- A–C Expression of different cytokines and phosphatases in RAW 264.7 cells and PEC infected with *Leishmania donovani* (*Ld*) parasites. A scheme of the experiments is shown in panel A. Cells at different time points of infection were harvested, and levels of various phosphatases were checked by Western blot analysis using antibodies specific for different phosphatases in both RAW 264.7 (B, left panel) and mouse peritoneal macrophage cells PEC (B, right panel). Cytokine mRNA levels like IL-10, TNF- α and IL-6 were quantified after 24 h of *Ld* infection in RAW 264.7 (C, upper panel mean \pm s.e.m., $n = 3$) and mouse peritoneal macrophage PEC (mean \pm s.e.m., $n = 3$) (C, lower panel).
- D, E Effect of *Ld* infection on Ago2 phosphorylation and its miRNA association. RAW 264.7 cells were transfected with FH-Ago2 expression construct, and infection was done for various time points followed by FH-Ago2 pull down using anti-FLAG beads. Phosphorylated Ago2 levels were checked during the course of *Ld* infection (D). Phosphorylation levels of Ago2 were measured by doing endogenous Ago2 pull down using Ago2-specific antibody after 4 h of infection and quantified along with Ago2-associated let-7a level measurement in primary macrophages (mean \pm s.e.m., $n = 2$) (E, left panel) and in RAW 264.7 cells (mean \pm s.e.m., $n = 3$) (E, right panel).
- F, G Schematic representation of *in vitro* phosphatase assay (F, upper panel). PP2A, MKP1, MKP3 or SHP1 was immunoprecipitated individually from naïve or *Leishmania*-infected macrophage cells and was incubated *in vitro* with FH-Ago2 isolated from FH-Ago2 stable HEK293 cells. Phosphorylated Ago2 level was detected by Western blot analysis using phosphotyrosine-specific 4G10 antibody (F, lower panel) and measured by densitometry. Relative intensity of 4G10 specific band against immunoprecipitated Ago2 was plotted (mean \pm s.e.m., $n = 3$) (G). BC: bead control.
- H, I Effect of PP2A knock-down on Ago2 phosphorylation and miRNA-Ago2 binding in RAW 264.7 cells infected with *Ld*. Cells were co-transfected with siRNA and FH-Ago2 expression plasmid. Phosphorylated Ago2 levels were detected after 4 h of infection in siCon- or siPP2A-transfected cells (H). Ago2-associated let-7a levels were also estimated and plotted (mean \pm s.e.m., $n = 4$) (I).
- J, K Effect of OA on Ago2 phosphorylation in *Ld*-infected RAW 264.7 cells and mouse PEC. Cellular levels of PP2A and Ago2 at different time points of *Ld* infection with or without OA treatment (100 nM) were detected. Cells were pre-treated with OA (100 nM) for 2 h before infection (J). β -Actin was used as loading control. Phospho-Ago2 level was measured in OA pre-treated; *Ld*-infected RAW 264.7 cells expressing FH-Ago2 and in PEC after 24 h of infection with or without OA pre-treatment. Phosphorylated Ago2 levels were also checked (K).
- L–N Subcellular compartmentalization of PP2A in *Ld*-infected RAW 264.7 cells. RAW 264.7 cells were infected with *Ld* for 6 h, and cell extract was analysed on a OptiPrep[®] density gradient to separate subcellular organelles and structures. Subcellular localization of Ago2 and PP2A in individual fractions was detected by Western blots. Alix was used as MVB marker, while Calnexin was used as ER marker (L). OptiPrep[®] fractions, positive for MVB (fraction number 2,3,4) and ER (fraction number 7,8,9) markers, were pooled separately, and Ago2 was immunoprecipitated using anti-FLAG beads. Phosphorylated Ago2 levels were quantified in Western blot done with phosphotyrosine-specific 4G10 antibody (M). PP2A percentage intensity plot for each fraction was done for control (Green line) and infected (Red line) samples (N).

Data information: In all experimental data, ns: non-significant and * represents P -value of < 0.05 estimated by using Student's t -test. HC: heavy chain of respective antibody used for immunoprecipitation. Exact P -values against each experimental set are presented in the Appendix Table S2. Positions of molecular weight markers are marked and shown in the Western blots used in different panels.

Source data are available online for this figure.

promastigote stage and has been reported to interact with several Toll-like receptors (TLRs) (Becker *et al*, 2003; Rojas-Bernabe *et al*, 2014; Chaparro *et al*, 2019). PP2A upregulation during *Ld* infection has been previously reported (Kar *et al*, 2010); however, the exact mechanism is unknown. We speculated that upregulation of PP2A could be mediated by TLR pathway upon interaction with LPG. To check whether LPG mediates PP2A upregulation, RAW 264.7 cells were treated with LPG isolated from *Ld*. Interestingly, LPG was found to upregulate PP2A mRNA level in a concentration-dependent manner (Fig EV2F–I). However, treatment of cells with anti-TLR4 antibody to block the TLR4 activation by LPS has been effective to reduce PP2A expression in RAW 264.7 cells and production of TNF- α mRNA there (Fig EV2F and G). Using the same anti-TLR4 antibody, we could reduce the expression of PP2A induced by LPG derived from *Ld* (Fig EV2H and I).

To confirm that the increased PP2A, present in the infected macrophage, is responsible for decreased Ago2 phosphorylation observed, we performed an *in vitro* phosphatase assay with affinity purified FH-Ago2 isolated from HEK293 cells and treated them with immunoprecipitated phosphatases from *Ld*-infected RAW 264.7 cells individually. Substantial decreases in Ago2 phosphorylation level were only observed upon interaction with PP2A immunoprecipitated materials suggesting PP2A as the major phosphatase present in *Ld*-infected cells that is responsible for decreased Ago2 phosphorylation (Fig 3F and G). The conclusion was substantiated in another set of experiments where cells were transfected with siRNAs against PP2A, and an increase in Ago2 phosphorylation and decrease in Ago2-bound miRNA content were noted in siPP2A-treated cells compared to control siRNA-treated cells upon *Ld*

infection (Fig 3H and I). Similarly, treatment of OA, the chemical inhibitor of PP2A, showed no effect on Ago2 levels but showed an increase in Ago2 phosphorylation in *Ld*-infected macrophage cells (Fig 3J and K).

The compartment where PP2A prevents the pro-inflammatory response via enhancing the miRNPs stability in *Ld*-infected cells was of interest, and we explored that in subsequent experiments. We isolated the different subcellular organelles over an Optiprep[®] density gradient that could separate out the organelles on the basis of their densities (Fig 3L). We noted an increased association of PP2A with the endosome enriched fraction in *Ld*-infected cells (Fig 3N). It is important to note that substrate of PP2A, the phosphorylated Ago2, is also known to get concentrated in these fractions as we had analysed them before both in macrophage and neuronal cells [Fig 3L and M (Mazumder *et al*, 2013; Patranabis & Bhattacharyya, 2016)]. Therefore, PP2A may act on its substrate phosphorylated Ago2 in the Optiprep density gradient fractions 2–4 that are positive for MVB marker protein Alix.

Protein phosphatase 2A-mediated stabilization of miRNPs ensures anti-inflammatory response and *Ld* infection in mammalian macrophages

Ld upregulate PP2A to promote anti-inflammatory responses (Kar *et al*, 2010). In support of this notion, we have identified the increased production of IL-10, the hallmark anti-inflammatory cytokine expressed in *Ld*-infected mammalian macrophages. Depletion of PP2A by siRNA or its inhibition by OA resulted in downregulation of IL-10 production in *Ld*-infected cells (Fig 4A). This was accompanied

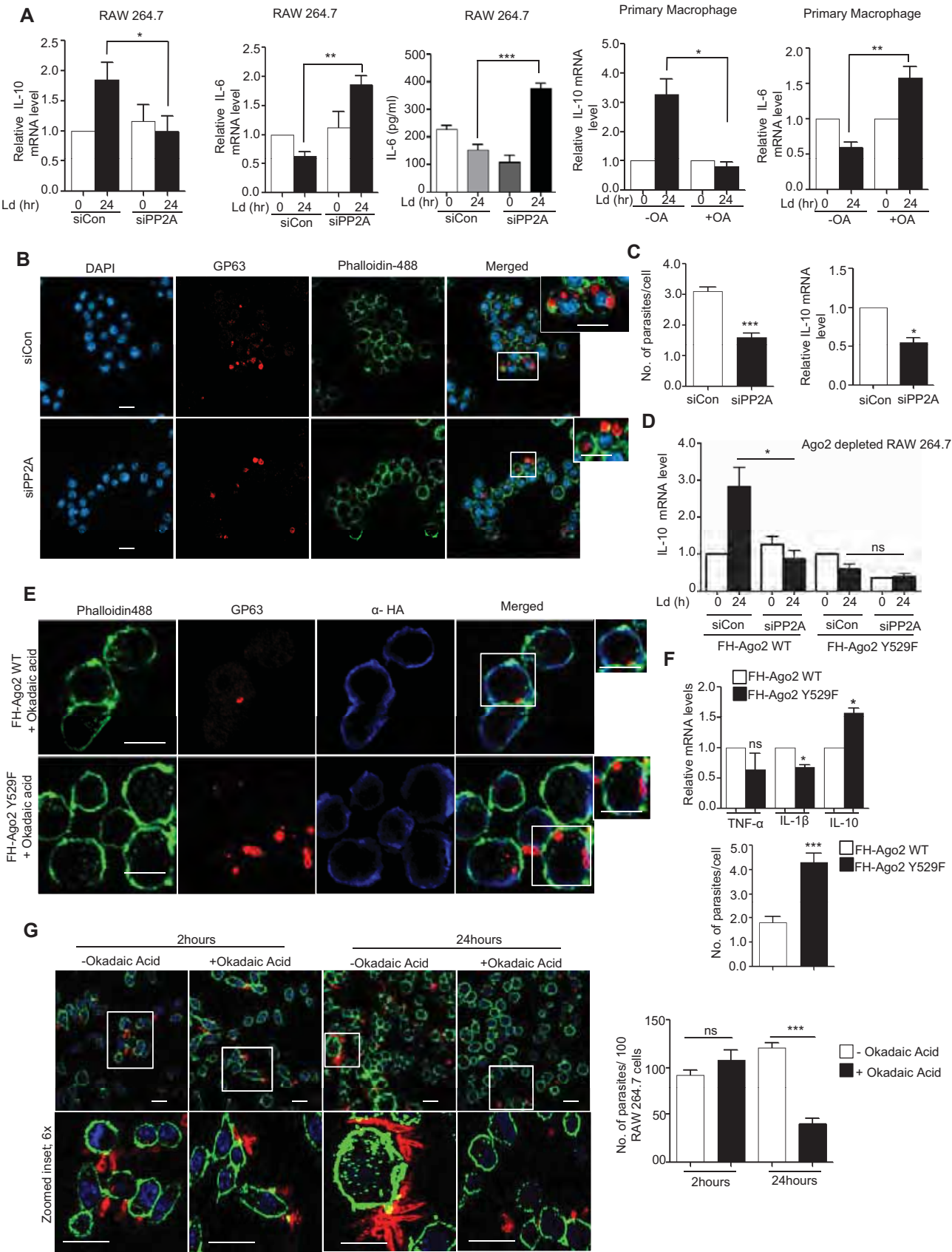


Figure 4.

Figure 4. PP2A-mediated dephosphorylation of Ago2 is necessary for *Leishmania donovani* infection of macrophage cells.

- A** Effect of PP2A downregulation or inhibition on pro- and anti-inflammatory cytokine levels in *Ld*-infected macrophage. IL-10 levels were measured after *Ld* infection in PP2A knocked-down RAW 264.7 cells (mean \pm s.e.m., $n = 3$) and in PEC (mean \pm s.e.m., $n = 3$). IL-6 was also measured in RAW cells after OA treatment (mean \pm s.e.m., $n = 5$) and also in PEC pre-treated with OA (mean \pm s.e.m., $n = 3$). Values obtained at 0 h (non-infected) or non-OA treated samples were considered as unit in each case. IL-6 protein level ($n = 5$) in cell supernatant was also measured by ELISA after *Ld* infection in PP2A knock-down RAW 264.7 cells.
- B, C** Effect of PP2A knock-down on parasite internalization and cellular IL-10 level. Internalized parasites were imaged in RAW 264.7 cells stained with Phalloidin-Alexa 488 (green) for actin cytoskeleton detection, and *Ld* was detected by indirect immunofluorescence done for parasite specific membrane protein GP63 (red) (B). Number of *Ld* internalized was measured in control and PP2A knock-down cells, and relative numbers of parasites within infected cells were plotted [C, left panel (mean \pm s.e.m., $n = 20$ cells)]. IL-10 mRNA levels were also quantified in those cells by qRT-PCR done for total cellular RNA [C, right panel (mean \pm s.e.m., $n = 3$)]. Scale bar 20 μ m. 4 \times Zoomed insets are shown.
- D** Effect of PP2A knock-down on IL-10 level in *Ld*-infected cells expressing phosphorylation defective mutant of Ago2. In RAW 264.7 cells, depleted for endogenous Ago2 (using a specific siRNA against the 3'UTR of Ago2 mRNA), either the wild type or Y529F mutant of FH-Ago2 (without having the 3'UTR of Ago2) was expressed in siCon- or siPP2A-treated RAW 264.7 cells. IL-10 mRNA level was measured subsequent to *Ld* infection. Relative IL-10 levels were plotted. Expression levels in non-infected siCon-treated cells in each case were designated as unit (mean \pm s.e.m., $n = 3$).
- E–G** Effect of PP2A inhibitor OA on *Ld* internalization and cytokine production in RAW 264.7 cells. In RAW 264.7 cells transfected with FH-Ago2 WT and Y529F mutant and pre-treated with OA, *Leishmania* internalization was measured microscopically. In images obtained, Ago2 was detected with α -HA (detected at 405 nm) and *Leishmania* was stained for GP63 (detected at 564 nm) (E). Quantitative measurement of GP63-positive structures was done, and quantitative data per 100 infected cells were plotted. Scale bar 10 μ m. RNA was isolated from different experimental sets, and TNF- α , IL-1 β and IL-10 mRNA levels were estimated (mean \pm s.e.m., $n = 3$) (F). RAW 264.7 cells with and without OA treatment were given *Ld* infection for 2 and 24 h. RAW 264.7 cells were stained with Phalloidin-Alexa 488 (green) for actin cytoskeleton, and *Ld* was stained for parasite specific protein GP63 (red) (G, left panel). Number of internalized parasites per 100 macrophages were calculated, and relative values were plotted (G, right panel) (mean \pm s.e.m., $n = 20$). Scale bar 20 μ m.

Data information: Zoomed parts are been highlighted with white boxes in the microscopic pictures. In all experimental data, ns: non-significant and *, ** and *** represent P -value of < 0.05 , < 0.01 and < 0.001 , respectively, quantified with the help of Student's t -test. For statistical analysis, all experiments are done minimum three times. Exact P -values against each experimental set are presented in the Appendix Table S2. Positions of molecular weight markers are marked and shown in the Western blots used in different panels.

Source data are available online for this figure.

by increased production of pro-inflammatory cytokine IL-6 both at mRNA and protein level (Fig 4A). Interestingly, internalization of the pathogen was reduced in the presence of siPP2A (Fig 4B and C, left panel). It was accompanied by decreased production of anti-inflammatory IL-10 in siPP2A-treated *Ld*-infected macrophages (Fig 4C, right panel). Importance of Ago2 dephosphorylation in the infection process was studied further in Ago2-depleted cells by expressing either the wild-type Ago2 or phosphorylation defective Y529F Ago2 mutant co-transfected either with siCon or siPP2A. Interestingly, unlike the FH-Ago2-expressing cells where depletion of PP2A strongly reduces IL-10 levels, there was little effect of PP2A depletion on IL-10 production in FH-Ago2Y529F mutant expressing cells (Fig 4D). This result supports the notion that the anti-inflammatory effect of PP2A induced by *Ld* infection is primarily through the control of phosphorylation–dephosphorylation cycle of Ago2 in infected cells. Therefore, PP2A has little effect on infection induced IL-10 level change in Ago2Y529F-expressing cell, as in those cells, Ago2Y529F is phosphorylation defective and therefore should not be responsive to the presence and absence of PP2A (Fig 4D). The importance of PP2A-mediated Ago2 dephosphorylation in infection process was further supported in other experiments where the expression of the Ago2Y529F mutant, compared to its wild-type counterpart, showed increased production of cytokine IL-10 and better internalization of parasite into the cells pre-treated with OA (Fig 4E). It was accompanied by a decrease in the expression of pro-inflammatory cytokine IL-1 β in OA-treated RAW 264.7 cells expressing Ago2Y529F (Fig 4F). In cells expressing wild-type Ago2, OA showed inhibition of *Ld* internalization and IL-10 production as PP2A is inhibited there. These data support the notion that in cells expressing a phosphorylation defective mutant of Ago2, the strong repression of pro-inflammatory cytokines would occur, and thus, they should be more susceptible to infection. The phosphorylation of Ago2 and its uncoupling with miRNA thus serve as an important mechanism of inflammatory response that got reversed during *Ld* infection in macrophage with wild-type Ago2 but

not in cells expressing Ago2Y529F (Fig 4D–G). These data also suggest a late effect of PP2A inhibition on internalized parasites as at early 2-h time no major change in internalized parasite number was detected (Fig 4G).

HuR-mediated export of miRNA is necessary and sufficient for pro-inflammatory immune response in mammalian macrophages

Balancing of pro-inflammatory responses by anti-inflammatory pathways in infected macrophage may need targeting of pro-inflammatory factors by the pathogen. In this context, miRNA derepressor protein HuR (Bhattacharyya et al, 2006) should have been an interesting candidate to explore as miRNA derepression due to miRNA-Ago2 uncoupling has been found to be a prerequisite for pro-inflammatory response in activated macrophage cells (Mazumder et al, 2013). Interestingly, there was increased level of HuR, the miRNA uncoupler, in macrophages activated with LPS (Fig 5A and B). It has been reported already that HuR is necessary and sufficient for miRNA export from mammalian hepatic cells under cellular stress (Mukherjee et al, 2016). Human ELAVL1 protein HuR has three RNA binding motifs, and it binds and sponges out specific miRNAs (Kundu et al, 2012; Poria et al, 2016). While HuR binds to mRNAs with AU-rich sequences, it could reversibly bind specific miRNA with AU/G sequences and may facilitate their export via exosomes, a special class of extracellular vesicles (EVs) (Mukherjee et al, 2016). As HuR level increases with increase in expression of canonical HuR target mRNAs like TNF- α in activated macrophages (Chen et al, 2006), the export of miRNAs is also expected to be accelerated in activated macrophages. HuR was found to be upregulated in those cells, and miRNAs that otherwise may play a repressive action on HuR target messages should be inactivated there. We explored the status of miRNA export from LPS-treated cells and noticed an accelerated miRNA export upon LPS exposure of macrophage cells. The characteristic profile of extracellular vesicles (EVs) isolated

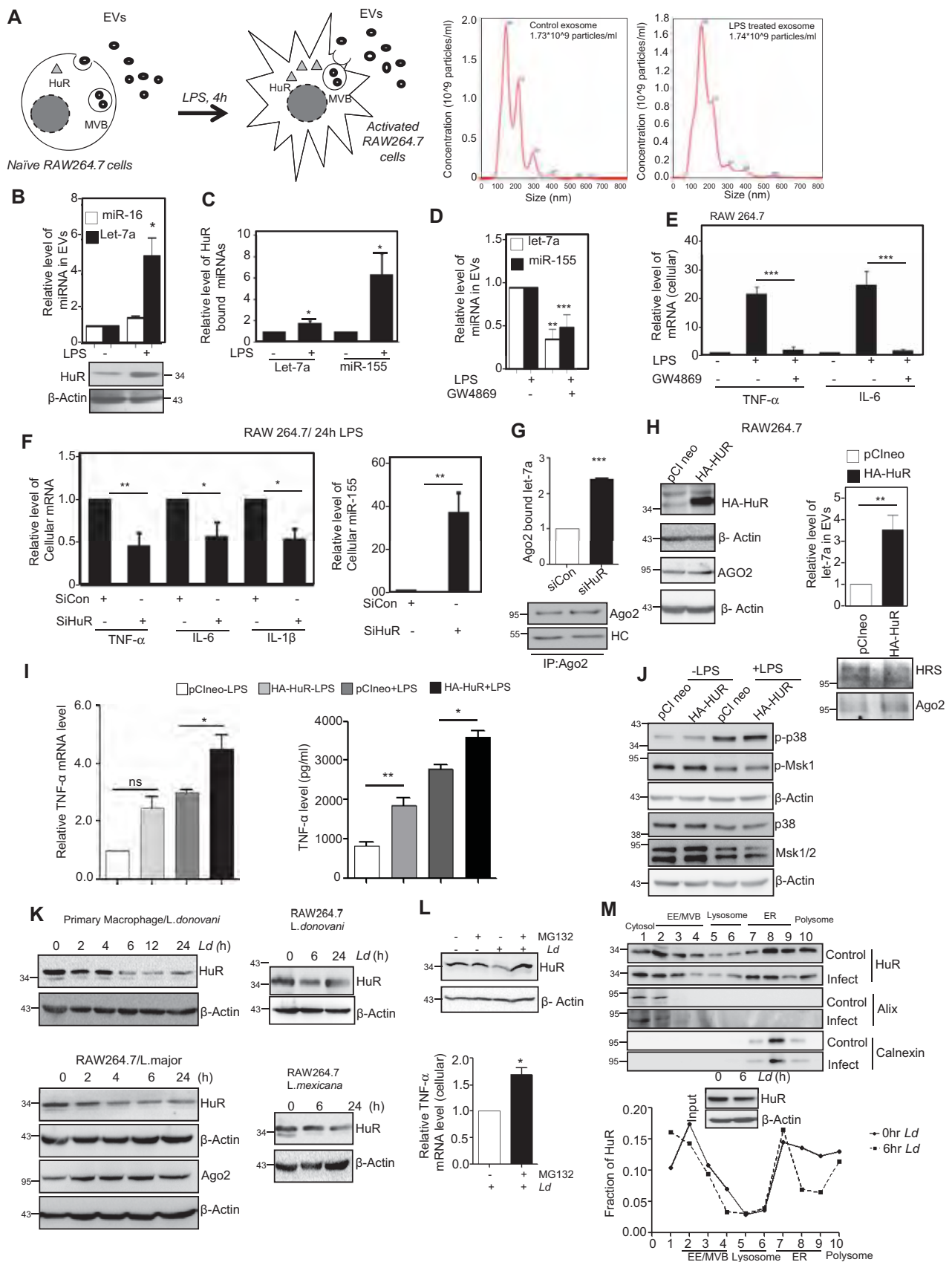


Figure 5.

Figure 5. HuR-mediated extracellular export of miRNA promotes pro-inflammatory responses in macrophage cells.

- A–C LPS induced miRNA export from mammalian macrophage cells. A schematic diagram of the experiments has been described in left panel of (A). Characterization and quantification of exosomes/EVs derived from control and LPS-activated RAW 264.7 cells by nanoparticle tracking analysis (NTA) done for isolated exosomes/EVs. Relative size distributions are shown (A, right panel). Levels of HuR and exosomal miRNA isolated from control and 24 h of LPS-treated RAW 264.7 cells. RNA content was normalized against total exosomal proteins (B). β -Actin was used as loading control for HuR Western blot. Binding of miRNAs with HuR after LPS exposure was measured. Amount of RNA was normalized against HuR content. Anti-GFP antibody was used for immunoprecipitation control (C). Values are mean \pm s.e.m. and $n = 3$.
- D Effect of GW4869, the inhibitor of exosome/EV-mediated miRNA export, on miRNA content of EVs released by LPS-stimulated cells. The level of miRNAs, let-7a and miR-155 was measured in exosomes (EVs) released from LPS-activated cell after GW4869 treatment. Values for EVs from naïve macrophages without GW4869 and LPS treatment were set as unit. Values are mean \pm s.e.m. and $n = 3$.
- E Effect of GW4869 on cellular cytokine levels in LPS-treated cells. The effect of GW4869 on cellular expression of pro-inflammatory cytokines IL-6 and TNF- α in LPS-activated macrophages was measured and normalized against 18S rRNA. Values in naïve RAW 264.7 cells without GW4869 and LPS treatment were set as unit. Values are mean \pm s.e.m. and $n = 3$.
- F, G Effect of siRNA-mediated downregulation of protein HuR on cellular expression of pro-inflammatory cytokines. In the left panel (F), effect of siRNA treatment on cellular cytokine mRNA levels in LPS-stimulated RAW 264.7 cells is shown. Relative levels measured against 18S rRNA are plotted. The effect of HuR depletion on cellular miR-155 content has been measured, and relative values normalized against U6 snRNA are plotted (right panel, F). The amount of let-7a bound to Ago2 after LPS stimulation in the presence and absence of siHuR has been calculated, and relative values have been normalized to immunoprecipitated Ago2 (G). Values are mean \pm s.e.m. and $n = 3$.
- H, I Effect of HuR expression on inflammatory responses in macrophage cells. Effect of ectopic expression of HuR on let-7a content of EVs in naïve macrophage cells (H, right panel). HA-HuR expression was checked by Western blot (H, left panel). The effect of HA-HuR expression on production of pro-inflammatory cytokine TNF- α in RAW 264.7 cells was measured. mRNA and protein level of TNF- α was quantified. Values obtained with pCIneo expression and without LPS treatment were taken as unit (I). Transfection was done either with pCIneo (control plasmid) of HA-HuR expression construct, and their effect on cellular pro-inflammatory cytokine mRNA levels in RAW64.7 cells was determined. Values in control set were taken as unit. Values are mean \pm s.e.m. and $n = 3$.
- J Effect of HA-HuR expression on p38-mediated activation of downstream signalling events. The levels of p-p38 and p-MSK1 and non-phosphorylated version of the p38 and MSK1/2 have been monitored by Western blotting done with cell extracts prepared from HA-HuR and control plasmid transfected, untreated and LPS-treated RAW 264.7 cells. β -Actin blot was used as loading control.
- K–M Downregulation of HuR in *Ld*-infected macrophages. HuR levels were monitored against time in *Ld*-infected primary macrophage cells (PEC) from BALB/c mice (K, upper left panel) as well as in *Ld*-infected RAW 264.7 cells (K, upper right panel). HuR levels were also monitored against time in *L. major*-infected RAW 264.7 cells (K, lower left panel) and *L. mexicana*-infected RAW 264.7 cells (K, lower right panel). Effect of proteasomal inhibitor MG132 treatment on HuR protein levels in control and 6 h of *Ld*-infected RAW 264.7 cells. In parallel assays, levels of pro-inflammatory cytokine TNF- α were measured in *Ld*-infected cells either with no treatment or pre-treated with MG132 (L). Values are mean \pm s.e.m. and $n = 3$. The isotonic cell lysates prepared from 6-h *Ld*-infected cells were analysed on an OptiPrep[®] density gradient, and HuR levels in individual fractions were determined. Input samples were monitored for HuR downregulation by Western blot. The presence of Alix (marker for early endosomes) and Calnexin (marker protein for ER) were used to confirm separation of organelles during density gradient fractionation. Loss of HuR from ER-associated fraction has been noted along with their reduction in total lysate after *Ld* infection (M upper panel). Densitometric analysis of individual fractions was done, and the respective values were plotted (M, lower panel).

Data information: HC: heavy chain. In all experimental data, ns: non-significant and *, ** and *** represent P -value of < 0.05 , < 0.01 and < 0.001 , respectively, calculated by Student's t -test. For statistical analysis, all experiments are done three times. Exact P -values against each experimental set are presented in the Appendix Table S2.

Positions of molecular weight markers are marked and shown in the Western blots used in different panels.

Source data are available online for this figure.

from naïve and activated macrophage did not differ significantly (Fig 5A, right panel). Interestingly, export of miRNA let-7a also got facilitated upon LPS exposure and was found to be HuR-associated (Fig 5B and C). Following the notion that the miRNA export from macrophage cells is responsible for elevated pro-inflammatory response, we noted decreased miRNA export and reduced expression of pro-inflammatory cytokine mRNAs in LPS-stimulated macrophages pre-treated with GW4869, the inhibitor of exosome-mediated miRNA export in mammalian cells [Fig 5D and E (Kosaka *et al*, 2010)]. We have also noted similar decrease in cytokine production upon LPS treatment in macrophages treated with siHuR compared to those treated with siCon. This was accompanied by increased cellular levels of miR-155 that HuR otherwise binds and facilitates its export from LPS-treated cells (Fig 5F). Interestingly let-7a uncoupling from Ago2 that happens in LPS-treated cells also got retarded in cells depleted for HuR (Fig 5G). In this context, miR-155 has been reported to target a TLR pathway adaptor protein Myd88 (Tang *et al*, 2010; Bandyopadhyay *et al*, 2014). Myd88 knock-down alters TNF- α , IL-1 β and IL-6 at various conditions suggesting a direct relation between miR-155 and cytokine production mediated by Myd88 (Morandini *et al*, 2013; Lin *et al*, 2015). This rather suggests EV-mediated export as a probable fate of the Ago2-decoupled miRNAs during early hours of LPS stimulation.

Ectopic expression of HuR does not have any major effect on Ago2 expression but increases EV-mediated miRNA export from cells expressing it (Fig 5H). Consistent with the idea of HuR-mediated miRNA export as the major mechanism for balancing inflammatory responses, HA-HuR expression in macrophage has been found to be both necessary and sufficient to cause elevated expression of pro-inflammatory cytokines such as TNF- α both at protein and RNA levels in macrophage cells (Fig 5I) and was accompanied by enhanced miRNA-Ago2 uncoupling noted in LPS-treated cells (unpublished data). However, ectopic expression of HuR did not show any major change in expression of cell signalling components that is known to get upregulated in macrophage upon LPS treatment (Fig 5J). This suggests, instead of a transcriptional surge governed by p38 MAPK-dependent activation of NF- κ B controlled pro-inflammatory cytokines, the stabilization of mRNAs due to export of repressive miRNAs by HuR could be necessary and sufficient for the observed pro-inflammatory response associated with HA-HuR expression. Therefore, HuR, here identified as an inducer of pro-inflammatory response, causes upregulation of pro-inflammatory cytokine mRNA levels possibly by facilitating export of cytokine repressor miRNAs. However, as certain cytokines also have AU-rich elements in their 3'-UTR, stabilization of these mRNAs by HuR may also contribute in a dual manner to the high levels of these mRNAs detected in HuR-expressing cells.

Leishmania downregulates HuR to ensure PP2A expression and anti-inflammatory response

The effect of HuR on cytokine mRNAs and miRNAs favours the pro-inflammatory response of the macrophage. It has been observed earlier that *Leishmania* affects the accumulation of miRNPs in the ER-associated fraction that cannot be exported out in *Ld*-infected cells (Chakrabarty & Bhattacharyya, 2017). On the other hand, during pro-inflammatory response, miRNAs are decoupled from Ago2 due to its phosphorylation and get exported out of the cells possibly in a HuR-dependent manner [(Mukherjee et al, 2016) Fig 5D and F]. The role of HuR is also evident on miRNA uncoupling from Ago2 (Mukherjee et al, 2016; Poria et al, 2016) and Fig 5G]. Therefore, the parasite could ensure a retarded miRNA export and poor pro-inflammatory response by targeting HuR.

To support this concept, we determined the expression status of probable HuR target mRNAs in *Ld*-infected human macrophages (Lebedeva et al, 2011; Mukherjee et al, 2011; Lu et al, 2014b). Certain HuR targets (56 mRNA) that could be upregulated on HuR knock-down were also found to be upregulated in *L. donovani*-infected human macrophages, and similarly, certain HuR targets (16 mRNA) that were found to be downregulated on HuR knock-down were also found to show reduced expression in *L. donovani*-infected isolated human macrophages (Appendix Table S1 and Fig S1).

To score the effect of *Ld* infection on cellular HuR levels, we performed a time course experiment with *Ld*-infected RAW 264.7 cells and followed HuR levels after *Ld* infection (Fig 5K). The HuR get cleaved in *Leishmania*-infected macrophage cells. *Leishmania major* and *L. mexicana* also showed HuR level reduction in PEC or RAW 264.7 cells upon infection. The decrease in HuR level could be blocked by inhibiting proteasome function by MG132 (Fig 5L upper panel). Blockage of proteasomal degradation of HuR also rescued the pro-inflammatory cytokine TNF- α level in *Ld*-infected RAW 264.7 cells (Fig 5L bottom panel). Interestingly, the majority of HuR was lost after 6 h of infection and the loss of HuR happens primarily from the endoplasmic reticulum (ER) and polysome attached fraction of *Ld*-infected cells (Fig 5M). Overall, these results suggest that the primary reason of HuR degradation in *Ld*-infected cells is to reduce pro-inflammatory cytokine production.

The degradation of HuR was also documented when RAW 264.7 cell lysate was incubated with *Ld* lysate (SLA) but that could be

blocked by Zn²⁺ chelator *ortho*-phenanthroline (OPT) (Fig EV3A). These data support the involvement of a *Leishmanial* Zn-metalloprotease in cleavage of HuR in infected cells. GP63 is the most prominent Zn-metalloprotease already identified for its role on cleavage of Dicer1 in *Ld*-exposed hepatocytes (Ghosh et al, 2013). We tested the purified GP63 and found it to target the cleavage of recombinant His-tagged HuR (data not shown) or cellular HA-HuR in RAW 264.7 cell lysate (Fig EV3B–D). This could be inhibited by Zn²⁺ chelator OPT (Fig EV3E). These data suggest that *Leishmanial* GP63 cleaves cellular HuR protein to ensure robust infection as well as downregulation of pro-inflammatory cytokine production in invaded macrophages. To make a direct relation of HuR cleavage and GP63 protein of *Ld*, we reconstituted liposomes with purified GP63 to treat RAW 264.7 cells to find that GP63 is sufficient to cause the degradation of HuR but not other proteins in GP63 liposome-treated cells (Fig EV3F–I). In multiple experiments, we detected HuR and known GP63 target Dicer1 to get downregulated without much change in β -actin level upon GP63-containing liposome treatment (Fig EV3I).

PP2A and HuR have common pathways to affect the immune response

Both in LPS-treated and in *Leishmania*-infected macrophage cells, PP2A and HuR expressions were regulated to control miRNA activity. During *Ld* infection, we have noticed increased production of PP2A. However, we observed a decrease in PP2A mRNA levels that could account for a decreased PP2A protein in HA-HuR-expressing cells (Fig 6A–C). In the infection context, the *Ld* infection induced upregulation of PP2A both at protein and mRNA levels (unpublished data) and enhanced the miRNA-mediated repression of pro-inflammatory cytokines. HuR, the negative regulator of PP2A, was noted to be downregulated by the pathogen, possibly to ensure robust anti-inflammatory response observed in infected macrophage cells. Therefore, it is likely that there are reciprocal ways of regulation on inflammatory response that both HuR and PP2A ensure by inversely regulating miRNP machineries targeting the pro-inflammatory cytokines in host cells. We have performed pathway analysis to identify probable regulatory mechanisms between HuR and PP2A (PPP2CA) and determined the common targets that both HuR and PP2A regulate in mammalian cells. Herein, we could identify that

Figure 6. Inverse regulation of pro-inflammatory pathways by miRNA regulators HuR (ELAVL1) and PP2A (PPP2CA) in mammalian macrophage cells.

- A–C Interaction routes between HuR (ELAVL1) and its target gene PP2A (PPP2CA). Alternate mechanism or regulatory steps that could be involved in establishing the regulatory relationship between HuR (ELAVL1) and its target genes have been investigated. A brief outline of possible alternate routes of regulation between HuR (ELAVL1) and PP2A (PPP2CA) via intermediates at the protein–protein interaction, cellular signalling or by miRNA has been outlined in panel A. In panels B and C, effect of HA-HuR expression on PP2A both at protein and RNA levels was scored. Values are mean \pm s.e.m. and $n = 3$.
- D–F Expression profiles of HuR, PP2A and miRNA let-7a are connected to IL-6 expression in RAW 264.7 cells. Data obtained from experiments described in previous figures are summed up to plot the changes in IL-6 mRNA levels against time of LPS treatment along with changes in PP2A, miRNA let-7a and HuR (D). Change in expression of IL-6 is connected to changes in let-7a concentration. The mathematical equation fitting the curve is shown here. Y represents concentration of IL-6, and X represents miRNA let-7a concentration. A1 is the initial IL-6 levels, and A2 is the changed level. LogX0 is the mid-point of value 0.34, a concentration of let-7a where IL-6 expression is reduced to half (E). The variations of IL-6 expression with the altered level of PP2A (black) and HuR (red). For both cases, the data were fitted to an equation, which is shown above. The parameter m denotes the expression level of PP2A/HuR which corresponds to the maximum IL-6 expression; w denotes the width of the distributions for both cases. For PP2A and HuR, the values of m were found to be 0.6 and 0.9, respectively, and A is a constant (F).

Data information: In all experimental data, ns: non-significant and * and ** represent P-value of < 0.05 and < 0.01 , respectively, calculated by Student's t -test. Exact P-values against each experimental set are presented in the Appendix Table S2. Positions of molecular weight markers are marked and shown in the Western blots used in different panels.

Source data are available online for this figure.

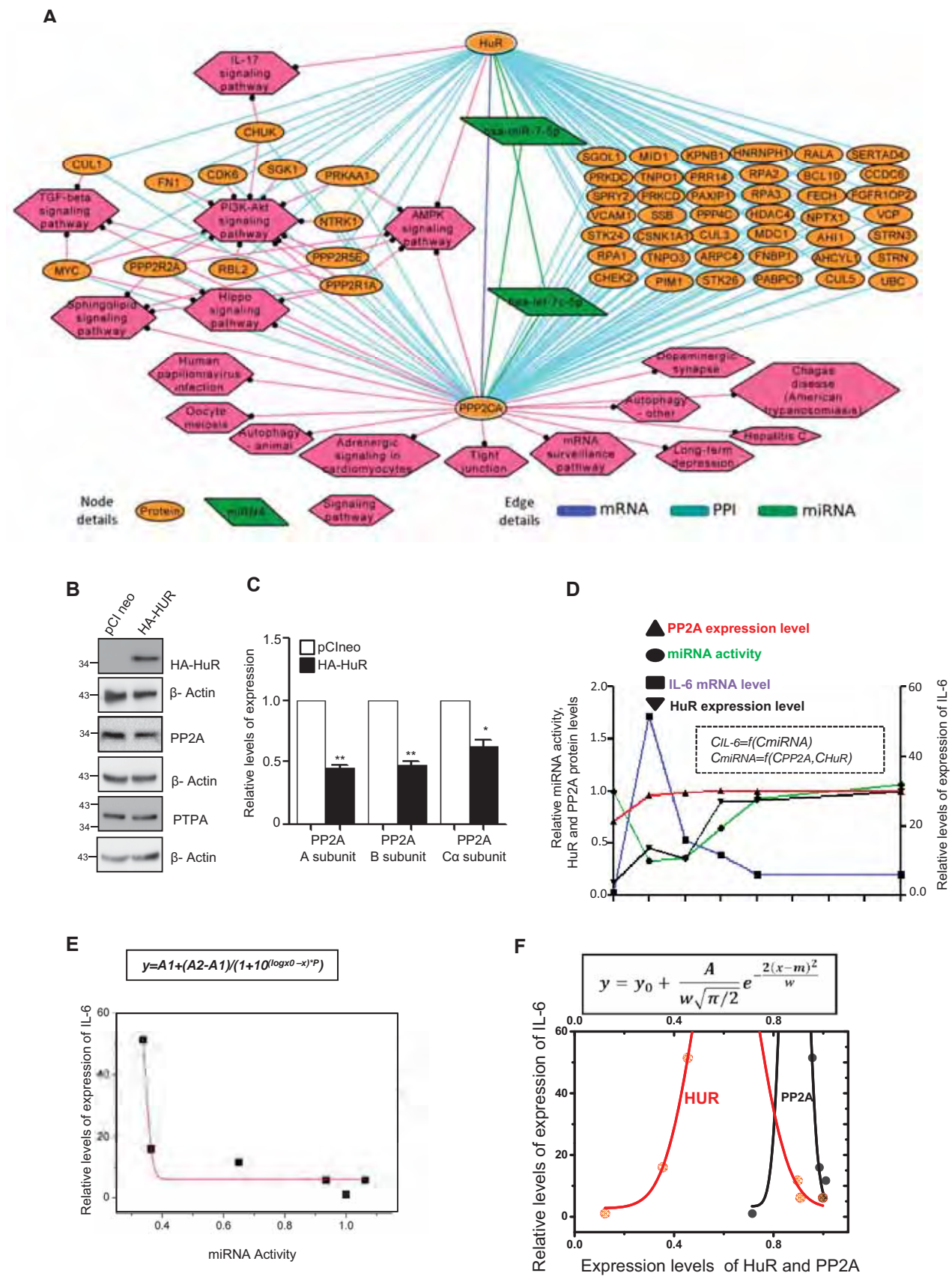


Figure 6.

PP2A (PPP2CA) is directly regulated by HuR at the mRNA level and indirectly regulated via multiple miRNAs (Fig 6A). Further, PP2A (PPP2CA) and HuR (ELAVL1) are commonly involved in regulating inflammatory responses in immune cells.

Using a candidate approach to verify this relation, we plotted the expression level changes of IL-6 mRNA, an important cytokine that is expressed in activated macrophage and regulated by let-7a miRNA (Mazumder *et al*, 2013), and followed the changes in its level in LPS-activated macrophage over time along with changes in miRNA let-7a (known to target IL-6), HuR and PP2A. Both HuR and PP2A control miRNA activity reciprocally and hence should influence the IL-6 expression level inversely (Fig 6D). IL-6 mRNA and miRNA let-7a were found to be in an inverse relationship. Relative changes in IL-6 mRNA levels are linked to let-7a activity as evident in the curve obtained, and the changes in their expression levels are depicted by the equation noted in Fig 6E. By connecting the LPS-mediated changes in IL-6 levels against concentration of PP2A and HuR, we have identified the unique relationship between HuR and PP2A. Mathematical modelling and curve fitting for IL-6 mRNA levels were done in LPS-stimulated macrophages. The equation fitting the data can explain the changes of IL-6 expression as a function of HuR and PP2A concentrations that resulted in a biphasic pattern of IL-6 regulation (Fig 6F). At lower concentration levels, a fluctuation of HuR can influence the IL-6 mRNA level prominently while at a higher concentration PP2A dominates over HuR to control IL-6 mRNA levels. It suggests a mutually exclusive effect of HuR and PP2A on IL-6 cytokine expression which is possibly governed by the action of these proteins on cellular miRNPs (Fig 6D–F).

HuR can counter PP2A-mediated anti-inflammatory response in *Ld*-infected cells and rescue infection *in vivo*

In the subsequent experiments, we have tested the importance of this biphasic regulation of cytokine expression by HuR and PP2A via miRNPs. As HuR is getting targeted during *Ld* infection, we were interested to test the effect of restoration of HuR expression on *Ld* infection. The number of internalized parasites in HA-HuR-positive cells was notably low compared to the neighbouring macrophage cells not expressing HA-HuR (Fig 7A and B). With HA-HuR expression, we also noted increased expression of TNF- α and IL-1 β and reduced expression of IL-10 in HA-HuR-expressing RAW 264.7 cells (Fig 7C). We wanted to see the effect of ectopic expression of HA-HuR on levels of infection *in vivo*. In infected mouse liver also, the level of HuR drops upon infection similar to what was observed in RAW 264.7 cells upon *Ld* infection (Figs 7D and 5K). Similar drop of HuR level in mouse liver could be documented in animals injected with liposomes containing leishmanial GP63 protein (Fig 7E). However, upon the tail vein injection of HA-HuR expression plasmid in infected animals, the expression levels of cytokines IL-10 dropped while the TNF- α expression had increased in liver, and interestingly, infection levels measured by *Ld* kinetoplastid DNA content dropped in mouse liver (Fig 7F–I). No detectable HA-HuR expression was noted in spleen of animals injected with HA-HuR plasmid through tail vein injection. Incidentally, no change in pro-inflammatory cytokine TNF- α could also be detected in spleen (Fig 7J and K). This was of no surprise as tail vein injection route is primarily used to express plasmid encoding genes predominantly in liver tissue (Ghosh *et al*, 2013).

Robust effect of drug-resistant *Leishmania Ld^R* on host PP2A expression can be reversed by simultaneous expression of HuR protein and PP2A inhibition

To combat visceral leishmaniasis or *kala-azar*, organic pentavalent antimonials were introduced in the Indian subcontinent almost nine decades ago with dramatic clinical success (Brahmachari, 1922). However, with time, resistance to the drug developed in Bihar, India, that leads to cessation of its further use in the Indian subcontinent. The antimonial drug-resistant form of the *Ld* parasite (*Ld^R*) is known for increased IL-10 production upon infection. This is also coupled with stronger reduction of pro-inflammatory cytokine production in the host (Mukherjee *et al*, 2013). Overall, the antimony-resistant *Ld* constitutes a unique example and a model of drug-resistant pathogens with traits of increased fitness and aggressive infection (Mukhopadhyay *et al*, 2015). We used one such strain BHU569 (Mukhopadhyay *et al*, 2011) to test the effect of *Ld^R* on the production of HuR and PP2A in RAW 264.7 cells.

Compared to drug-sensitive (*Ld^S*) Ag83 strain of *Ld*, the drug-resistant BHU 569 strain (*Ld^R*) showed increased IL-10 expression with low TNF- α expression and strong induction of ERK phosphorylation in host cells. It also showed increased drug resistance-associated protein MDR1 expression in RAW 264.7 cells (Fig 8A–D). We also noticed that *Ld^R* had an equivalent effect on HuR and a stronger effect on PP2A levels compared to control drug-sensitive *Ld^S* Ag83 strain (Fig 8E). Interestingly, unlike what happened to *Ld^S* Ag83 strain, HA-HuR expression in RAW 264.7 cells had no effect on internalized parasite number or expression of pro-inflammatory cytokines upon infection with *Ld^R* BHU569 strain (Fig EV4). This suggests a strong anti-inflammatory response that *Ld^R* raises in RAW 264.7 cells is possibly due to high PP2A expression. The high PP2A effect cannot be counteracted alone by expression of the pro-inflammatory response inducer HuR. However, the mild effect of blockage of PP2A activity by OA on increased IL-1 β and TNF- α expression was augmented by the ectopic expression of pro-inflammatory immune response stimulator protein HA-HuR in *Ld^R* BHU569-infected cells (Fig 8F). This also holds true in mouse model of infection with *Ld^R*. In BALB/c mice infected with *Ld^R*, we detected no change in internalized parasite number or cytokine expression in mouse liver by either HuR expression or PP2A inhibition alone. However, like in *ex vivo* experiments simultaneous targeting of pro-inflammatory pathway by HuR expression and PP2A inhibition increased pro-inflammatory response significantly and ensured clearance of *Ld^R* from infected mice liver (Fig 8G–I). During *Ld^R* infection, the balance should have shifted to anti-inflammatory pathways due to HuR lowering and PP2A upregulation (Fig 8J). However, the reciprocal action of HuR and PP2A in mammalian macrophages in regulation of immune response through their action on miRNP machineries could be utilized to cure infection by *Ld^R* when both pathways are targeted.

Discussion

The expression of cytokines determines the activation status of a macrophage, and the expression of pro-inflammatory cytokines like IL-1 β , TNF- α or IL-6 signifies the pro-inflammatory activation state

of the macrophage, whereas increased expression of IL-10 signifies the anti-inflammatory state of the cells. Switching to anti-inflammatory pathway is dominated by suppression of pro-inflammatory cytokine production both at pre- and post-transcriptional stages

(Mosser & Edwards, 2008). The repressive action of miRNAs that targets the pro-inflammatory cytokine encoding mRNAs is considered as the prerequisite for the switching to anti-inflammatory stage (Squadrito et al, 2013).

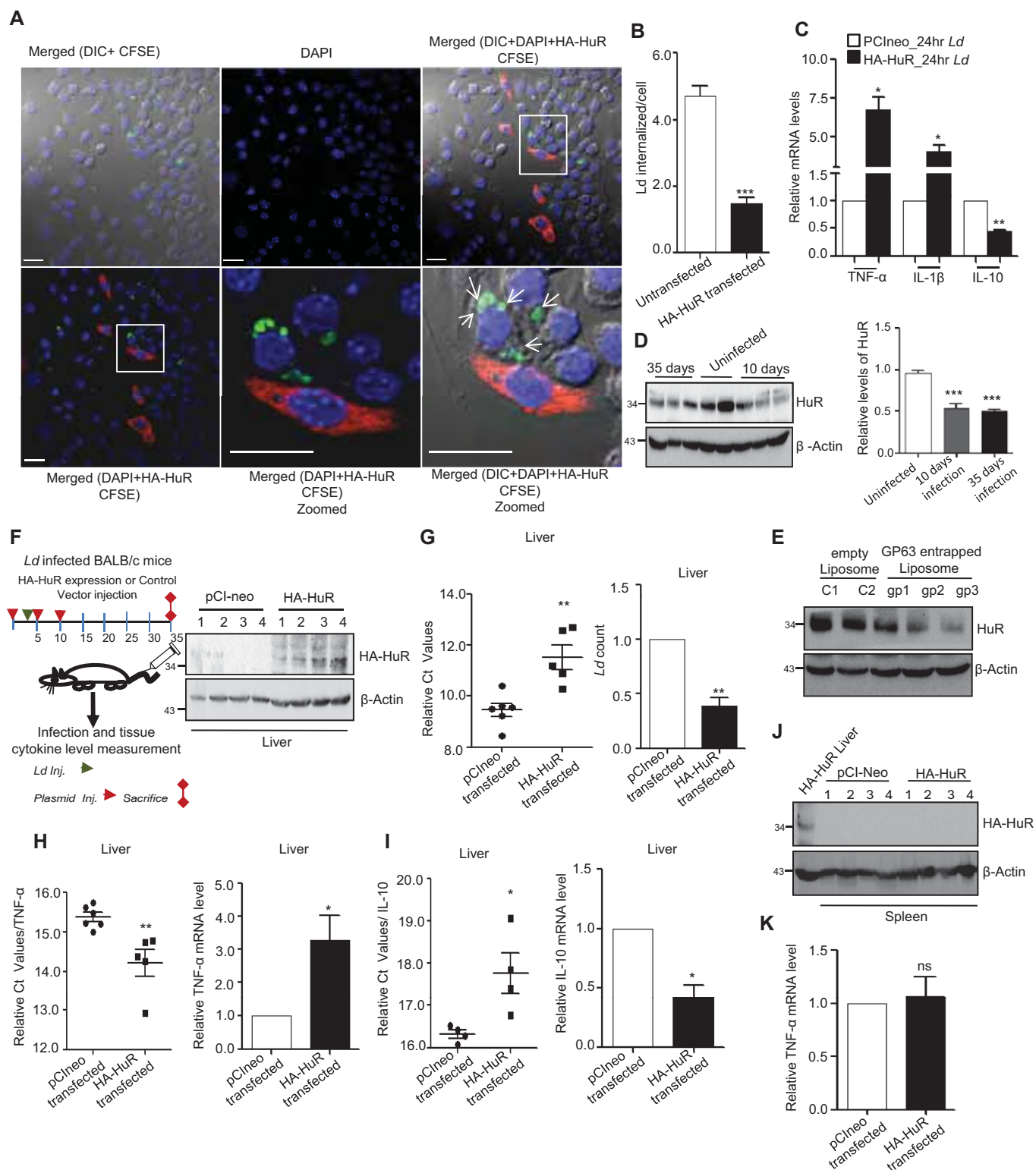


Figure 7.

Figure 7. *Leishmania donovani* infection could be counteracted by ectopic expression of HuR.

- A–C Effect of HA-HuR expression on *Ld* infection of RAW 264.7 cells. Effect of HuR expression on internalized parasite number and cytokine expression in RAW 264.7 cells. HA-HuR was transfected to RAW 264.7 cells, and infection was given for 24 h at a host to parasite 1:10 ratio. *Ld* was stained with CFSE dye, and parasite internalization was detected by counting the CFSE-positive structures inside the cells. HA-HuR was immunostained with anti-HA antibody and detected by secondary antibody tagged with Alexa[®]564 (A). Zoomed part of the merged picture are used to show the internalized parasite. Internalized parasites present in HA-HuR-positive cells were counted and compared against untransfected cells without HA-HuR expression (B). Levels of expression of different cytokines are measured in control or HA-HuR-expressing RAW 264.7 cells infected with *Ld* (C). Scale bar 20 μ m. Values are mean \pm s.e.m. and $n = 3$.
- D, E Effect of *Ld* infection on the HuR expression in mouse liver. BALB/c mice of 6 weeks of age were infected with *Ld* via cardiac puncture. Animals were sacrificed after subsequent days; protein was extracted from liver tissue followed by Western blot analysis for HuR. β -Actin was used as loading control (D, left panel). Each lane have extracts of livers from individual animal. In each case, HuR level was normalized by respective β -Actin bands (D, right panel mean \pm s.e.m., $n = 5$). Animals were injected with GP63-containing liposome (gp1–3) or empty liposome (C1–2), and after 24 h of injection, HuR level was checked against β -Actin used as loading control (E).
- F–I Effect of expression of HA-HuR on *Ld* infection in mice liver. Scheme for animal experiments done by expressing HA-HuR in mouse liver is shown. HA-HuR level was detected in the liver tissue by Western blot analysis using anti-HA antibody (F). Parasite load in liver tissues was estimated by measuring *Ld* DNA in infected tissue using specific primer for *Ld* minicircle kDNA. Values are mean \pm s.e.m. and $n = 5$ (G). TNF- α (values are mean \pm s.e.m. and $n = 5$) and IL-10 (values are mean \pm s.e.m. and $n = 4$) mRNA levels were checked from RNA isolated from liver tissues, and 18S rRNA normalized C_t values were plotted (H and I, left panels). Relative fold change was calculated by $\Delta\Delta C_t$ method and the values plotted for *Ld* count, TNF- α and IL-10 mRNA levels [G mean \pm s.e.m. ($n = 5$), H mean \pm s.e.m. ($n = 6$) and I mean \pm s.e.m. ($n = 4$), right panel].
- J, K Effect of HA-HuR plasmid tail vein injection on mice spleen. Levels of HA-HuR were undetectable in mice spleen after HA-HuR expression plasmid was injected. Sample from one liver tissue of HA-HuR injected group was used as a positive control of HA-HuR expression in mouse liver after tail vein injection of HuR encoding plasmid (J). Simultaneously, TNF- α mRNA levels were checked in spleen total RNA (K). Values are mean \pm s.e.m. and $n = 4$.

Data information: In all experimental data, ns: non-significant and *, ** and *** represent P -value of < 0.05 , < 0.01 and < 0.001 , respectively, calculated by using Student's t -test. For statistical analysis, all experiments are done three times. Exact P -values against each experimental set are presented in the Appendix Table S2. Positions of molecular weight markers are marked and shown in the Western blots used in different panels. Source data are available online for this figure.

miRNA-mediated regulation controls varieties of genes including several cytokine encoding genes (Palanisamy *et al*, 2012). It has also been observed that reversible uncoupling of miRNA from Ago2 ensures switching of miRNA activity in mammalian cells (Mazumder *et al*, 2013; Patranabis & Bhattacharyya, 2016). It has also been noted that *Ld* infection controls expression of several miRNAs including those that act as repressor of pro-inflammatory cytokine mRNAs (Chakrabarty & Bhattacharyya, 2017). In infected cells, a general increase in miRNA stability was observed and increased miRNAs were found to be associated with the ER attached fraction. The increased stability of miRNAs can be attributed to decreased miRNA export. HuR is known to be involved in exosome-mediated export of miRNAs. In cells, infected with *Ld*, we noted a decrease in HuR levels. However, the role of PP2A is important also in *Ld*-infected macrophage where its high expression ensures restriction of Ago2 in its dephosphorylated and miRNA-bound form. HuR expression is both necessary for unbinding of miRNAs and their extracellular export. The pathogens which reside within the macrophage tame the pro-inflammatory response and achieved this by targeting pro-inflammatory cytokine mRNA production both at pre- and post-transcriptional level. It has been reported earlier that induction of PP2A phosphatase is required for inactivation of p38/MAPK pathways, and thus, PP2A prevents not only the expression of pro-inflammatory cytokine mRNAs at transcriptional levels by targeting NF- κ B pathway and related signalling events (Kar *et al*, 2010) but also it helps to keep Ago2 in its dephosphorylated miRNA-bound active form to repress the existing mRNAs. In this process, inactivation of p38 pathways possibly ensures the down-regulation of nucleocytoplasmic shuttling of HuR shown to be essential for HuR action on its targets (Tiedje *et al*, 2012) and to restrict subsequent miRNA turnover and export by cytoplasmic HuR. Opposite event happens during LPS activation phase where the cytoplasmic HuR promotes the export of miRNAs and ensures the miRNA recycling prerequisite for restoration of miRNA-mediated

repression of excess cytokine mRNAs otherwise detrimental for activated macrophage cells. HuR has a negative role on PP2A mRNA expression and as expected should be useful to downregulate PP2A expression to ensure maximum activation of macrophage during LPS exposure. However, the HuR-mediated downregulation mechanism of PP2A is not clear. On the contrary, PP2A level increases during late phase of LPS activation, and thus, it can be concluded that PP2A may dominate over HuR during late phase of activation. This is also supported by the mathematical model of macrophage activation. However, HuR gets downregulated during *Ld* invasion of macrophage. This possibly ensures a robust downregulation of pro-inflammatory response associated with *Ld* infection.

From the mechanistic angle, the contribution of subcellular structures and compartments involved in immune response of *Ld* invaded macrophages is an underexplored question, and it is not clear why the majority of miRNPs are usually associated with ER while the PP2A and phosphorylated Ago2 get accumulated in endosomal membrane (Patranabis & Bhattacharyya, 2016; Chakrabarty & Bhattacharyya, 2017). Perhaps, by ensuring compartmentalization of miRNA loading and miRNP phosphorylation to ER and endosomes, respectively, the spatio-temporal control of macrophage activation process is achieved to ensure a robust regulation at post-translational level.

In the context of infection by drug-resistant pathogen, these findings have some direct implications. Interestingly, 78% of the recent clinical isolate of *L. donovani* (*Ld*) from endemic zone of Bihar show resistance to organic pentavalent antimonials (Mukhopadhyay *et al*, 2011). The resistant parasite (*Ld^R*) induces production of disease-promoting cytokines like IL-10 from macrophages (Mukherjee *et al*, 2013). It also upregulates multidrug resistance-associated protein-1 (MDR-1) in infected macrophages (Mukherjee *et al*, 2013). These attributes are essentially absent when macrophages are infected with antimony-sensitive *Ld* parasites (*Ld^S*). The mechanism by which *Ld^R* induce aggressive infection is not clearly known. *Ld^R* upregulates miR-466i in macrophages that binds to 3'-UTR causing

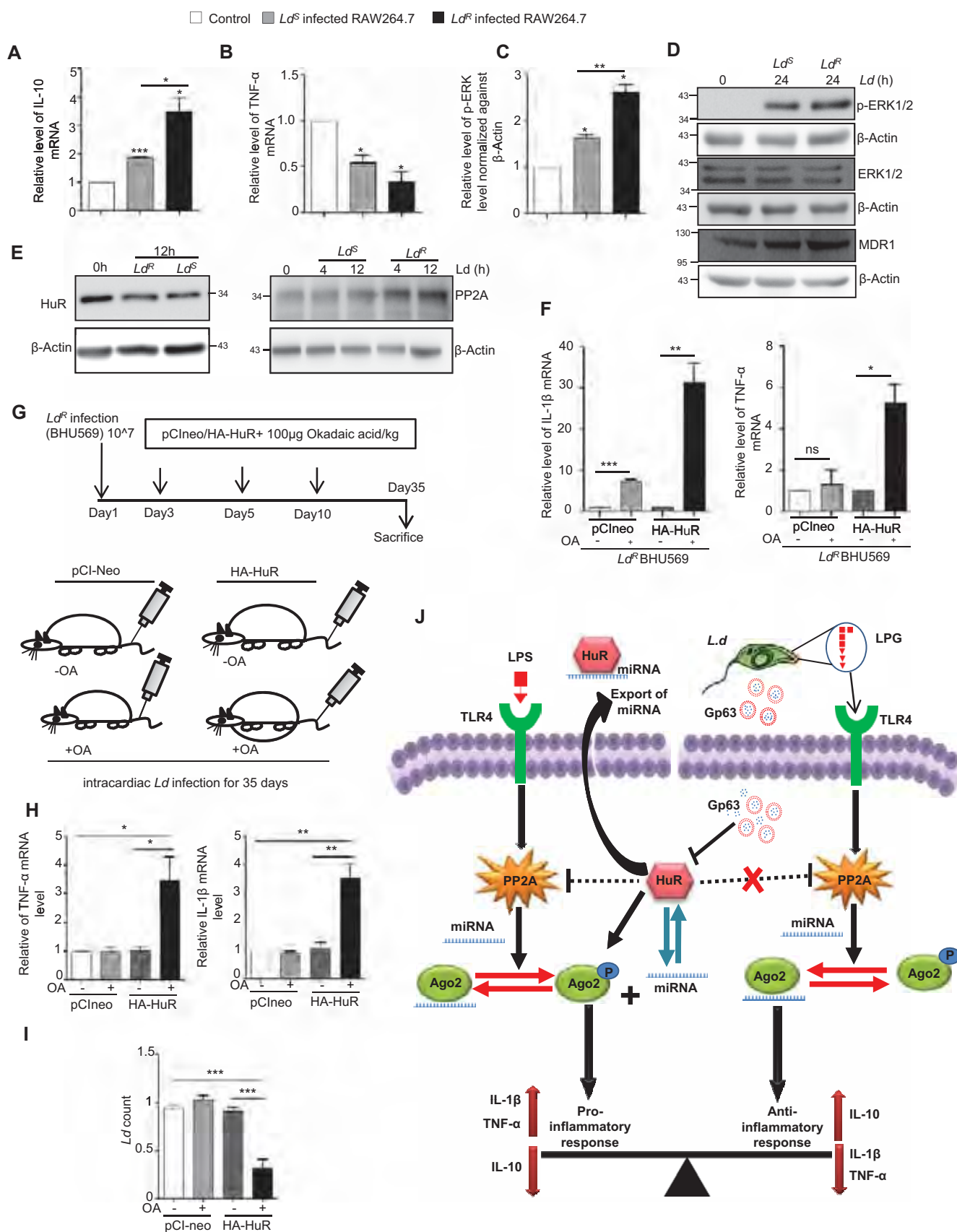


Figure 8.

Figure 8. Requirement of simultaneous activation of HuR and deactivation of PP2A driven processes in mammalian macrophage to prevent infection by antimonial drug-resistant *Leishmania* parasite.

- A–D Effect of antimonial drug-resistant and drug-sensitive forms of the *Ld* (Ld^R and Ld^S) on cellular cytokine levels as well as on phospho-ERK and MDR1 levels. RAW 264.7 cells were infected with antimony-sensitive (Ld^S -Ag83) and antimony-resistant (Ld^R -BHU569) form of *Ld* for 24 h along with uninfected cells kept as control. IL-10 (A) and TNF- α (B) were measured at mRNA level by qRT-PCR after infection (mean \pm s.e.m. and $n = 4$). p-ERK, ERK and MDR1 levels were also measured by Western blot (D). Densitometry analysis was done for p-ERK level by ImageJ, and relative values were plotted (C). β -Actin was used as loading control. Values are mean \pm s.e.m. and $n = 3$.
- E Effect of antimony-sensitive and antimony-resistant form of the *Ld* on HuR and PP2A. RAW 264.7 cells were infected with Ld^S and Ld^R for 12 h, and HuR level was measured by Western blot (left panel). PP2A level was also measured by Western blot after 4 h and 12 h of Ld^S and Ld^R infection (right panel). β -Actin was used as loading control.
- F Effect of ectopic expression of HuR and PP2A inhibitor OA treatment on Ld^R infection of macrophage cell. RAW 264.7 cells were transfected with HA-HuR or pCIneo followed by 2 h of pre-treatment with OA. These cells were then infected with Ld^R for 24 h. Pro-inflammatory cytokines TNF- α (right panel; mean \pm s.e.m., $n = 3$) and IL-1 β (left panel; mean \pm s.e.m. and $n = 4$) were measured at mRNA level, and relative values are plotted. Values without OA treatment were set as control.
- G–I Effect of HuR over expression on Ld^R infection in mice liver. A scheme for animal experiment done with Ld^R infection followed by HA-HuR expression and OA treatment is shown (G). Pro-inflammatory cytokines TNF- α (left panel) and IL-1 β (right panel) levels were measured at mRNA level in liver (H). Parasite load was measured in infected liver tissue by using specific primer against kinetoplastid minicircle DNA of *Ld* (I). Values are mean \pm s.e.m. and $n = 6$.
- J The model depicts inter-regulatory balance between PP2A and HuR in controlling pro-inflammatory and anti-inflammatory response by altering Ago2 phosphorylation–dephosphorylation cycle and exosomal export of miRNAs in mammalian macrophage cells. Left half of the model shows lipopolysaccharide (LPS)-induced PP2A upregulation via TLR4 pathway during late hours of treatment which results in Ago2 dephosphorylation. Right half of the scheme represents *Leishmania*-induced PP2A increase mediated by membrane glycolipid lipophosphoglycan (LPG). Interestingly, the RNA binding protein HuR plays a central role in both the contexts. Inhibitory effect of HuR on PP2A ensures phosphorylated form of Ago2 to dominate which in turn facilitates miRNA unbinding to Ago2 and miRNA export via exosome thereby promoting pro-inflammatory cytokine response. On the contrary, *Ld* induced downregulation of HuR via a zinc-metalloprotease, GP63 which results in PP2A upregulation that facilitates anti-inflammatory response necessary for the parasite survival and proliferation.

Data information: In all experimental data, ns: non-significant and *, ** and *** represent P -value of < 0.05 , < 0.01 and < 0.001 , respectively, quantified by using Student's t -test. For statistical analysis, all experiments are done three times. Exact P -values against each experimental set are presented in the Appendix Table S2. Positions of molecular weight markers are marked and shown in the Western blots used in different panels. Source data are available online for this figure.

downregulation of MyD88 and resulting in elevated IL-10/IL-12 ratio (Mukherjee et al, 2015). This elevated IL-10 over IL-12 may cause aggressive pathology in BALB/c mice when infected with Ld^R as compared to sensitive counterpart. It is also known that Ld^R attenuates the therapeutic efficacy of antimonials by inhibiting dendritic cells, the key regulators of anti-leishmanial immune responses (Hal-dar et al, 2010). Drug resistance represents one of the main problems for the use of chemotherapy to treat leishmaniasis. Additionally, it could provide some advantages to *Leishmania* parasites, such as a higher capacity to survive in stress conditions. Further to this, intracellular amastigotes from resistant lines present a higher capacity to survive inside the macrophages than those of the control line. Our results suggest that resistant parasites acquire an overall fitness increase than the sensitive counterpart (Roy et al, 2014) and that can be reversed by changing the balance of pro-over anti-inflammatory response controlled by miRNPs and its modulators HuR and PP2A.

The drug-resistant BHU569 strain used in this work is one of the clinical isolates previously characterized in terms of their sensitivity towards anti-leishmanial drug sodium stibogluconate (SSG) in macrophage culture system by Mukhopadhyay et al (2011). Also, they had studied a series of genes related to SSG transport in the parasites itself. The resistant parasites were shown to overexpress MRPA gene higher than the sensitive one along with the higher expression of an unique terminal glycoconjugate *N*-acetyl-D-galactosaminyl on cell membrane of resistant parasites. Higher IL-10 production and higher level of MDR1 expression in macrophages infected with of Ld^R strain comparative to the Ld^S strains were also reported by them (Mukhopadhyay et al, 2011).

Later, the same group revealed the molecular mechanism behind higher IL-10 production and MDR1 expression in case of resistant strain infection which showed that the terminal glycoconjugate

interacts with TLR2/6 which resulted in more IL-10 production via upregulation of phospho-ERK level than the sensitive one (Ag83). The higher MDR1 expression was found to be IL-10-driven (Mukherjee et al, 2013).

Here, our observation reveals that the BHU569 strain can produce more IL-10 upon infection via ERK1/2 pathway by higher upregulation of phospho-ERK1/2 level than the sensitive Ag83 strain. In this work, we have found Ld^R infection to trigger PP2A level more than that in the Ld^S strain. It also produces more IL-10. However, no direct relation has been found between higher IL-10 production and higher PP2A level. One such work reported previously in case of experimentally generated paromomycin-resistant *L. donovani* increased level of MRPA, MDR1 and PP2A was found in the resistant parasites than their sensitive counterparts along with increased IL-10 production upon infection (Bhandari et al, 2014). Other groups have reported that a protein Tyrosine phosphatase PTPN3 gene expression increases in cisplatin and doxorubicin-resistant ovarian cancer cells (Li et al, 2016). All these previous reports suggest that somehow protein phosphatases are involved in drug resistance phenomenon.

Our observation reveals higher expression of IL-10 and MDR1 along with PP2A upon Ld^R infection. Hence correlating with previous reports, it can be assumed that PP2A might be involved in regulation of MDR1 expression and responsible for their increased pathogenicity and drug resistance phenomenon of these antimony resistance parasites. However, our unpublished data indicate similar increase in PP2A in macrophage upon infection with another Ld^R strain, and blockage of ERK pathway by chemical inhibitor could retard the PP2A expression in infected cells. This suggests importance of ERK signalling in PP2A expression.

HuR is primarily known to associate with specific upstream/downstream sequences of target mRNAs, for instance, U/AU-rich

sequences either at 3'-untranslated regions (UTRs) or within pre-mRNA introns (Srikantan & Gorospe, 2011). Since RNA-HuR interactions have been extensively characterized in PAR-CLIP analysis considering HeLa or HEK293 cells in previous works (Lebedeva *et al*, 2011; Mukherjee *et al*, 2011), we have utilized the data provided to generate a list of HuR target mRNAs that may be regulated also in macrophages. During *Ld* infection, HuR expression goes down. Hence, the underlying assumption was that as the binding sites of the target genes would be present in the macrophage cell mRNA as well, HuR-mediated regulation of target genes' expression would also be altered during *Ld* infection. Subsequently, by determining whether any of the probable HuR targets are differentially expressed when human macrophages are infected with *Ld*, we could predict 165 likely mRNA targets of HuR that may have a role in macrophages in *Ld* infection scenario. Additionally, considering RNAseq profile of mRNA from HuR (*Elavl1*) knockout murine bone marrow-derived macrophages (Lu *et al*, 2014a) described in the GEO dataset (GSE63199), we could observe that 129 among the previously predicted 165 targets show differences in their expression profile under these conditions as well.

Mechanism by which pro-inflammatory cytokine mRNA expression was upregulated by HuR is not entirely clear. While due to defined AU-rich HuR binding site of TNF- α mRNA can account for its stabilization and expression against miRNA-mediated repression, the situations with other pro-inflammatory factor are elusive. Interesting work by other groups has shown previously that HuR regulates TNF- α -induced IL-6 production by stabilizing IL-6 mRNA that otherwise gets negatively regulated by another RNA binding protein TTP (Shi *et al*, 2012). Consistent with this finding, other groups have reported LPS-induced p38 pathway mediates phosphorylation of TTP which alters its inhibitory effect on IL-1 β mRNA levels (Chen *et al*, 2006; Neuder *et al*, 2009). IL-1 β also has binding sites for HuR; thus, HuR directly also can influence its expression. IL-10 mRNA expression was undetectable in HA-HuR-expressing cells, and thus, we could not comment on that.

The immunogenic properties of the EV are dependent on the cargos they carry. The immunostimulatory role has already been reported for liver-specific miR-122 that can be transferred via EVs to neighbouring macrophage cells to get them stimulated (Saha *et al*, 2018; Xu *et al*, 2018). Similar to what has been described in our previous paper where role of HuR in enhancing EV-mediated export of miR-122 has been described, we can attribute a role of HuR in contributing the inflammatory response propagation in that context (Basu & Bhattacharyya, 2014; Mukherjee *et al*, 2016). Therefore, the effect could be very much contextual. In macrophage, HuR by exporting out repressive let-7a or similar miRNAs during early phase of LPS stimulation allows pro-inflammatory cytokines to get expressed and thus ensures pro-inflammatory response to set in HuR-expressing cells. Interestingly, miR-155, a pro-inflammatory miRNA (Squadruto *et al*, 2013), also get exported out from macrophage expressing HuR. This pro-inflammatory signal is communicated to neighbouring naive macrophages to get them stimulated via a secondary pathway. Therefore, the data are not inconsistent with previously published data rather in line with the findings by us and others on both pro- and anti-inflammatory role of EVs. It could be determined by the cargos they carry.

Interestingly, the findings described in this manuscript suggest that the balance of anti- and pro-inflammatory responses is

delicately achieved via miRNA-mediated regulation and by targeting the miRNA modulators, in this case HuR and PP2A. One can arbitrate the immunological response of host macrophage to control parasite infection. This should hold true for other context like in tumour microenvironment or in auto-immune complications where pro- and anti-inflammatory behaviours of the immune cells are context-dependent and may also be regulated in similar manners by separate sets of miRNA modulators and HuR-like factors.

Materials and Methods

Chemicals and plasmid constructs

The macrophage cells were stimulated with 1 ng/ml *Escherichia coli* O111:B4 LPS (Calbiochem, La Jolla, CA). For PP2A-specific inhibition, 100 nM okadaic acid (Calbiochem, CA) was used. Exosome secretion blocker GW4869 (Calbiochem, CA) was used at 10 μ M concentration. Plasmid information about pRL-con and pRL-3XBulge-Let7a was published previously (Pillai *et al*, 2005) and was a kind gift from Witold Filipowicz. HA-HuR-expressing plasmid was obtained from Witold Filipowicz which was cloned into pCIneo backbone and described previously (Kundu *et al*, 2012). FH-Ago2 and FH-Ago2Y529F were obtained as kind gifts from Gunter Meister. Tet-inducible precursor miR-122 was cloned in pTRE-tight-BI vector (Clontech) and described in previous report (Ghosh *et al*, 2015). All siRNAs were purchased from Dharmacon Inc. (On Target Plus siRNAs).

Cell culture and reagents

RAW 264.7 cells were grown in RPMI 1640 medium (Gibco) supplemented with 2 mM L-glutamine, 0.5% β -mercaptoethanol, 1% Pen-strep (Gibco) and 10% heat-inactivated foetal calf serum (complete media). The cell line was obtained from ATCC.

Peritoneal exudate cells (PEC) of BALB/c mice were elicited by 4% starch injected in the mouse peritoneal cavity, and 24 h after starch boost, mice were sacrificed, skin was carefully removed, and peritoneal lavage containing the PEC was extracted with cold 1 \times PBS. Cells were spin down and resuspended in complete RPMI media. All experiments were done after 48 h of cell isolation. PEC was isolated from adult BALB/c mice from any sex.

For macrophage activation, 1 ng/ml LPS was used. For all okadaic acid (OA) treatment experiments, 100 nm OA was used to pre-treat the cells for 2 h before further treatment either with LPS or infection.

Parasite infection of macrophage cells

Leishmania donovani strain AG83 (MAOM/IN/1083/AG83) was originally obtained from an Indian visceral leishmaniasis ("kala-azar") patient and maintained in golden hamster. To infect RAW 264.7 cells, 2nd–4th passage cultures of *Ld* promastigotes were used in 10:1 ratio for all experiments to infect RAW 264.7 or PEC. Sodium stibogluconate-resistant clinical isolate of *Ld* strain MHOM/IN/09/BHU569/0 was also maintained by similar method.

Stationary phase *L. major* (Friedlin strain) and *L. mexicana* (M379) parasites from 3rd to 5th passage were maintained in M199

media supplemented with 10% FBS (Gibco) and 1% Pen-strep solution (Gibco). Infection was given to the RAW 264.7 cells at 1:10 host:parasite ratio. *Leishmania major* was maintained by infecting hamster footpad with 10^7 parasites; thereby, amastigotes were isolated from footpad after 6–8 weeks of infection.

Cell transfection

For luciferase assay, 25 ng of RL reporters and 400 ng of FF reporters were transfected using Lipofectamine 2000 following manufacturer's protocol in 12-well format. Transfection of HA-HuR, pCIneo and FH-Ago2 plasmids was transfected by Eugene HD (Promega) in 1:5 ratio (μg of DNA: μl of Eugene HD). For co-transfection of siRNA and plasmids, Lipofectamine 2000 was used.

Immunoprecipitation

For immunoprecipitation, protein G agarose beads (Life technologies) for endogenous Ago2 or FLAG-M2 agarose beads (Sigma) for exogenous FLAG-tagged Ago2 were washed with $1\times$ IP buffer (20 mM Tris-HCl, pH7.5; 150 mM KCl, 1 mM MgCl_2). For endogenous Ago2, beads were blocked with 5% BSA in lysis buffer ($1\times$ IP buffer with 0.5% Triton X-100) for 1 h before antibody addition (1:50 dilution) for overnight at 4°C . Cells were lysed in $1\times$ lysis buffer for 30 min at 4°C followed by 10-s sonication for three times with 5-min incubation on ice in between. Lysate was pre-cleared by centrifugation at $16,000\times g$ at 4°C after lysis. Lysate was then added to the antibody-bound beads for 4 h after which beads were washed with IP buffer for three times at 4°C . Proteins and RNAs were extracted from the beads for further analysis either with $1\times$ SDS sample buffer or Trizol LS (Invitrogen) reagent.

Exosomes isolation and characterization

Cell culture supernatants were used for exosome isolation. For exosome isolation, cells were grown in exosome-depleted media to prevent any background levels of exosomes present in FBS used to prepare the culture medium. Briefly, the cell supernatant was centrifuged at $3,000\times g$ for 15 min to remove cell debris. Next, the cell supernatant was collected and centrifuged at $10,000\times g$ for 30 min. The supernatant that was obtained was passed through $0.22\ \mu\text{m}$ filter units to further remove debris. This was followed by ultracentrifugation of the supernatant at $100,000\times g$ for 90 min. After ultracentrifugation, the pellet was resuspended in either PBS or complete media for further use.

For nanoparticle tracking analysis (NTA), exosome from 10^6 cells was resuspended in 1 ml PBS. Exosome was 10-fold diluted, 1 ml of diluted exosome was injected into the sample chamber of nanoparticle tracker (Nanosight NS300), tracking were done, and video was captured.

Luciferase assay

Control Renilla (RL-con) and/or let-7a reporter RL-3XBulge-let-7a containing three miRNA binding sites was used to check the miRNA let-7a activity. Firefly (FF) reporter plasmid was used for normalization of transfection. The Renilla and Firefly levels were measured using Dual Luciferase Assay Kit (Promega) using manufacturer's

protocol. The ratio of FF normalized RL-con to FF controlled RL-3XBulge-let-7a was used to measure the repression level (Mazumder et al, 2013).

OptiPrep™ density gradient centrifugation

OptiPrep™ (Sigma-Aldrich, USA) was used to prepare a 3–30% gradient in a buffer containing 78 mM KCl, 4 mM MgCl_2 , 8.4 mM CaCl_2 , 10 mM EGTA and 50 mM HEPES (pH 7.0) in a 4 ml ultracentrifuge tube. The protocol has been standardized for separation of subcellular organelles as described previously (Ghosh et al, 2015). RAW 264.7 cells were washed with PBS and homogenized with a Dounce homogenizer in a buffer containing 0.25 M sucrose, 78 mM KCl, 4 mM MgCl_2 , 8.4 mM CaCl_2 , 10 mM EGTA, 50 mM HEPES pH 7.0 supplemented with 100 $\mu\text{g}/\text{ml}$ of cycloheximide, 5 mM vanadyl ribonucleoside complex (VRC) (Sigma-Aldrich), 0.5 mM DTT and $1\times$ protease inhibitor (Roche). The lysate was clarified by centrifugation at $1,000\times g$ for 5 min two times and layered on top of the prepared gradient. The tubes were centrifuged at $110,000\times g$ for 5 h for separation of gradient on a SW60 Ti rotor. About 400 μl of each fraction was collected by aspiration from the top for subsequent analysis.

Estimation of total cellular and Ago2-bound mRNA and miRNAs

For miRNA estimation, cellular miRNA levels were detected using TaqMan-based miRNA specific assay kit started with 50 ng of total RNA concentration. U6 was used for normalization. Ago2-bound miRNA was estimated after immunoprecipitation of Ago2 using equal volume of RNA extracted after immunoprecipitation. Value normalized against total amount of Ago2 immunoprecipitated in each case. Real-time PCR was performed with 25 ng of cellular RNA and 200 ng of EV RNA unless specified otherwise, using specific primers for human let-7a (assay ID 000377), human miR-122 (assay ID 000445), human miR-16 (assay ID 000391), human miR-146a (assay ID 000468) and human miR-155 (assay ID 002571). U6 snRNA (assay ID 001973) was used as an endogenous control. The reverse transcription mix was used for PCR amplification with TaqMan® Universal PCR Master Mix No AmpErase (Applied Biosystems) and analysed in triplicates for each biological replicates. The comparative C_t method which typically included normalization, by the U6 snRNA, was used for quantification.

For mRNA estimation, mRNA levels were estimated by SYBR Green-based real-time cDNA estimation using specific primer for respective genes. For that, 200 ng of total RNA was used. For Ago2-bound mRNA estimation, equal volume of RNA extracted after immunoprecipitation was used. Value normalized against total amount of Ago2 immunoprecipitated in each case. Ago2 protein level quantified using ImageJ software done for blots obtained after Western blot analysis of immunoprecipitated Ago2. The comparative C_t method which typically included normalization by the GAPDH mRNA or 18S rRNA was used for quantification.

Immunofluorescence

Cells were fixed using 4% para-formaldehyde (PFA) for 20 min. Blocking and permeabilization was done by 1% BSA, 10% goat serum and 0.1% triton X-100 for 30 min. *Ld* promastigotes were stained by 1 μM carboxyfluorescein succinimidyl ester (CFSE) dye (Green) for

30 min at 22°C rocking followed by washing with 1× PBS thrice before infecting RAW 264.7 cells. The anti-HA (Rat) and anti-GP63 (Mouse) were used at 1:1,000 dilutions. Secondary Alexa Fluor^R 405 and 568-labelled anti-rat and anti-mouse antibodies were used at 1:500 dilutions. Cells were observed under Zeiss LSM800 confocal microscope. In HA-HuR overexpressed cells, primary anti-HA and Alexa Fluor^R 568 anti-rat secondary antibody was used. For calculating per cent of infected cells, minimum of 100 cells were counted.

In vitro phosphatase assay

FH-Ago2 was immunoprecipitated from stable transfected HEK293 cells expressing FH-Ago2. The phosphatases were pulled down using specific antibody from RAW 264.7 cell extracts prepared under different reaction conditions. The beads were washed with 1× phosphatase buffer (50 mM Tris-HCl, pH 7.5, 1 mM MgCl₂, 100 μM EDTA, 4.5 mg BSA, 1× protease inhibitor) prior to the reaction. FA-Ago2 was eluted and mixed with immunoprecipitated phosphatase containing beads, and volume was adjusted to 100 μl using 1× phosphatase buffer and incubated at 37°C for 30 min before the reaction is stopped with 1× SDS sample dye containing phosphatase inhibitor OA. The reaction was analysed on SDS-PAGE, and quantity of HA-Ago2 and phospho-Ago2 was determined by HA and phosphotyrosine-specific 4G10 antibodies, respectively.

SLA and GP63 purification

Soluble *Leishmania* antigens (SLA) and GP63 purification were done by following the published protocol (Bhowmick *et al*, 2008; Ghosh *et al*, 2013). Briefly, 1×10^{10} promastigotes cells were used as a starting material, and after series of thorough lysis, ultracentrifugation and affinity-based purification, GP63 was successfully purified.

In vitro HuR cleavage assay

RAW 264.7 cell lysate was incubated with *Leishmania*-derived soluble *Leishmania* antigen (SLA) or purified GP63 at 37°C for 30 min. The reaction was terminated using 5× SDS buffer. *Ortho*-phenanthroline was used as GP63 inhibitor. SLA was pre-treated with 10 μM *ortho*-phenanthroline for 30 min on ice before the reaction. The reaction was performed in a buffer containing 10 mM Tris-HCl pH 7.5, 100 mM KCl, 1 mM DTT and 1× protease inhibitor (Roche).

Animal experiments

BALB/c female mice of age 4–6 weeks were infected with 1×10^7 promastigotes via cardiac puncture maintained and sacrificed after 10th day and 35th day of infection. For the exogenous expression of HA-HuR experiment, mice were injected with 25 μg pCIneo or HA-HuR expression plasmid. On the third day, 1×10^7 promastigotes were used to infect the mice by cardiac puncture. Booster doses of plasmid were given on the 5th and the 10th day after the 1st day of plasmid administration. All mice were sacrificed on 35th day of infection, and tissues were snap frozen for future use. Approximately 10 mg tissue slice was collected and homogenized using 1× RIPA buffer for protein estimation and Western blotting. TriZol was directly added to the tissue slices, homogenized rigorously for thorough lysis before RNA isolation. DNA isolation was done following

manufacturer's protocol using Promega Wizard DNA isolation Kit. All animals were maintained in individually ventilated cages having sterile air supply and regulated temperature. For isolation, peritoneal macrophage adult female mice were used. All procedures were performed in accordance with a protocol approved Institutional Animal Ethics Committee. All the experimentations were performed according to the National Regulatory Guidelines issued by the Committee for the Purpose of Supervision of Experiments on Animals, Ministry of Environment and Forest, Govt. of India. All the experiments involving animals were carried out with prior approval of the Institutional Animal Ethics Committee. All mice were housed in individually ventilated caging system with 12 h/12 day/night cycle.

LPG purification and treatment

LPG was extracted was described previously with modifications (Piedrafita *et al*, 1999). Briefly, parasites were cultured and grown to a density of 10^7 cells/ml. The parasites were centrifuged at $200 \times g$ for 10 min. Cells were resuspended in 2 ml of chloroform: methanol:water (1:2:0.5, v/v) for 2 h at room temperature. The insoluble pellet was used for LPG extraction. De-lipidation of LPG was done with 9% butanol in water for 1 h each time for twice ($2 \times 250 \mu\text{l}$), and the fractions were pooled and vacuum dried. A total of 10^8 cells were used for LPG extraction. The overall extraction was resuspended in 100 μl of 1× filtered PBS and sonicated before treatment. As LPG was extracted from 10^8 cells and resuspended in 100 μl of PBS, 1 μl of the extract corresponds to approx 10^6 cell equivalent of LPG.

GP63 entrapment to liposome and treatment

GP63 entrapment in liposome was done using a previously described procedure (Ghosh *et al*, 2013) with slight modifications. Briefly, 12 mg phosphatidylcholine (Avanti Polar Lipids) (100 mg/ml), 8.7 mg cholesterol (Sigma) (100 mg/ml) (1:1.5 of cholesterol to PC molar ratio) and 6 mg *n*-octyl-β-D-glucopyranoside (Sigma) were dissolved in chloroform. The lipid mixture was coated as a uniform layer in a round glass bottle and kept in the desiccator. The lipid layer was solubilized in PBS containing either 250 μg purified GP63 or in the absence of GP63 and resuspended. The solution was sonicated in a bath sonicator for 15 min on ice water. The liposomes were ultracentrifuged at $100,000 \times g$ at 4°C for 1 h to remove unincorporated protein and lipid particles. The liposomal pellet was resuspended in normal saline for animal or cell treatment. Approximately 20 μg of GP63 entrapped liposome was administered to the animal (BALB/c female adult mice) via intracardiac route. Mice were sacrificed after 24 h of administration. Liver tissues were collected for Western blot analysis. It has been shown by Ghosh *et al* (2013) that most of the administered liposome gets accumulated in the liver. For RAW 264.7 cell treatment, 1 μg of GP63 entrapped liposome were used for 10^6 cells.

Real-time PCR for detection of *Leishmania*

The real-time detection to estimate *Ld* count was done as previously described (Nicolas *et al*, 2002). Briefly, DNA was collected from liver tissue of mice and 200 ng of isolated DNA was used for the

real-time detection. 18S rRNA was used as endogenous control. The *Ld* count was calculated from relative values obtained by $\Delta\Delta C_t$ analysis. Appendix Table S3 has information related to all primers used.

Northern and Western blot

Northern blotting of total cellular RNA was performed following the methods described previously (Ghosh *et al*, 2015). For miRNA detection, ^{32}P -labelled 22 nt anti-sense LNA-modified probes specific for respective miRNAs or U6 snRNA were used. Densitometry of the blot was performed in Cyclone Plus Storage Phosphor System (Perkin Elmer), and Optiquant software (Perkin Elmer) was used for quantification.

Western analyses of different proteins were performed as described elsewhere. Detailed list of antibodies used for Western blot and immunoprecipitation is available as Appendix Table S4. Imaging of all Western blots was performed using an UVP BioImager 600 system equipped with VisionWorks Life Science software (UVP) V6.80 which was also used for quantification.

Bio-informatics-based analysis of regulatory relationship between HuR and its target genes

An extensive list of HuR target genes (1,877) was compiled by utilizing the data from two previous analyses which had identified HuR targets either in HeLa cells or HEK293 cells by PAR-CLIP analysis (Lebedeva *et al*, 2011; Mukherjee *et al*, 2011). Target genes (1,103) that had binding site information, scored a log odds ratio (LOD) ≥ 0 [where LOD is indicative of probability of an mRNA being associated with HuR], were differentially expressed either at protein/mRNA level upon HuR knock-down in HEK293 cells were compiled from Mukherjee *et al* (2011). Similarly, another set of target genes (875) identified based on PAR-CLIP analysis that showed differential expression either at mRNA/protein level upon HuR knock-down in HeLa cells were obtained from Lebedeva *et al* (2011). Further, based on the assumption that HuR may have similar target genes in macrophages, differentially expressed HuR target genes in isolated *Ld*-infected human macrophages (16 h) [fold change: 1.5, *P*-value: 0.05] were determined considering the GEO dataset GSE360 (Chaussabel *et al*, 2003). Additionally, RNAseq profile of mRNA from HuR (*Elavl1*) knockout murine bone marrow-derived macrophages (Lu *et al*, 2014a) was determined considering the GEO dataset (GSE63199) (Afghan *et al*, 2018). Possible regulatory events that could be involved in this interaction between HuR and its target gene (PPP2CA) either directly at the mRNA level or via intermediates at the protein–protein interaction level (Szklarczyk *et al*, 2015), signalling level (Kanehisa & Goto, 2000) and miRNA level (Lebedeva *et al*, 2011) have been identified.

Statistical analysis

All graphs and statistical significance were calculated using GraphPad Prism 5.00 (GraphPad, San Diego). Experiments were done for minimum of three times to get the *P* values. The sample size was chosen by convenience, and no exclusion criteria were used. All the animals and samples were used in the analyses. Subjective randomization was used. *In vitro* analyses were not blind but occasionally verified by independent researchers within the

The paper explained

Problem

Maintaining inflammatory homeostasis is an important event in immune cells. Macrophages, that act as first line defence against any invading pathogens, need to show balanced immune response to safeguard themselves from self-destruction at the time of pathogen killing. Parasites like *Leishmania* have developed clever strategy to evade the immune sentinels and continue to propagate within macrophages. Sodium stibogluconate (SSG)-resistant clinical isolates are of serious clinical concern as they shifted the immune balance of the infected macrophage more towards a strong anti-inflammatory one. How to stimulate the infected macrophage to a pro-inflammatory setting to clear the residing drug-resistant pathogens is a major challenge from the clinical point of view.

Results

We have identified two major players HuR, a miRNA depressor protein, and PP2A, a phosphatase that favours the pro or anti-inflammatory responses, respectively. During *Ld* infection, the parasite reciprocally modulates HuR and PP2A which ensure parasite survival within the macrophage. Although HuR overexpression could successfully control the drug-sensitive strain of *Leishmania* (*Ld*^S), it was not sufficient alone to clear the resistant form (*Ld*^R). HuR restoration along with PP2A inhibition however effectively counters the strong anti-inflammatory response induced by *Ld*^R. Interestingly, both the factors work by influencing the phosphorylation of miRNA effector protein Ago2 to regulate miRNA activity against target cytokines.

Impact

Our data suggest intricate regulation of inflammatory response by PP2A and HuR that works primarily by modulating Ago2 phosphorylation during infection and inflammation. This might hold true for any disease that involves alteration of inflammatory homeostasis. Therefore, HuR and PP2A would be new drug targets not only to treat inflammatory diseases but also to affect anti-inflammatory responses during invasion of host cells by pathogens like *Leishmania* or mycobacterium.

group. In all experiments, the variance was similar between groups. Individual *P*-values were calculated by using Student's *t*-test. Curve fitting, the mathematical modelling, was done with OriginLab data analysis and Graphing software. The animal selection and analysis process were blind as injection/numbering, and tissue collection was done independently.

Ethics statement

BALB/c mice were obtained from CSIR-Indian Institute of Chemical Biology animal facility. Experiments were done according to the national regulatory guidelines stated by the Committee for the Purpose of Supervision of Experiments on Animals, Ministry of Environment and Forest, Govt of India. Prior permission related to mice experiments was obtained through Institutional Animal Ethics Committee.

Expanded View for this article is available online.

Acknowledgements

We acknowledge Witold Filipowicz and Gunter Meister for different plasmids constructs. SNB is supported by The Swarnajayanti Fellowship (DST/SJF/LSA-

03/2014-15) from Dept. of Science and Technology, Govt. of India, while AG, KM, AM, SG and IM received their support either from CSIR, India, University Grant Commission (UGC) or Dept. of Science and Technology, Govt. of India. SR is supported by J C Bose Fellowship, DST, Govt. of India (SB/S2/JCB-65/2014). The work also received support from a Indo-Swiss Bilateral Project Grant from Department of Biotechnology, Govt of India (BT/IN/Swiss/53/SNB/2018-19) and a High Risk High Reward Grant (HRR/2016/000093) from Dept. of Science and Technology, Govt. of India.

Author contributions

AG, KM, AM and SG done all the experiments. Appendix Fig S1 and part of Fig 6 done by IM and KC. SNB conceptualized the idea, analysed data and wrote the manuscript along with AG, KM, AM and SG. KM also contributed in idea conceptualization and manuscript language editing. SC, SR and SS helped in planning some of the experiments described in Figs 6 and 8.

Conflict of interest

The authors declare that they have no conflict of interest.

References

- Aderem A, Underhill DM (1999) Mechanisms of phagocytosis in macrophages. *Annu Rev Immunol* 17: 593–623
- Afgan E, Baker D, Batut B, van den Beek M, Bouvier D, Cech M, Chilton J, Clements D, Coraor N, Gruning BA et al (2018) The Galaxy platform for accessible, reproducible and collaborative biomedical analyses: 2018 update. *Nucleic Acids Res* 46: W537–W544
- Akilbekova D, Philip R, Graham A, Bratlie KM (2015) Macrophage reprogramming: influence of latex beads with various functional groups on macrophage phenotype and phagocytic uptake *in vitro*. *J Biomed Mater Res A* 103: 262–268
- Bandyopadhyay S, Long ME, Allen LA (2014) Differential expression of microRNAs in *Francisella tularensis*-infected human macrophages: miR-155-dependent downregulation of MyD88 inhibits the inflammatory response. *PLoS ONE* 9: e109525
- Bartel DP (2018) Metazoan microRNAs. *Cell* 173: 20–51
- Basu S, Bhattacharyya SN (2014) Insulin-like growth factor-1 prevents miR-122 production in neighbouring cells to curtail its intercellular transfer to ensure proliferation of human hepatoma cells. *Nucleic Acids Res* 42: 7170–7185
- Becker I, Salaiza N, Aguirre M, Delgado J, Carrillo-Carrasco N, Kobeh LG, Ruiz A, Cervantes R, Torres AP, Cabrera N et al (2003) Leishmania lipophosphoglycan (LPG) activates NK cells through toll-like receptor-2. *Mol Biochem Parasitol* 130: 65–74
- Bhandari V, Sundar S, Dujardin JC, Salotra P (2014) Elucidation of cellular mechanisms involved in experimental paromomycin resistance in *Leishmania donovani*. *Antimicrob Agents Chemother* 58: 2580–2585
- Bhattacharyya SN, Habermacher R, Martine U, Closs EI, Filipowicz W (2006) Relief of microRNA-mediated translational repression in human cells subjected to stress. *Cell* 125: 1111–1124
- Bhowmick S, Ravindran R, Ali N (2008) gp63 in stable cationic liposomes confers sustained vaccine immunity to susceptible BALB/c mice infected with *Leishmania donovani*. *Infect Immun* 76: 1003–1015
- Bode JG, Ehrling C, Haussinger D (2012) The macrophage response towards LPS and its control through the p38(MAPK)-STAT3 axis. *Cell Signal* 24: 1185–1194
- Brahmachari UN (1922) A new form of cutaneous leishmaniasis-dermal leishmanoid. *Ind Med Gaz* 57: 125–127
- Chakrabarty Y, Bhattacharyya SN (2017) *Leishmania donovani* restricts mitochondrial dynamics to enhance miRNP stability and target RNA repression in host macrophages. *Mol Biol Cell* 28: 2091–2105
- Chaparro V, Leroux LP, Zimmermann A, Jardim A, Johnston B, Descoteaux A, Jaramillo M (2019) *Leishmania donovani* lipophosphoglycan increases macrophage-dependent chemotaxis of CXCR6-expressing cells via CXCL16 induction. *Infect Immun* 87: e00064-19
- Chaussabel D, Semnani RT, McDowell MA, Sacks D, Sher A, Nutman TB (2003) Unique gene expression profiles of human macrophages and dendritic cells to phylogenetically distinct parasites. *Blood* 102: 672–681
- Chen YL, Huang YL, Lin NY, Chen HC, Chiu WC, Chang CJ (2006) Differential regulation of ARE-mediated TNFalpha and IL-1beta mRNA stability by lipopolysaccharide in RAW264.7 cells. *Biochem Biophys Res Comm* 346: 160–168
- Contreras I, Gomez MA, Nguyen O, Shio MT, McMaster RW, Olivier M (2010) Leishmania-induced inactivation of the macrophage transcription factor AP-1 is mediated by the parasite metalloprotease GP63. *PLoS Pathog* 6: e1001148
- Courret N, Frehel C, Gouhier N, Pouchelet M, Prina E, Roux P, Antoine JC (2002) Biogenesis of leishmania-harboring parasitophorous vacuoles following phagocytosis of the metacyclic promastigote or amastigote stages of the parasites. *J Cell Sci* 115: 2303–2316
- Fernandez JJ, Cadenas ML, Souto ML, Trujillo MM, Norte M (2002) Okadaic acid, useful tool for studying cellular processes. *Curr Med Chem* 9: 229–262
- Ghosh J, Bose M, Roy S, Bhattacharyya SN (2013) *Leishmania donovani* targets Dicer1 to downregulate miR-122, lower serum cholesterol, and facilitate murine liver infection. *Cell Host Microbe* 13: 277–288
- Ghosh S, Bose M, Ray A, Bhattacharyya SN (2015) Polysome arrest restricts miRNA turnover by preventing exosomal export of miRNA in growth-retarded mammalian cells. *Mol Biol Cell* 26: 1072–1083
- Haldar AK, Yadav V, Singhal E, Bisht KK, Singh A, Bhaumik S, Basu R, Sen P, Roy S (2010) *Leishmania donovani* isolates with antimony-resistant but not -sensitive phenotype inhibit sodium antimony gluconate-induced dendritic cell activation. *PLoS Pathog* 6: e1000907
- Halle M, Gomez MA, Stuibler M, Shimizu H, McMaster WR, Olivier M, Tremblay ML (2009) The *Leishmania* surface protease GP63 cleaves multiple intracellular proteins and actively participates in p38 mitogen-activated protein kinase inactivation. *J Biol Chem* 284: 6893–6908
- Janssens V, Van Hoof C, Merlevede W, Goris J (1998) PTPA regulating PP2A as a dual specificity phosphatase. *Methods Mol Biol* 93: 103–115
- Kanehisa M, Goto S (2000) KEGG: kyoto encyclopedia of genes and genomes. *Nucleic Acids Res* 28: 27–30
- Kar S, Ukil A, Sharma G, Das PK (2010) MAPK-directed phosphatases preferentially regulate pro- and anti-inflammatory cytokines in experimental visceral leishmaniasis: involvement of distinct protein kinase C isoforms. *J Leukoc Biol* 88: 9–20
- Kosaka N, Iguchi H, Yoshioka Y, Takeshita F, Matsuki Y, Ochiya T (2010) Secretory mechanisms and intercellular transfer of microRNAs in living cells. *J Biol Chem* 285: 17442–17452
- Kozicky LK, Sly LM (2015) Phosphatase regulation of macrophage activation. *Semin Immunol* 27: 276–285
- Kumar A, Das S, Mandal A, Verma S, Abhishek K, Kumar V, Ghosh AK, Das P (2018) Leishmania infection activates host mTOR for its survival by M2 macrophage polarization. *Parasite Immunol* 40: e12586
- Kundu P, Fabian MR, Sonenberg N, Bhattacharyya SN, Filipowicz W (2012) HuR protein attenuates miRNA-mediated repression by promoting miRISC dissociation from the target RNA. *Nucleic Acids Res* 40: 5088–5100

- Lebedeva S, Jens M, Theil K, Schwanhauser B, Selbach M, Landthaler M, Rajewsky N (2011) Transcriptome-wide analysis of regulatory interactions of the RNA-binding protein HuR. *Mol Cell* 43: 340–352
- Li S, Cao J, Zhang W, Zhang F, Ni G, Luo Q, Wang M, Tao X, Xia H (2016) Protein tyrosine phosphatase PTPN3 promotes drug resistance and stem cell-like characteristics in ovarian cancer. *Sci Rep* 6: 36873
- Lin X, Kong J, Wu Q, Yang Y, Ji P (2015) Effect of TLR4/MyD88 signaling pathway on expression of IL-1beta and TNF-alpha in synovial fibroblasts from temporomandibular joint exposed to lipopolysaccharide. *Mediators Inflamm* 2015: 329405
- Liu D, Uzonon JE (2012) The early interaction of *Leishmania* with macrophages and dendritic cells and its influence on the host immune response. *Front Cell Infect Microbiol* 2: 83
- Lloberas J, Valverde-Estrella L, Tur J, Vico T, Celada A (2016) Mitogen-activated protein kinases and mitogen kinase phosphatase 1: a critical interplay in macrophage biology. *Front Mol Biosci* 3: 28
- Lu L, Zheng L, Si Y, Luo W, Dujardin G, Kwan T, Potochick NR, Thompson SR, Schneider DA, King PH (2014a) Hu antigen R (HuR) is a positive regulator of the RNA-binding proteins TDP-43 and FUS/TLS: implications for amyotrophic lateral sclerosis. *J Biol Chem* 289: 31792–31804
- Lu YC, Chang SH, Hafner M, Li X, Tuschl T, Elemento O, Hla T (2014b) ELAVL1 modulates transcriptome-wide miRNA binding in murine macrophages. *Cell Rep* 9: 2330–2343
- Mazumder A, Bose M, Chakraborty A, Chakrabarti S, Bhattacharyya SN (2013) A transient reversal of miRNA-mediated repression controls macrophage activation. *EMBO Rep* 14: 1008–1016
- Meisner NC, Filipowicz W (2011) Properties of the regulatory RNA-binding protein HuR and its role in controlling miRNA repression. *Adv Exp Med Biol* 700: 106–123
- Mogensen TH (2009) Pathogen recognition and inflammatory signaling in innate immune defenses. *Clin Microbiol Rev* 22: 240–273
- Morandini AC, Chaves Souza PP, Ramos-Junior ES, Souza Costa CA, Santos CF (2013) MyD88 or TRAM knockdown regulates interleukin (IL)-6, IL-8, and CXCL12 mRNA expression in human gingival and periodontal ligament fibroblasts. *J Periodontol* 84: 1353–1360
- Mosser DM, Edwards JP (2008) Exploring the full spectrum of macrophage activation. *Nat Rev Immunol* 8: 958–969
- Mukherjee N, Corcoran DL, Nusbaum JD, Reid DW, Georgiev S, Hafner M, Ascano M Jr, Tuschl T, Ohler U, Keene JD (2011) Integrative regulatory mapping indicates that the RNA-binding protein HuR couples pre-mRNA processing and mRNA stability. *Mol Cell* 43: 327–339
- Mukherjee B, Mukhopadhyay R, Bannerjee B, Chowdhury S, Mukherjee S, Naskar K, Allam US, Chakravorty D, Sundar S, Dujardin JC et al (2013) Antimony-resistant but not antimony-sensitive *Leishmania donovani* up-regulates host IL-10 to overexpress multidrug-resistant protein 1. *Proc Natl Acad Sci USA* 110: E575–E582
- Mukherjee B, Paul J, Mukherjee S, Mukhopadhyay R, Das S, Naskar K, Sundar S, Dujardin JC, Saha B, Roy S (2015) Antimony-resistant *Leishmania donovani* exploits miR-466i to deactivate host MyD88 for regulating IL-10/IL-12 levels during early hours of infection. *J Immunol* 195: 2731–2742
- Mukherjee K, Ghoshal B, Ghosh S, Chakrabarty Y, Shwetha S, Das S, Bhattacharyya SN (2016) Reversible HuR-microRNA binding controls extracellular export of miR-122 and augments stress response. *EMBO Rep* 17: 1184–1203
- Mukhopadhyay R, Mukherjee S, Mukherjee B, Naskar K, Mondal D, Decuypere S, Ostyn B, Prajapati VK, Sundar S, Dujardin JC et al (2011) Characterisation of antimony-resistant *Leishmania donovani* isolates: biochemical and biophysical studies and interaction with host cells. *Int J Parasitol* 41: 1311–1321
- Mukhopadhyay D, Mukherjee S, Roy S, Dalton JE, Kundu S, Sarkar A, Das NK, Kaye PM, Chatterjee M (2015) M2 polarization of monocytes-macrophages is a hallmark of Indian post kala-azar dermal leishmaniasis. *PLoS Negl Trop Dis* 9: e0004145
- Neuder LE, Keener JM, Eckert RE, Trujillo JC, Jones SL (2009) Role of p38 MAPK in LPS induced pro-inflammatory cytokine and chemokine gene expression in equine leukocytes. *Vet Immunol Immunopathol* 129: 192–199
- Nicolas L, Prina E, Lang T, Milon G (2002) Real-time PCR for detection and quantitation of leishmania in mouse tissues. *J Clin Microbiol* 40: 1666–1669
- Olivier M, Gregory DJ, Forget G (2005) Subversion mechanisms by which *Leishmania* parasites can escape the host immune response: a signaling point of view. *Clin Microbiol Rev* 18: 293–305
- Palanisamy V, Jakymiw A, Van Tubergen EA, D'Silva NJ, Kirkwood KL (2012) Control of cytokine mRNA expression by RNA-binding proteins and microRNAs. *J Dent Res* 91: 651–658
- Patranabis S, Bhattacharyya SN (2016) Phosphorylation of Ago2 and subsequent inactivation of let-7a RNP-specific microRNAs control differentiation of mammalian sympathetic neurons. *Mol Cell Biol* 36: 1260–1271
- Piedrafitra D, Proudfoot L, Nikolaev AV, Xu D, Sands W, Feng GJ, Thomas E, Brewer J, Ferguson MA, Alexander J et al (1999) Regulation of macrophage IL-12 synthesis by *Leishmania phosphoglycans*. *Eur J Immunol* 29: 235–244
- Pillai RS, Bhattacharyya SN, Artus CG, Zoller T, Cougot N, Basyuk E, Bertrand E, Filipowicz W (2005) Inhibition of translational initiation by Let-7 microRNA in human cells. *Science* 309: 1573–1576
- Podinovskaia M, Descoteaux A (2015) *Leishmania* and the macrophage: a multifaceted interaction. *Future Microbiol* 10: 111–129
- Poria DK, Guha A, Nandi I, Ray PS (2016) RNA-binding protein HuR sequesters microRNA-21 to prevent translation repression of proinflammatory tumor suppressor gene programmed cell death 4. *Oncogene* 35: 1703–1715
- Ready PD (2014) Epidemiology of visceral leishmaniasis. *Clin Epidemiol* 6: 147–154
- Rojas-Bernabe A, Garcia-Hernandez O, Maldonado-Bernal C, Delegado-Dominguez J, Ortega E, Gutierrez-Kobeh L, Becker I, Aguirre-Garcia M (2014) *Leishmania mexicana* lipophosphoglycan activates ERK and p38 MAP kinase and induces production of proinflammatory cytokines in human macrophages through TLR2 and TLR4. *Parasitology* 141: 788–800
- Roy K, Naskar K, Ghosh M, Roy S (2014) Class II MHC/peptide interaction in *Leishmania donovani* infection: implications in vaccine design. *J Immunol* 192: 5873–5880
- Rudel S, Meister G (2008) Phosphorylation of Argonaute proteins: regulating gene regulators. *Biochem J* 413: e7–e9
- Saha B, Momen-Heravi F, Furi I, Kodys K, Catalano D, Gangopadhyay A, Haraszti R, Satishchandran A, Iracheta-Velhe A, Adejumo A et al (2018) Extracellular vesicles from mice with alcoholic liver disease carry a distinct protein cargo and induce macrophage activation through heat shock protein 90. *Hepatology* 67: 1986–2000
- Shi JX, Su X, Xu J, Zhang WY, Shi Y (2012) HuR post-transcriptionally regulates TNF-alpha-induced IL-6 expression in human pulmonary microvascular endothelial cells mainly via tristetraprolin. *Respir Physiol Neurobiol* 181: 154–161
- Soulart D, Bogdan C (2017) Function of macrophage and parasite phosphatases in leishmaniasis. *Front Immunol* 8: 1838

- Squadrito ML, Etzrodt M, De Palma M, Pittet MJ (2013) MicroRNA-mediated control of macrophages and its implications for cancer. *Trends Immunol* 34: 350–359
- Srikantan S, Gorospe M (2011) UneCLIPsing HuR nuclear function. *Mol Cell* 43: 319–321
- Szklarczyk D, Franceschini A, Wyder S, Forslund K, Heller D, Huerta-Cepas J, Simonovic M, Roth A, Santos A, Tsafou KP et al (2015) STRING v10: protein-protein interaction networks, integrated over the tree of life. *Nucleic Acids Res* 43: D447–D452
- Tang B, Xiao B, Liu Z, Li N, Zhu ED, Li BS, Xie QH, Zhuang Y, Zou QM, Mao XH (2010) Identification of MyD88 as a novel target of miR-155, involved in negative regulation of *Helicobacter pylori*-induced inflammation. *FEBS Lett* 584: 1481–1486
- Tiedje C, Ronkina N, Tehrani M, Dhamija S, Laass K, Holtmann H, Kotlyarov A, Gaestel M (2012) The p38/MK2-driven exchange between tristetraprolin and HuR regulates AU-rich element-dependent translation. *PLoS Genet* 8: e1002977
- Xu T, Li L, Hu HQ, Meng XM, Huang C, Zhang L, Qin J, Li J (2018) MicroRNAs in alcoholic liver disease: recent advances and future applications. *J Cell Physiol* 234: 382–394



License: This is an open access article under the terms of the Creative Commons Attribution 4.0 License, which permits use, distribution and reproduction in any medium, provided the original work is properly cited.

Leishmania donovani Targets Dicer1 to Downregulate miR-122, Lower Serum Cholesterol, and Facilitate Murine Liver Infection

June Ghosh,^{1,2} Mainak Bose,¹ Syamal Roy,² and Suvendra N. Bhattacharyya^{1,*}

¹RNA Biology Research Laboratory, Molecular and Human Genetics Division

²Infectious Diseases and Immunology Division

CSIR-Indian Institute of Chemical Biology, Kolkata 700032, India

*Correspondence: sb@csiricb.in

<http://dx.doi.org/10.1016/j.chom.2013.02.005>

Open access under CC BY license.

SUMMARY

Leishmania donovani causes visceral leishmaniasis (VL) where the parasite infects and resides inside liver and spleen tissue macrophages. Given the abnormal lipid profile observed in VL patients, we examined the status of serum lipids in an experimental murine model of VL. The murine VL liver displayed altered expression of lipid metabolic genes, many of which are direct or indirect targets of the liver-specific microRNA-122. Concomitant reduction of miR-122 expression was observed in VL liver. High serum cholesterol caused resistance to *L. donovani* infection, while downregulation of miR-122 is coupled with low serum cholesterol in VL mice. Exosomes secreted by the infective parasites caused reduction in miR-122 activity in hepatic cells. *Leishmania* surface glycoprotein gp63, a Zn-metalloprotease, targets pre-miRNA processor Dicer1 to prevent miRNP formation in *L. donovani*-interacting hepatic cells. Conversely, restoration of miR-122 or Dicer1 levels in VL mouse liver increased serum cholesterol and reduced liver parasite burden.

INTRODUCTION

Visceral leishmaniasis (VL) is caused by the protozoan parasite *Leishmania donovani* or *Leishmania infantum* and is the most fatal form of this parasitic disorder (Murray et al., 2005). The parasite infects the spleen and liver of infected individuals and resides within the macrophages to escape host immune response (Olivier et al., 2005). It shows a dimorphic life cycle, residing as flagellate promastigotes in the midgut of the sand fly vector and as aflagellate amastigotes in the mammalian host (Desjardins and Descoteaux, 1998; Engwerda et al., 2004). Liver is the primary organ that gets infected in the early phase of infection where the parasites survive within the tissue macrophage Kupffer cells, while the liver parenchyma remains noninfected (Beattie et al., 2010).

VL patients show hypolipidemia characterized by reduced serum total cholesterol and lipoproteins (Lal et al., 2007). Inter-

estingly, hyperlipidemia is associated with resistance to VL (Ghosh et al., 2012). In experimental VL, reduced membrane cholesterol in infected macrophages leads to increased membrane fluidity affecting its antigen-presenting ability (Chakraborty et al., 2005). Liposomal formulation of cholesterol is known to offer protection in infected hamsters (Banerjee et al., 2009). Although the involvement of cholesterol in controlling VL is evident from these studies, little is known about the influence of *Leishmania* on host lipid metabolism.

MicroRNAs (miRNAs), the 20–22 nt long posttranscriptional regulators, mediate gene repression primarily by inducing translational repression or degradation of target mRNAs to affect almost all physiological processes including metabolic processes in higher eukaryotes (Filipowicz et al., 2008; Krützfeldt and Stoffel, 2006). Precursors to miRNAs, primary miRNA transcripts (pri-miRNAs) are processed by microprocessor Drosha-DGCR8 in the nucleus to generate precursor miRNAs (pre-miRNAs), which are subsequently processed to the mature form by RNase III endonuclease Dicer1 in the cytoplasm (Filipowicz et al., 2008). The miRNA encoding strand of miRNA duplex gets loaded to Argonaute proteins by DICER1 and TAR RNA-binding proteins (TRBPs) to form active microRNA ribonucleoprotein complexes (miRNPs). miR-122, a miRNA expressed abundantly in liver, modulates a wide range of liver functions. miR-122 comprises more than 70% of the liver miRNA pool and is largely responsible for liver homeostasis and lipid metabolism (Chang et al., 2004; Girard et al., 2008). Antisense oligonucleotides against miR-122 confirmed its role in fatty acid and cholesterol metabolism (Elmén et al., 2008; Esau et al., 2006). Therefore, it is an interesting possibility that parasite infection controls liver miR-122 in order to modulate serum cholesterol.

L. donovani interacts with its target cell either by cell-cell contact or by secreting exosomes containing virulence factors (Silverman et al., 2010). The surface metalloprotease gp63, a membrane-bound glycosylphosphatidylinositol (GPI)-anchored glycoprotein of 63 kDa, is a known virulence factor present in *Leishmania* exosomes that serves as a ligand for the macrophage complement receptor (Brittingham et al., 1995). This *Leishmania* surface protease cleaves multiple intracellular proteins and participates in p38 mitogen-activated protein (MAP) kinase inactivation (Hallé et al., 2009). gp63 is also responsible for selective degradation of eIF4E in *L. donovani*-infected macrophages (Jaramillo et al., 2011).



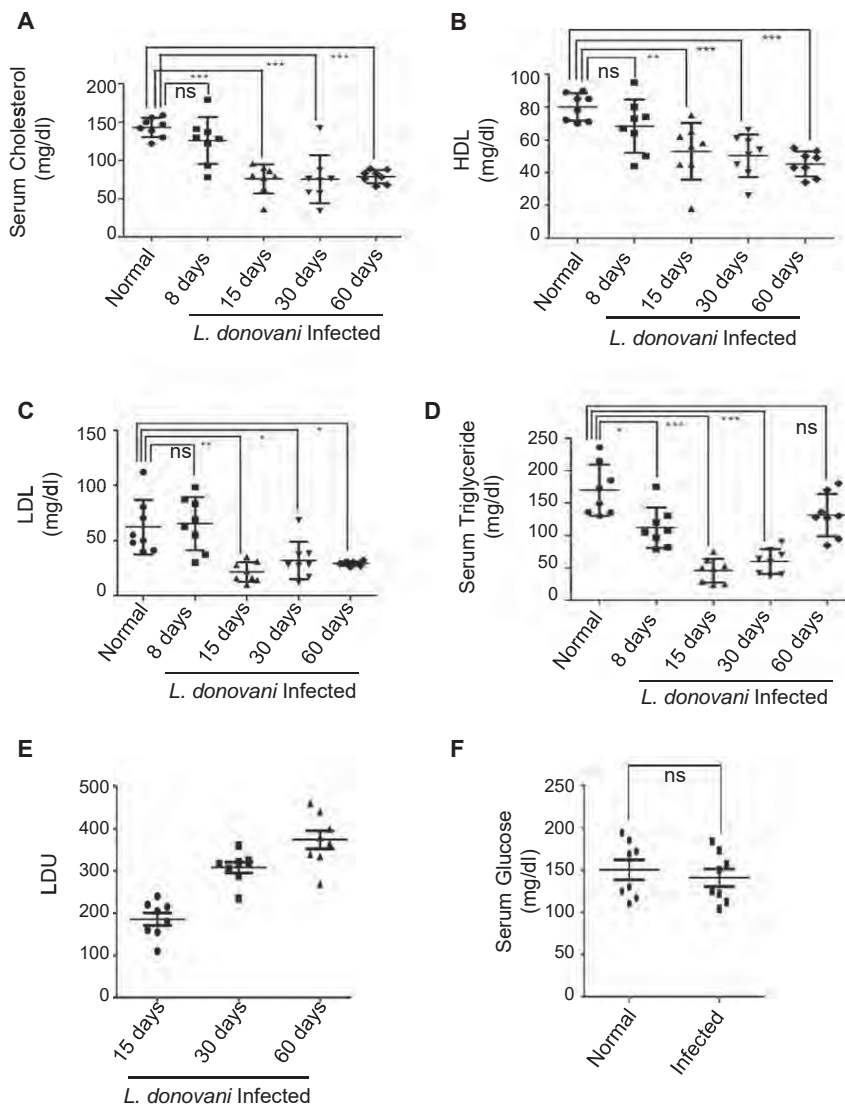


Figure 1. Reduction in Serum Lipids with Progress of *L. donovani* Infection in Mouse Liver

(A) Level of total serum cholesterol in *L. donovani*-infected BALB/c mice. Serum cholesterol levels in mice infected for 8, 15, 30, or 60 days were measured and plotted individually.

(B–D) Levels of HDL (B), LDL (C), and triglyceride (D) in the blood serum of 8, 15, 30, or 60 days of infected or age-matched normal animals.

(E) Liver parasite load in individual animals from different experimental groups estimated and plotted as LDU against infection time.

(F) Level of serum glucose in *L. donovani*-infected (1 or 2 months) and normal animals. Data represent mean \pm SEM. For each experiment $n = 8$. Significance levels: ns (not significant), $p > 0.05$, * $p < 0.05$, ** $p < 0.001$, *** $p < 0.0001$. See also Table S1 and Figure S1.

cholesterol with almost 50% reduction at 60 days postinfection (p.i.) in *L. donovani*-infected BALB/c mice. Major serum lipoproteins like high-density lipoprotein (HDL) and low-density lipoprotein (LDL) also showed similar trends (Figures 1A–1C). Serum triglyceride dropped up to 65% until 30 days p.i. with a partial recovery at 60 days p.i. (Figure 1D). An inverse correlation between serum cholesterol level and parasite load was evident (Figure 1E and Table S1). Histological examination of the infected liver section also revealed a gradual increase in both number and size of granuloma, with progress of infection where parasites were also visible (Figures S1A and S1B). Overall, we observed a substantial difference in serum lipid profiles in *L. donovani*-infected animals, whereas

serum glucose level remained unaffected (Figure 1F). Similar changes in serum cholesterol were also documented in *L. donovani* amastigote-infected mouse livers (Figures S1C and S1D).

Altered Expression of Lipid Metabolic Genes in *Leishmania*-Infected Mouse Liver

In order to dissect the cause of these abnormalities in the lipid profile of *L. donovani*-infected animals, we checked the expression levels of lipid metabolic genes in infected mouse liver. A whole-genome microarray analysis was done using an Illumina Mouse WG-6 v2 BeadChip gene expression array. Of 45,200 total transcripts analyzed, 9,659 showed a differential expression (5,501 were downregulated, and 4,148 were upregulated) with more than or equal to 2-fold changes in their expression in infected livers (Figure 2A). The whole microarray data have been uploaded to the Gene Expression Omnibus database (accession number GSE38985).

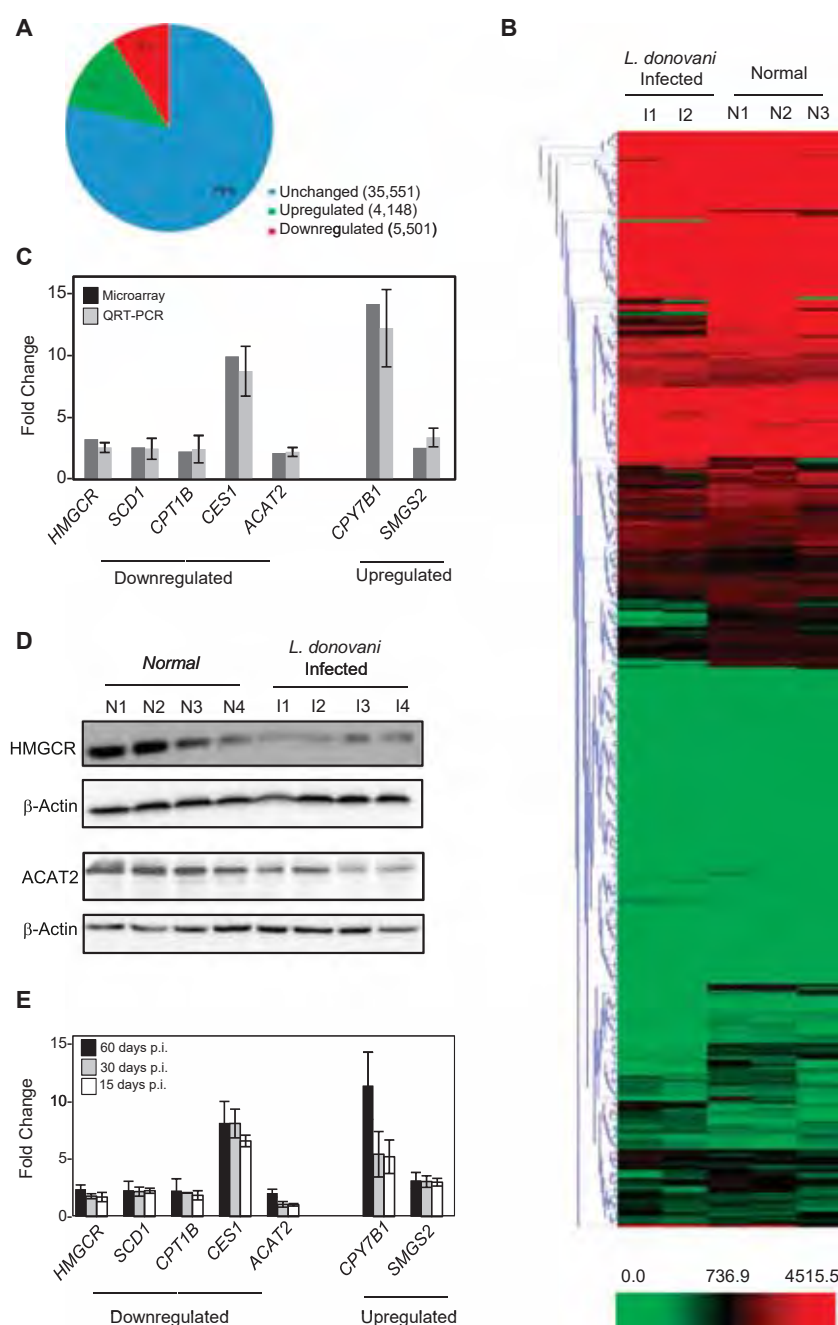
Scrutiny of differentially expressed gene clusters revealed that a large number of genes showing reduced expression in infected

We have shown in this study that *L. donovani* infection downregulates miR-122 and genes involved in cholesterol biosynthesis in infected mouse livers to reduce serum cholesterol. We have also found that restoration of miR-122 induces revival of serum cholesterol and reduction in liver parasite count. *Leishmania* metalloprotease gp63, a component of *Leishmania* exosomes, gets internalized to degrade Dicer1 in hepatic cells. It inhibits Dicer1-mediated pre-miR-122 processing to restrict miRNP formation and prevents miR-122 activity in *L. donovani*-interacting hepatocytes.

RESULTS

L. donovani Alters Serum Lipid Profiles of Infected Animals

Abnormal lipid profiles identified in VL patients (Ghosh et al., 2011; Liberopoulos et al., 2002) made us interested to look at the status of serum lipids in *L. donovani*-infected mice. Measurement of total cholesterol showed a gradual lowering in serum



livers are related to lipid metabolism (83 showed more than or equal to 2-fold changes among 476 genes considered). A heatmap was generated showing differences in expression of lipid metabolizing genes between normal ($n = 3$) and infected ($n = 2$) groups (Figure 2B). A list comprising lipid metabolizing genes with fold change (upregulated or downregulated) greater than or equal to two are provided as a table (Table S2). In summary, the gene expression data suggest that a major alteration in lipid metabolism occurs in *L. donovani*-infected mouse liver. Among the genes listed, *HMGCR* (hydroxyl-3-methylglutaryl coenzyme A reductase), the rate-limiting enzyme for de novo cholesterol

Figure 2. Altered Expression of Lipid Metabolizing Genes in the Livers of *L. donovani*-Infected Animals

(A–C) Whole-genome microarray analysis revealed differentially expressed genes in *L. donovani*-infected liver. A pie chart representation of number of genes that showed altered expression in mouse livers after 60 days p.i. is shown. RNA was isolated from normal ($n = 3$) or infected ($n = 2$) livers, and whole genome microarray analysis was done (A). Heatmap of lipid metabolic genes (B). Fold changes obtained from both real-time quantification and microarray analysis were plotted for the key lipid metabolizing genes that showed either an increased or decreased expression in infected livers (C).

(D) Decreased expression of cholesterol anabolic proteins *HMGCR* or *ACAT2* in infected mouse liver. Liver tissue extracts were western blotted for *HMGCR* or *ACAT2* detection. β -actin was used as loading control. $n = 4$ for noninfected control and 60 days p.i.

(E) Changes in expression of important lipid metabolic genes in infected animal livers with progress of infection. Respective fold changes in expression were quantified by real-time PCR. For all real-time estimations, $n \geq 3$. SD was from three independent measurements. Data represented as \pm SEM. See also Table S2.

biosynthesis (fold downregulation = 2.9), and *CYP7B1* (25-hydroxycholesterol-7 α -hydroxylase), a member of the monooxygenase cytochrome P450 superfamily that catalyzes the first step of catabolism of cholesterol to bile acid (fold upregulation = 12.71), are of key importance in cholesterol metabolism. The validation of the microarray data was performed by real-time quantification of seven (five showed downregulation and two showed upregulation in microarray analysis) of these genes. All of them showed proportional changes in their expression in infected mouse livers (Figure 2C). Changes in protein levels for *HMGCR* and *ACAT2* were also confirmed by western blot analysis (Figure 2D). Interestingly, these genes showed altered expression even during the early stage of infection when the serum cholesterol level also starts to decrease

(Figure 2E). The microarray data suggested an overall downregulation in cholesterol-synthesizing genes and selective upregulation of cholesterol catabolic genes that result in the lowering of serum cholesterol in *Leishmania*-infected mice.

Leishmania Infection Reduces miR-122 Levels in Mouse Liver

A more detailed analysis of the microarray data highlighted an interesting finding: several lipid-metabolizing genes showing differential expression in the livers of infected animals are direct or indirect targets of miR-122 (Table S3). Among them, *HMGCR*,

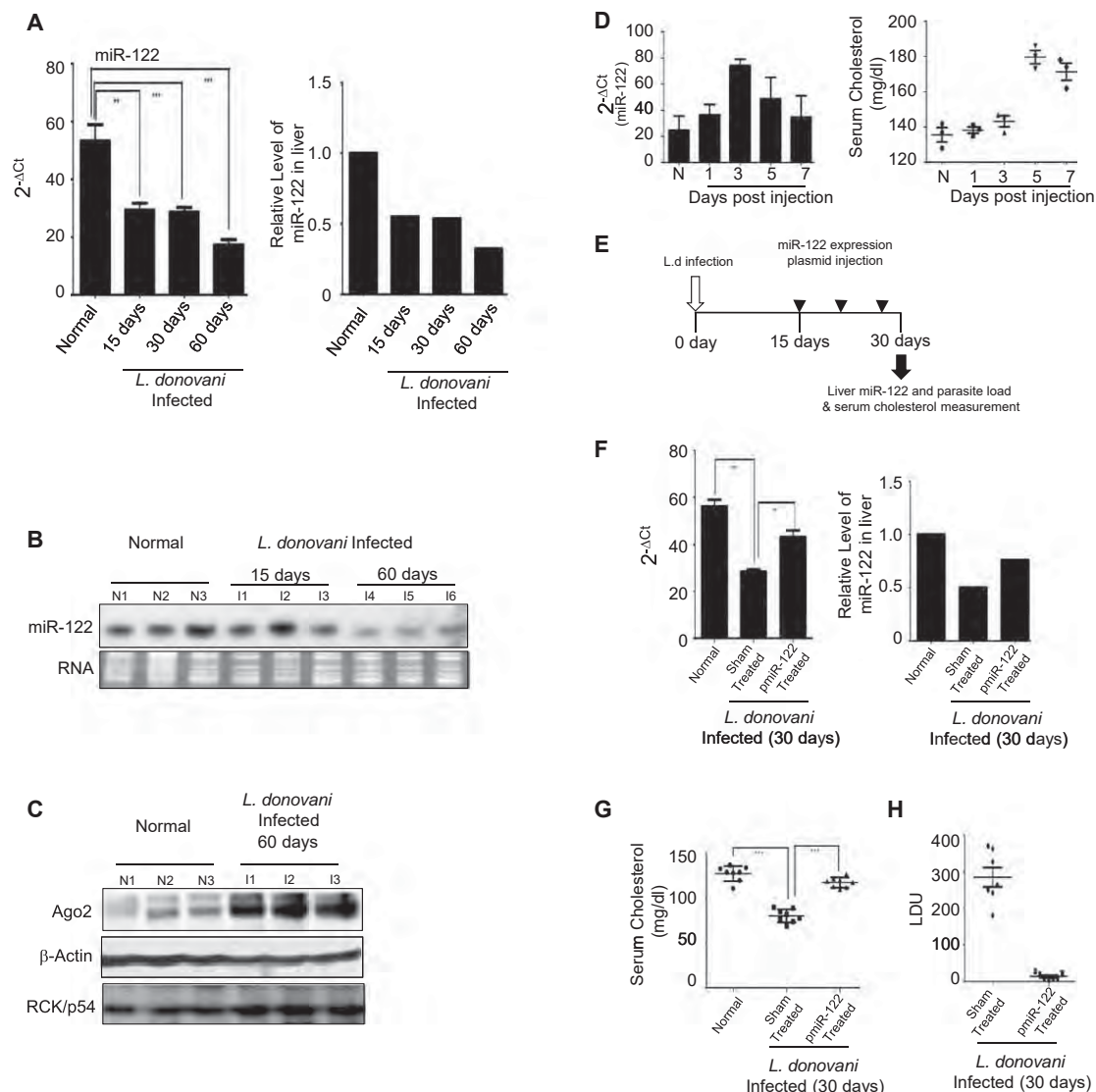


Figure 3. miR-122 Acts as a Modulator of Parasitic Infection in *L. donovani*-Infected Mouse Liver

(A and B) Downregulation of miR-122 in *L. donovani*-infected mouse liver. Liver miR-122 levels in *L. donovani*-infected BALB/c mice were quantified by real-time quantification. U6 small nuclear RNA (snRNA) was used for normalization. miR-122 content in age-matched noninfected animals were used as reference value (A). Northern blot to detect miR-122 changes in infected mouse livers (B). Ethidium bromide (EtBr)-stained gel was used for loading control. For real-time quantification $n = 8$ for each time point.

(C) Levels of AGO2 and RCK/p54 protein in *L. donovani*-infected mice. Western blot analysis for AGO2 and RCK/p54 proteins in liver extracts from normal and infected animals. β -actin was used as loading control.

(D) Changes in expression of miR-122 and the serum cholesterol level in mice after introduction of miR-122 expression plasmid pmir122 through tail vein injection. Animals were sacrificed after indicated time; liver miR-122 and serum cholesterol levels were measured.

(E) A schematic representation of the time course of exogenous miR-122 expression in infected mouse liver. Infection time is marked by a white arrow, and the black arrow defines the time of sacrifice 30 days p.i. The black arrowheads mark the injection time of miR-122 expression plasmids.

(F–H) Effect of upregulation of miR-122 on infection level in mouse livers. Infected animals were treated as per the schedule described in (E) and were sacrificed after a month. Relative miR-122 expression (F), serum cholesterol level (G), and hepatic parasite load (H) were compared in pmir122-treated versus sham-treated groups. Data represent mean \pm SEM. For all experiments, $n = 8$. *** $p < 0.0001$, ** $p < 0.001$. L.d, *L. donovani*. See also Table S3 and Figure S2.

a rate-determining enzyme in cholesterol biosynthesis (fold downregulation = 2.9), and *FASN* (fatty acid synthase), controlling fatty acid synthesis (fold downregulation = 2.7), are known to be reciprocally regulated by miR-122 (Esau et al., 2006). Connection between miR-122 and lipid metabolism is well documented in mammals (Girard et al., 2008). Therefore, we

may expect reduced miR-122 activity in *L. donovani*-infected livers. Levels of miR-122 in the total RNA isolated from the livers of normal and infected animals were determined. Real-time quantification revealed a gradual downregulation of miR-122 in mouse livers with progressive infection (Figure 3A). Northern blot analysis corroborated this finding (Figure 3B). A

similar decrease in the miR-122 level was also observed in animals infected with *L. donovani* amastigotes (Figure S2A). Reduced miR-122 activity could not be due to lower expression of miRNP components, as we did not find any reduction in miRNP-interacting protein RCK/p54 in infected livers (Figure 3C). Interestingly, AGO2, the key miRNP component, showed an increased expression in infected liver. Therefore, *L. donovani* infection reduces liver miR-122 to control the serum cholesterol level.

Exogenous Expression of miR-122 Can Rescue Serum Cholesterol and Clear Hepatic Parasite Load

In order to understand the significance of miR-122 downregulation during the *L. donovani* infection process, we aimed to complement the reduced miR-122 level in the livers of infected animals. To that end, we injected pmir122, a miR-122 expression plasmid with a constitutive U6 promoter, in noninfected mouse via tail vein and monitored miR-122 levels in its liver until 7 days postinjection. The miR-122 level was increased and was at a maximum after 3 days, whereas the serum cholesterol level started to show changes at 3 days and reached a maximum at 5 days p.i. (Figure 3D). To highlight the protective role of miR-122, we injected miR-122 expression plasmid in animals after 15 days p.i. when initial infection was already established. Animals received three doses of pmir122 injection, and the parasite load was monitored at 30 days p.i. (Figure 3E). We documented an increase in miR-122 level with a concomitant elevation in serum cholesterol (Figures 3F and 3G). This also induced reversal of expression of key cholesterol metabolic genes (data not shown). Interestingly, the hepatic parasite load was reduced significantly compared to sham-treated control animals (Figure 3H) showing the protective action of miR-122 against *L. donovani* infection.

L. donovani Interacts with Human Hepatocytes and Impairs miRNA-Mediated Repression

The in vivo experiments described above confirmed the lowering of miR-122 in *L. donovani*-infected mouse liver. In liver, *L. donovani* infects the tissue macrophage K pffer cells, but how the infection of K pffer cells induces miR-122 downregulation in hepatocytes is not known. To understand the mechanism of hepatic miR-122 downregulation in infected animals, we used human Huh7 hepatoma cells that express miR-122. Huh7 cells were transfected with a *Renilla* luciferase reporter either with no miRNA binding sites (RL-con) or with three imperfect miR-122 binding sites (RL-3xbulge-miR-122; Figure 4A) to assess the miR-122 activity in Huh7 cells before and after interaction with *L. donovani*.

To imitate the liver microenvironment, we cocultured Huh7 cells (expressing RL reporters) with isolated human peripheral blood mononuclear cells (PBMC) in the presence and absence of *Leishmania* parasites at different cell-to-parasite ratios; the monocyte in PBMC served as the parasite host and Huh7 cells as hepatocytes. There was essentially no change in miR-122 activity when Huh7 and PBMC were cultured in the absence of the parasite (data not shown). For a fixed number of Huh7 cells, with an increase in PBMC-to-parasite ratio, there was a moderate change in miR-122-mediated repression in Huh7 cells (Figure 4C). It is possible that a host secretory factor, probably

a pro- or anti-inflammatory cytokine, secreted by the infected macrophage/monocyte cells changes the hepatic microenvironment that leads to compromised miR-122 activity. To test this hypothesis, we cultured Huh7 cells with *Leishmania*-infected whole PBMC supernatant. No significant changes were observed, even at the highest PBMC-to-parasite ratio (Figure 4B).

From the above experiments it was evident that the parasite itself is the probable candidate to cause the effect on hepatic miR-122. In order to ascertain the importance of direct interaction between Huh7 and *Leishmania* for impairment of miR-122 activity in hepatocytes, we used isolated amastigotes or transformed promastigotes of *L. donovani* to test their effect, if any, on miR-122 activity in human hepatoma cells. Huh7 cells were incubated with *L. donovani* promastigotes at different cell-to-parasite ratios for 24 hr. There was a gradual reduction in repression level with an increasing parasite number per Huh7 cell (Figure 4D). A similar result was obtained when the amastigote form of the parasite was used (Figure 4E). Although upon interaction with the parasite no appreciable change in cellular transcription machineries was observed, a drastic reduction in protein translation was evident in *L. donovani*-treated Huh7 with an overall decrease in proliferation of *L. donovani*-interacting Huh7 cells (Figures S3A–S3C).

Is a parasite-derived secretory factor required for downregulation of miR-122 activity in target cells? Huh7 cells were treated with cell-free *L. donovani* culture supernatant grown at 22 C, the temperature of leishmanial growth at the gut of the sandfly vector. The supernatant could not show any effect on miR-122 activity in Huh7 cells (Figure 4F), but supernatant of the *Leishmania* culture grown at 37 C, the temperature the parasite encounters in mammalian hosts, can reduce miR-122 activity in Huh7 cells (Figure 4F). Thus, *Leishmania*-free culture media at 37 C should contain a factor(s) that can mediate the anti-miR-122 activity in hepatocytes.

Leishmania Glycoprotein gp63 Is Responsible for Reversal of miR-122-Mediated Repression in Huh7

Leishmania exosomes, the secretory vesicles released by the parasite, have been documented previously as the carrier of the virulence factors for cellular communication. It is also known that high temperature and low pH increase the rate of exosome secretion by *Leishmania* (Silverman et al., 2010). Hence, we speculate that the exosomes released by the parasites grown at 37 C may contain the key component(s) required for the lowering of miR-122 activity in Huh7 cells. In order to investigate this possibility, we purified exosomes from cell-free *Leishmania* culture supernatant grown at 37 C.

Isolated *L. donovani* exosomes showed reduced miR-122-mediated repression, whereas control exosomes isolated from the culture media kept at 37 C without the parasite showed no difference in miR-122-mediated fold repression compared to untreated cells (Figures 4G and 4H). Previous exploration of the *Leishmania* exosomal cargo proteins revealed that one of the virulence factors, gp63 (a Zn²⁺ dependent metalloprotease), is an abundant protein in *Leishmania* exosomes (Silverman et al., 2010). Preincubation of *Leishmania* exosomes with o-Phenanthroline, a Zn²⁺ chelator and an inhibitor of Zn²⁺ metalloproteases, had an inhibitory effect on the ability of *Leishmania*

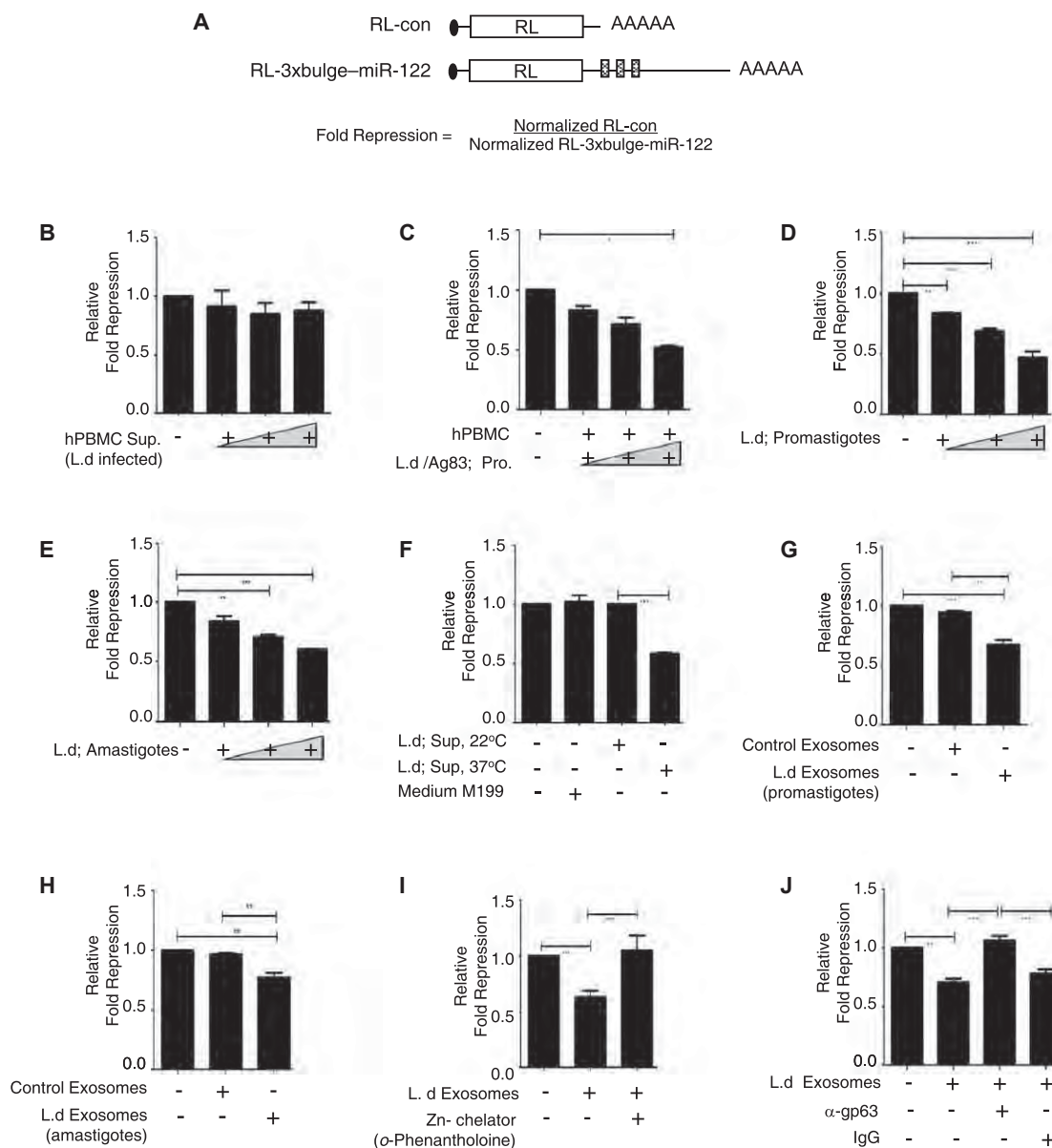


Figure 4. Inhibition of miR-122 in Huh7 Cells by *L. donovani*

(A) Schematic picture of the miR-122 reporter used to measure the miR-122 activity in Huh7 cells. For relative fold repression, the calculation level of repression for controls was always settled to 1.

(B–E) Modulation of miR-122 activity in Huh7 cells by *L. donovani*. Huh7 expressing either the RL-con or RL-3 × bulge-miR-122 *Renilla* luciferase reporter along with firefly luciferase encoding control mRNA were grown and treated differently (as described below) before the luciferase activities were measured and relative fold repression values calculated. (B) Huh7 cultured with *Leishmania*-infected human PBMC supernatant. (C) Huh7 cocultured with human PBMC and with increasing numbers of *L. donovani* parasite. Huh7 cultured with *L. donovani* promastigotes (1:1, 1:10, 1:100) (D) or amastigotes (1:1, 1:10, 1:100) (E).

(F–J) Exosomes released by *L. donovani* affects miR-122 activity in Huh7 cells. As described above, Huh7 cells expressing miR-122 reporter or control mRNAs were treated with *L. donovani* culture supernatant (grown at either 22°C or 37°C) or control medium used for parasite growth (M199), and fold repression values were calculated (F). Exosomes isolated from the *L. donovani* promastigote-grown (G) or amastigote-grown (H) medium or control medium were also used to test its effect on miR-122-mediated repression. In similar experiments, *L. donovani* exosomes either pretreated with the Zn-chelator α -Phenanthroline (I) or anti-gp63 antibody (J) were used to score their effect on exosome-dependent inhibition of miRNA-mediated repression. Normal IgG was used as a control. Data represent mean \pm SEM. Significance level, * $p < 0.05$, ** $p < 0.001$, *** $p < 0.0001$. Ld, *Leishmania donovani*. See also Figure S3 and Movie S1.

exosomes to reverse miRNA action in Huh7 cells (Figure 4I). A rabbit polyclonal antibody raised against *L. donovani* gp63 was used to block its activity in vitro (Bhowmick et al., 2008). Exosomes preblocked with this anti-gp63 antibody could not

prevent the miRNA repression, whereas pretreatment with normal rabbit immunoglobulin G (IgG) failed to reverse the inhibitory role of leishmanial exosomes on miR-122 activity in Huh7 cells (Figure 4J). Overall, these experiments suggest that gp63

glycoprotein, a *Leishmania* exosomal component, is responsible for the anti-miR122 activity observed in Huh7 cells.

Internalization of *Leishmania* Exosomes Is Essential for miR-122 Downregulation in Hepatocytes

Entry of *L. donovani* or parasite-derived exosomes into host cells is well documented (Silverman et al., 2010). No such direct evidence is reported for cellular entry of either intact *Leishmania* or *L. donovani* exosomes in liver parenchymal cells. From the previous experiments it was evident that the exosomes caused downregulation of miR-122 activity in human hepatoma cells, but it was not clear whether the internalization of the exosomes in hepatocytes is required or if its interaction with the membrane of Huh7 cells is sufficient for lowering miR-122 activity. Immunofluorescence analysis showed internalization of gp63 in Endo-GFP-expressing Huh7 cells that were treated with *L. donovani* exosomes. In exosome-treated Huh7 cells, the Endo-GFP-tagged early endosomes were either colocalized or showed proximal localization with gp63 (Figure S3D). Three-dimensional reconstitution of the z-stacked images obtained with a spinning disc confocal microscope was used to confirm the colocalization of the gp63 signal with early endosomes (Figure S3E; Movie S1). Therefore, the entry pathway of *Leishmania* gp63 to Huh7 cells is possibly endosomal. In subsequent experiments with Endo-GFP-expressing Huh7 cells treated with siRNA against dynamin 2, a GTPase involved in membrane trafficking of vesicles (Durieux et al., 2010) showed no internalization or co- or proximal localization of gp63 with Endo-GFP inside the hepatocytes. GFP-tagged endosomes in cells treated with control siRNA showed dynamin 2 colocalization with Endo-GFP and gp63 (Figures S3F and S3G). Downregulation of gp63 internalization in dynamin 2-compromised cells also reduced the effect of exosomes on miR-122-mediated repression in Huh7 (Figure S3H).

Do intact parasites internalize inside the hepatocytes? When incubated with live *L. donovani*, parasitic nuclear DNA stained with DAPI and proximally localized with gp63 signals in intact parasites was absent in Huh7 cells but visible in murine peritoneal macrophages. This suggests an absence of intracellular parasites in infected hepatic cells (Figure S4A and S4B).

In infected mouse liver, immunofluorescence staining for gp63 identified infected regions with elevated gp63 signal that faded out with distance from the zone of infection. Interestingly, apart from the intracellular signals of gp63 inside the hepatocytes surrounding the infected region, strong signals from gp63-positive vesicles/bodies along the intercellular space between hepatocytes were evident (Figure S4C).

Accumulation of Pre-miR-122 and Failed miRNP-122 Formation Accounts for the Reduced miR-122 Activity in *L. donovani*-Treated Huh7 Cells

Interestingly, unlike the mature form, the pre-miR-122 increased in both parasite-infected mouse livers and *L. donovani*-treated Huh7. Real-time quantification of pre-miR-122 confirmed accumulation of the precursor form with progressive infection, which augmented to 3-fold higher than its normal level at 60 days p.i. (Figure 5A). The pre-miR-122 also increased 2.5-fold in Huh7 cells after its interaction with *L. donovani* (Figure 5B).

Why should the precursor accumulate in *L. donovani*-interacting hepatic cells? In eukaryotes, pre-miRNAs are cleaved and

processed by an RNase III enzyme, DICER1. This protein processes the pre-miRNAs and loads the processed mature miRNA to AGO proteins to form active miRNPs (Bartel, 2004). When the AGO2 protein was immunoprecipitated from normal and infected Huh7 cell lysates, we documented a 6-fold reduction of miR-122 association with immunoprecipitated AGO2 in *L. donovani*-treated Huh7 (Figure 5C). The observation was similar when miR-16 association with AGO2 was measured (data not shown). These results signify an impaired processing of precursor miRNAs as a mechanism that leads to reduced miRNP formation, which accounts for lowered miRNP activity in *L. donovani*-interacting hepatic cells.

gp63 Cleaves DICER1 to Prevent Effective miRNP Formation and Inhibits miR-122 Activity in Human Hepatocytes

From the previous experiments it was evident that AGO2 failed to get loaded with miR-122 and form active miRNP in *L. donovani*-exposed hepatic cells. Hence, it was essential to look at the status of Dicer1 in infected tissue samples. We detected a low level of Dicer1 in infected livers after 60 days p.i. as well as in Huh7 treated with *L. donovani* (Figure 5D). Over-expressed DICER1 in Huh7 cells inhibited the derepression of miR-122 activity by *L. donovani* (Figure 5E). Interestingly, when a miR-122 mimic that does not require the DICER1 processing step was transfected in Huh7 cells, the inhibition of miRNA activity by *Leishmania* was lost. However, in Huh7 cells expressing exogenous pre-miR-122 that required DICER1 processing to generate miRNP-122, *L. donovani*-mediated reversal of miR-122 activity was unaffected (Figure 5F). These results further confirm Dicer1 as the primary target of *Leishmania* to downregulate miR-122 activity in mammalian liver. We anticipate degradation of DICER1 by a *Leishmania*-derived factor in target hepatic cells. We observed that HA-tagged DICER1 expressed in Huh7 cells was cleaved in the presence of *Leishmania* lysate when incubated in vitro (Figure 5G). The cleavage of DICER1 was primarily by a Zn-metalloprotease, as the DICER1 degradation was prevented in the presence of o-Phenanthroline (Figure 5G). This experiment indicates that gp63, the most abundant Zn-metalloprotease present in leishmanial exosomes, is responsible for DICER1 cleavage. That was further tested when purified gp63 was incubated with DICER1 in an in vitro reaction. Purified gp63 cleaved DICER1 and generated the same fragments obtained with the leishmanial extract. A cleaved N-terminal fragment of 180 kDa was generated along with a shorter C-terminal half (Figure 5H). The specificity of gp63 in Dicer1 cleavage reaction was further confirmed in experiments in which blocking with a polyclonal antibody reduced the activity of purified gp63. Interestingly, the monoclonal antibody treatment augmented the activity of gp63 (Figure 5I), possibly due to a change in its conformation upon antibody binding as reported earlier for few other enzymes (Benito et al., 1996; Cooper and King, 1986). DICER1 associates and transfers the processed mature miRNA to AGO2 to form miRNPs. In cell extract treated with gp63, we also found reduced association of AGO2 with full-length DICER1, resulting in decreased pre-miR-122 processing (Figure 5J). Therefore, *L. donovani* targets DICER1 to prevent active miRNP formation.

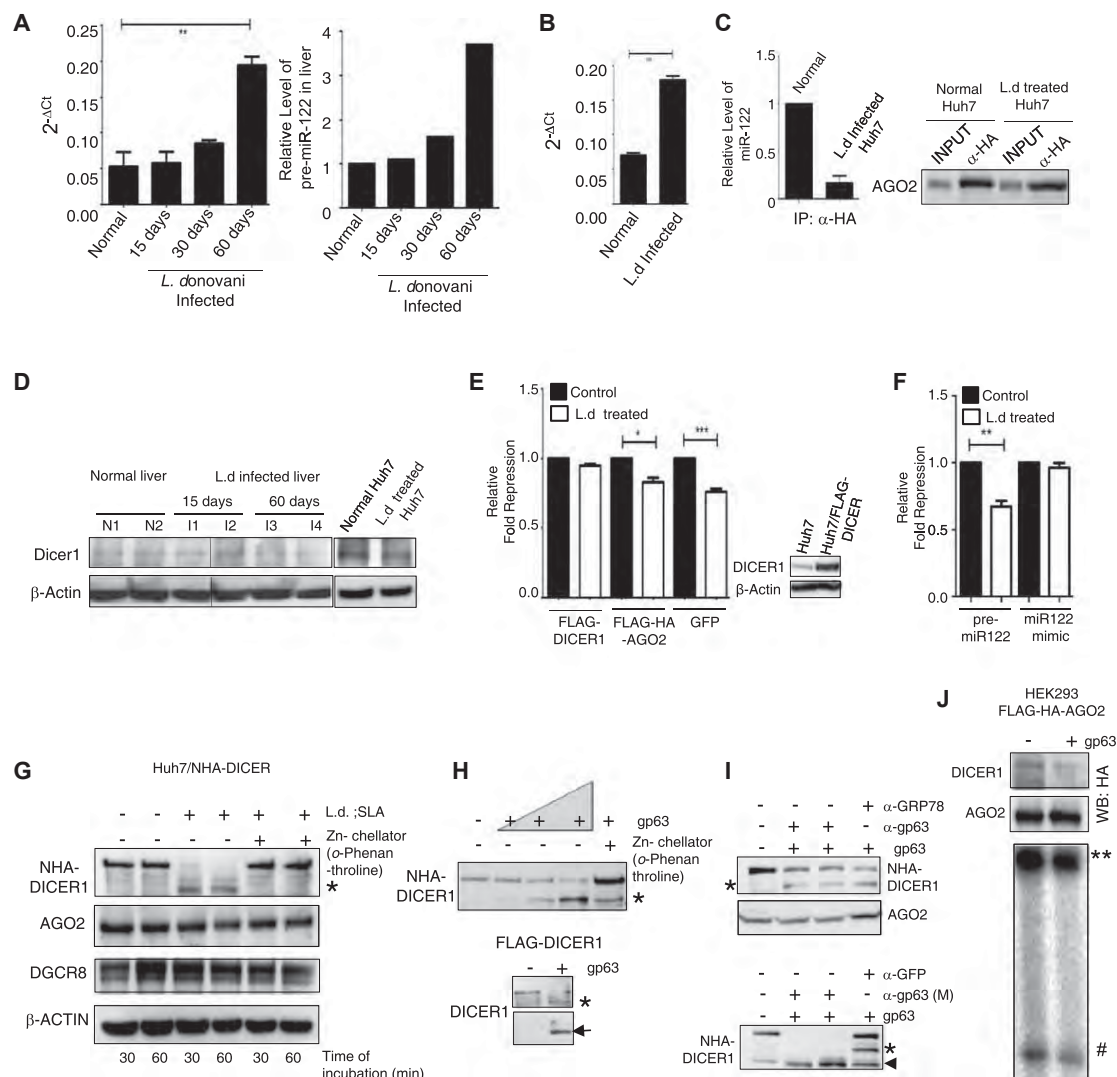


Figure 5. *L. donovani* Downregulates DICER1 and Prevents miRNP Formation in Huh7 Cells

(A) *L. donovani* increases pre-miR-122 levels in livers of *L. donovani*-infected animals. RNA isolated from the livers of BALB/c mice after 15, 30, or 60 days infected were subjected to real-time analysis, and β-actin mRNA levels were used for normalization. n = 6 for each group.

(B) pre-miR-122 levels in Huh7 cells before and after treatment with *L. donovani* promastigotes for 24 hr. Real-time quantification for pre-miR-122 was performed. SDs were from three independent measurements.

(C) Association of miR-122 with AGO2 in Huh7 cells interacted with *L. donovani*. RNA was isolated from immunoprecipitated (IP) materials from normal and infected cell lysates, and miR-122 levels were quantified by real-time quantification and normalized against immunoprecipitated AGO2. Quantification data are the mean values obtained from three IP reactions. Western blot was used to detect AGO2 in immunoprecipitated materials.

(D) Dicer1 levels in *Leishmania*-infected animal livers. Protein extracts were prepared from normal and infected mouse livers (15 or 60 days p.i.) and western blotted for Dicer1. Huh7 cells treated with *L. donovani* also showed reduction in DICER1 levels.

(E) Exogenous expression of DICER1 inhibits *L. donovani*-mediated inhibition of miR-122 activity in Huh7 cells. Cells expressing RL reporters were transfected with plasmids encoding FLAG-DICER1, FLAG-HA-AGO2, or GFP, and the effects of *L. donovani* on miR-122 activity was scored. DICER1 overexpression was confirmed by western blot.

(F) Unlike pmir-122 overexpressed cells, cells transfected with miR-122 mimics can escape *L. donovani*-mediated repression of miR-122 activity. miR-122 repressive activity was measured in normal and *L. donovani*-interacting Huh7 cells expressing pre-miR-122 or miR-122 mimic.

(G) DICER1 can be specifically cleaved by the Zn-metalloprotease present in the SLAs. Huh7 extracts were incubated with SLA in the presence and absence of Zn-chelator for 30 or 60 min at 37°C and were western blotted for HA-DICER1, AGO2, and DGCR8. β-actin was used as loading control.

(H) *L. donovani* surface protease gp63 cleaves DICER1 and generates two fragments in vitro. Lysates of HEK293T cells expressing NHA-DICER1 were incubated with an increasing concentration of purified gp63 in the absence and presence of Zn-chelator, and cleaved product was visualized by western blot using an HA-specific antibody. It detected a shortened DICER1 band that was ~180 KDa after cleavage of full-length protein by gp63. Digestion of FLAG-DICER1 also generated a 180 KDa fragment (marked by *). The N-terminal and short C-terminal half (marked by an arrowhead) of DICER1 were both detected with a DICER1-specific antibody.

(I) Treatment with specific polyclonal and/or monoclonal antibody modify gp63 activity in vitro. Blocking of gp63 with a polyclonal antibody raised against the recombinant protein reduces DICER1 cleavage activity. Anti-GRP78 antibody was used as control (upper panel). Pretreatment of gp63 against a monoclonal

(legend continued on next page)

Restoration of Dicer1 Expression in Parasite-Infected Livers Rescues miR-122 Expression and Reduces Liver Parasite Burden

When expressed exogenously, NHA-DICER1 expression was found to be low in *L. donovani*-infected mouse livers (Figure 6A). This observation was consistent with the prediction of Dicer1 as a target that *L. donovani* degrades to downregulate miR-122 in infected mouse liver. With infection, the level of gp63 was increased in mouse livers (Figure 6B). To confirm that gp63 can downregulate Dicer1 in vivo, purified gp63 from *L. donovani* extract was entrapped in liposomes before being delivered to Huh7 cells. Interestingly, a substantial decrease in miR-122 activity was noted in cells receiving gp63-containing liposomes (Figure 6C). These liposomes were found to be more enriched in mouse livers 24 hr after in vivo delivery (Figure S5A) and were subsequently used for in vivo administration of gp63 in BALB/c mice expressing NHA-DICER1. Delivery of gp63 to liver was confirmed by western blot (Figure 6D). Interestingly, the level of NHA-DICER1 was significantly low in the livers of animals treated with gp63-containing liposomes (Figure 6E). During infection, exosomes may be the vehicles for gp63 transfer to hepatocytes (Figures S3 and S4C). Delivery of purified *L. donovani* exosomes downregulated DICER1 in animal livers (Figure 6F).

To see whether DICER1 overexpression can clear *L. donovani* from infected mouse liver, we administered NHA-DICER1-expressing plasmids (Figure 6G). Excess Dicer1 in liver increased liver miR-122 expression and restored the serum cholesterol level (Figures 6H and 6I). This was accompanied with a drastic reduction in liver parasite load (Figure 6J). Importantly, no apparent change in liver cell morphology, tissue integrity, or production of serum albumin was documented (Figures S5B and S5C).

DISCUSSION

In *L. donovani*-infected mouse liver, almost 20% of the total genes showed an altered expression. Several genes of cholesterol metabolism that are indirect targets and reciprocally regulated by miR-122 (Elmén et al., 2008) were downregulated along with miR-122 in *L. donovani*-infected liver. Animals manipulated to have excess miR-122 levels in their livers showed resistance to *L. donovani* infection (Figures S2B–S2E). This observation further supports the existence of a balance of liver miR-122 and serum cholesterol that get influenced and exploited by *Leishmania* parasites in infected mammals. Therapy against VL is still a big challenge, and recently, the emergence of drug resistance has added to the problem (Croft et al., 2006). Overexpressing miR-122 in infected liver tissue showed appreciable clearance of hepatic parasite burden with a recovery of serum cholesterol. Therefore, the therapeutic potential of miR-122 alone and in combination with cholesterol can open up avenues to combat this deadly disease.

L. donovani infection in mice shows a decrease in liver DICER1 expression accompanied by a concomitant increase of its substrate pre-miR-122. Pre-let-7a RNA also showed similar accumulation in infected mouse livers (data not shown). Therefore, this might be a general mechanism for *Leishmania* to lower the activities of miRNAs in the host cell. Interestingly, *L. donovani* infection also leads to the lowering of Dicer1 and let-7a miRNA in infected mouse macrophages (J.G., Y. Chakraborty, and S.N.B., unpublished data).

Inactivation of specific miRNA by virus-encoded target RNAs or virus-encoded miRNA binding proteins in virus infected cells has been reported previously (Belair et al., 2011; Cazalla et al., 2010; Libri et al., 2012). Here, we report a leishmanial protease gp63 that targets Dicer1 to reduce miRNA activity in hepatic cells. But how the gp63, produced by the Küpffer cell resident parasites, gets transferred to the neighboring target hepatocytes is an unsolved issue. The *Leishmania* exosomes may act as the vehicles for transport of gp63 cargo to the hepatocytes in mouse liver. This idea was supported by downregulation of DICER1 expression in liver upon exposure to *Leishmania* exosomes (Figure 6F). Interestingly, mammalian macrophages are also known to secrete exosomes and microvesicles that are used for intracellular transport and signal communication (Bhatnagar et al., 2007). Therefore, it may be possible that parasite-released gp63 get trapped within the exosomes secreted by the host cells and get delivered to hepatocytes to target Dicer1 and reduce miRNA activity. Immunofluorescence detection of gp63 in infected livers was suggestive of propagation of this protease through the intercellular spaces in *L. donovani*-infected livers.

Overall, the present study deals with an interesting connection between altered lipid metabolism during *L. donovani* infection and liver miR-122 levels. We report an alteration of a miRNA in a parasite-infected tissue that can account for an important metabolic change necessary for pathogenesis. This also documents a unique strategy that the parasite evolved to combat regulatory RNA function in host cells. With human hepatic cells, we have shown that leishmanial metalloprotease gp63 targets DICER1 in human hepatic cells to reduce miR-122 activity. A similar mechanism is operative for downregulation of miRNA activity in *L. donovani*-infected mouse liver. It will be interesting to investigate whether other members of the Trypanosomatidae family have evolved a similar mechanism for their survival in infected host.

EXPERIMENTAL PROCEDURES

Infection Delivery and Postinfection Analysis

L. donovani strain AG83 (MAOM/IN/1083/AG83) was used to infect 4- to 6-week old BALB/c mice with 2nd passage promastigotes or amastigotes (10⁷ parasites/animal) by the intracardiac route. After stipulated days of infection, blood serum was collected and liver extract was used for RNA or protein analysis. Liver sections were used for histological examination,

antibody augments its activity in DICER1 cleavage assay (lower panel). Anti-GFP antibody was used as control. The arrowhead denotes a secondary cleaved product increased in the presence of anti-gp63 monoclonal antibody.

(J) The cleavage of AGO2-associated NHA-DICER1 by gp63 and its effect on pre-miRNA processing. Extracts of HEK293 stably expressing FLAG-HA-AGO2 and transfected with NHA-DICER1 were digested with purified gp63 and subsequently FLAG-HA-AGO2 was immunoprecipitated. FLAG-HA-AGO2-associated DICER1 was detected by western blot, and pre-miR-122 processing activities associated with immunoprecipitated materials were quantified. ** denotes the pre-miR-122 substrate; # denotes the mature miR-122 formed; WB, western blot. Data represent mean \pm SEM. See also Figure S4.

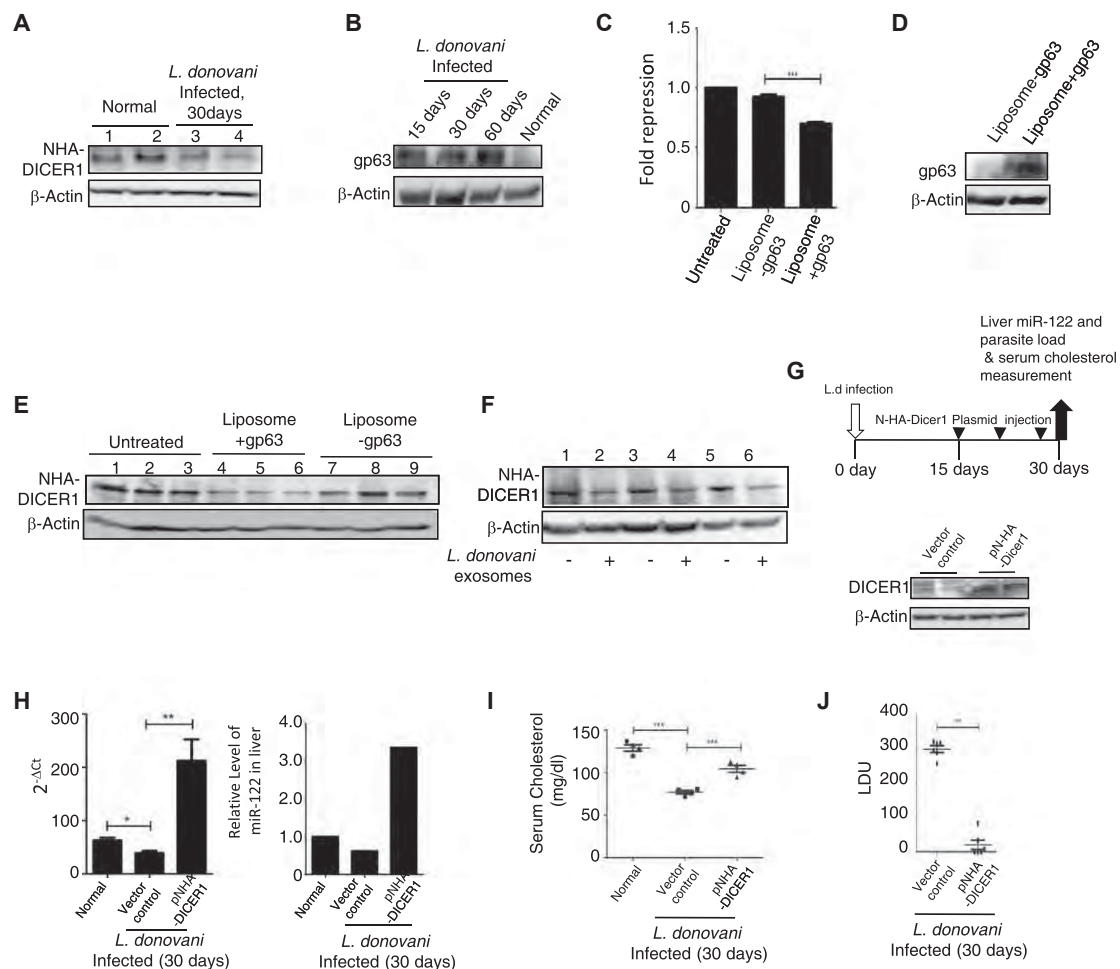


Figure 6. Restoration of Dicer1 Expression Rescues Serum Cholesterol Levels and Lowers Hepatic Parasite Load in *L. donovani*-Infected Mouse Livers

(A) Dicer1 expression in *L. donovani*-infected mouse liver. Expression of NHA-DICER1 in the livers of control or infected (30 days p.i.) *L. donovani* BALB/c mice three days postinjection of NHA-DICER1 expression plasmid through tail vein.

(B) Increase of gp63 in infected mouse liver extracts western blotted for gp63.

(C) Effects of liposomal delivery of gp63 on miR-122 activity in Huh7 cells. Liposomal formulations with or without purified gp63 were delivered to cells expressing miR-122 reporter, and fold repression was calculated.

(D) Treatment with gp63-containing liposomes delivers the protein to animal liver. Western blot detection of gp63 was done in liver lysates from control and liposome-treated animals using an anti-gp63 antisera.

(E) Effect of gp63-containing liposomes on liver DICER1. Adult BALB/c mice were injected first with NHA-DICER1-expressing plasmids and then with liposomes (100 μ l liposome suspension with or without 100 μ g of purified gp63). Liver lysates were prepared after 24 hr of liposome injection and western blotted for NHA-DICER1.

(F) Effect of *L. donovani* exosome treatment on the mouse liver DICER1 level. Adult BALB/c mice expressing NHA-DICER1 protein were injected through the intracardiac path with *L. donovani* exosomes secreted by 5×10^7 parasites. After 24 hr of exosome treatment, liver lysates were prepared and western blotted for the NHA-DICER1.

(G) Expression of NHA-DICER1 increases cellular Dicer levels in mouse livers. Schematic representation of protocol of NHA-DICER1 expression in BALB/c mice livers (upper panel). Endogenous Dicer1 levels in both normal and NHA-DICER1 expression-plasmid-injected mouse livers after 3 days of plasmid injection (Lower panel).

(H–J) NHA-DICER1 can prevent infection progression in mice. *L. donovani*-infected animals were injected with NHA-DICER1 expression plasmids and sacrificed as per the schedule in (G). Relative miR-122 expression (H), serum cholesterol level (I), and hepatic parasite load (J) were compared between NHA-DICER1 plasmids injected and control groups. For all experiments, n was either 4 or 6, and representative western blots were shown. For all western blot experiments β -actin was used as loading control. Data represent mean \pm SEM. ***p < 0.0001, **p < 0.001, *p < 0.01. See also Figure S5.

and parasite count was accomplished by microscopic evaluation of Giemsa-stained tissue imprints. Leishman-Donovan unit (LDU) = number of amastigotes/1,000 nucleated cells \times weight of spleen or liver (g).

All animal experiments approved by the institutional animal ethics committee were carried out following the national guidelines set by the government of India.

Parasite Transformation, Amastigote Isolation, Culture Supernatant Collection, and Soluble Leishmanial Antigen Preparation

Amastigotes were isolated from *L. donovani*-infected golden hamsters. They were either used directly or transformed to promastigotes and maintained until the second to fourth passage cultures before the promastigotes were used. Culture supernatants used for in vitro assays were collected from

cultures grown at 22°C and 37°C. Soluble leishmanial antigen (SLA) was prepared after sonication of the promastigotes as described elsewhere (Saha et al., 1991).

Whole-Genome Microarray Analysis

Microarray analysis was done on an Illumina Sentrix Chip (Mouse WG-6 v2.0 Beadchip) using total RNA isolated from normal mouse livers and *L. donovani*-infected mouse liver after 60 days. TCGA Catalyzing Genomics (New Delhi, India) performed the analysis, and the data were analyzed after background noise correction and normalization. Differential expression analysis was done using Illumina custom algorithm. All the data have been filtered based on detection; differential p value ≤ 0.05 . The whole microarray data have been uploaded in Gene Expression Omnibus database (accession number GSE38985).

Exogenous Expression of miR-122 and Dicer in Mouse Liver

Exogenous expression studies were conducted according to a published hydrodynamic injection strategy (Tada et al., 2006; Andrianaivo et al., 2004). To overexpress miR-122 or NHA-DICER1 in mouse livers, pmiR-122, the pre-miR-122 expression plasmid, or the pCIneoNHA-DICER1 plasmid was injected through the tail vein of mice at a dose of 25 μ g plasmid DNA dissolved in 100 μ l saline. Animals weighing 20–25 g were used and sacrificed at 1, 3, 5, and 7 days postinjection to determine liver miR-122 levels. For NHA-DICER1 expression examination, animals were sacrificed after 3 days. In experimental animals, injections were delivered to *L. donovani*-infected mice in three individual doses starting from 15 days p.i. at intervals of 6 days. Mock plasmid-treated (100 μ l each) animals were kept as sham-treated controls. Animals were sacrificed at 30 days p.i. along with the control group of animals, and serum lipid profile, liver parasite burden, and miR-122 expression levels were determined.

Cell Culture, Transfection, Treatment, and Luciferase Assays

Huh7 cells were cultured, and all transfections were performed using Lipofectamine 2000 (Invitrogen) following manufacturer's instructions. *Renilla* luciferase (RL) and firefly luciferase (FL) activities were measured using a Dual-Luciferase Assay Kit (Promega) measured on a VICTOR X3 Plate Reader system (PerkinElmer), and fold repression was calculated.

Northern and Western Blot Analyses

Total RNA isolated from mouse liver was electrophoresed in 15% denaturing TBE-Urea polyacrylamide gel and transferred to Immobilon-NY+ transfer membrane. It was probed with 5' end 32 P-labeled oligonucleotide probes against hsa-miR-122 at 37°C for 16 hr in a hybridization oven. Phosphorimaging was performed with a Cyclone Plus Storage Phosphor System (PerkinElmer). Liver tissue proteins were extracted in RIPA buffer, separated using SDS-PAGE, transferred to polyvinylidene fluoride (PVDF) membrane, and western blotted for different proteins using specific antibodies. β -actin was used as a loading control. gp63 was detected in liposome-treated mouse livers by western blot against antisera to gp63.

Real-Time Quantitative RT-PCR

The miR-122, miR-16, and U6 levels were quantified with a real-time RT-PCR detection assay kit (Applied Biosystems) from total RNA following the manufacturer's instructions. mRNA and pre-miRNA quantifications were done using the SYBR Green Real-Time PCR Assay Kit (Invitrogen). The results were normalized against 18S ribosomal RNA (rRNA) for mRNAs and against β -actin for pre-miR-122.

Exosome Isolation and Treatment

Stationary-phase *L. donovani* promastigote or amastigote ($\sim 5.0 \times 10^7$ cells/ml) culture was kept at 37°C overnight. As a control, M199 medium supplemented with 10% fetal calf serum (FCS), but without the parasites, was used. Exosomes were isolated as described earlier (Raposo et al., 1996) with minor modifications. For further treatment, exosomes (100 μ g protein per assay) were incubated for 1 hr at room temperature with *o*-Phenanthroline or 4°C overnight with anti-gp63 antibody before the exosomes (treated or untreated) were used in subsequent assays with Huh7 cells.

Immunoprecipitation

For immunoprecipitation (IP) reactions, HA-AGO2-transfected cells were lysed and incubated with anti-HA (Roche) bound protein G agarose beads overnight at 4°C. As control, anti-GFP bound protein G agarose beads (Invitrogen) were used. After that, the beads were washed thrice with IP buffer, and the bound proteins were analyzed by western blot. Half of the beads separated during washing steps were used for RNA extraction.

In Vitro DICER1 Cleavage Assay

For in vitro cleavage assay, NHA-DICER1 expressing Huh7 cell extract was incubated with *L. donovani* SLA or purified gp63 in buffer containing 10 mM Tris-HCl (pH 7.5), 1 mM DTT, 100 mM KCl, and 1 \times protease inhibitor cocktail. Incubation was done at 37°C for 30 or 60 min. The reactions were stopped with SDS sample buffer. For the *o*-Phenanthroline treatment, SLA was preincubated with 10 μ M *o*-Phenanthroline for 30 min on ice before being used for the assay. For testing the purity of isolated gp63, a mouse monoclonal and a polyclonal anti-gp63 antibody were used to block gp63 activity at 1:10 and 1:25 dilutions overnight. Anti-GFP and anti-GRP78 were used at the same dilutions as the control. The samples were run in 8% SDS-PAGE, and western blot was performed using anti-HA antibody to detect NHA-DICER1.

In Vitro Pre-miRNA Processing Assay

The NHA-DICER1 expressing HEK293 cell lysate was incubated with purified gp63 followed by immunoprecipitation with anti-FLAG M2 affinity gel. Washed beads were used for pre-miR122 processing assay with 10 nM pre-miR122, and the products were analyzed on a 12% denaturing (8 M Urea) polyacrylamide gel and visualized in a phosphorimager.

Introduction of Liposomes and *L. donovani* Exosomes in BALB/c Mice

Adult BALB/c mice were injected with NHA-DICER1-expressing plasmids via tail vein. After 2 days, liposomal formulations or leishmanial exosomes were injected through the intracardiac route. After 24 hr, mice were sacrificed, liver lysates were prepared, and exogenous DICER1 levels were detected by western blot analysis using anti-HA antibody. For liposome treatment of Huh7 cells, luciferase reporter transfected cells were treated with 200 μ l liposome suspension.

Other Experimental Procedures and Details

Additional experimental procedures and other essential details on plasmids, oligos, and antibodies used have been provided as [Supplemental Experimental Procedures](#).

ACCESSION NUMBERS

The Gene Expression Omnibus (GEO) accession number for the whole-genome microarray expression data reported in this paper is GSE38985.

SUPPLEMENTAL INFORMATION

Supplemental Information includes five figures, three tables, one movie, and Supplemental Experimental Procedures and can be found with this article online at <http://dx.doi.org/10.1016/j.chom.2013.02.005>.

ACKNOWLEDGMENTS

We acknowledge support from the Wellcome Trust, UK International Senior Research Fellowship fund; the Career Development Award fund of HFSP, and CSIR research grant BSC0114. J.G. and M.B. were supported by the University Grant Commission (UGC) and CSIR fellowship. S.R. acknowledge support from CSIR Network Project NWP0005. We are also thankful to Witold Filipowicz and Nahid Ali for providing us with plasmid constructs and antibodies. We acknowledge Kshudiram Naskar, Rajan Guha, and Sukanta Jash for technical help.

Received: July 23, 2012
Revised: November 20, 2012
Accepted: February 8, 2013
Published: March 13, 2013

REFERENCES

- Andrianaivo, F., Lecocq, M., Wattiaux-De Coninck, S., Wattiaux, R., and Jadot, M. (2004). Hydrodynamics-based transfection of the liver: entrance into hepatocytes of DNA that causes expression takes place very early after injection. *J. Gene Med.* 6, 877–883.
- Banerjee, S., Ghosh, J., Sen, S., Guha, R., Dhar, R., Ghosh, M., Datta, S., Raychaudhury, B., Naskar, K., Haldar, A.K., et al. (2009). Designing therapies against experimental visceral leishmaniasis by modulating the membrane fluidity of antigen-presenting cells. *Infect. Immun.* 77, 2330–2342.
- Bartel, D.P. (2004). MicroRNAs: genomics, biogenesis, mechanism, and function. *Cell* 116, 281–297.
- Beattie, L., Peltan, A., Maroof, A., Kirby, A., Brown, N., Coles, M., Smith, D.F., and Kaye, P.M. (2010). Dynamic imaging of experimental *Leishmania donovani*-induced hepatic granulomas detects Kupffer cell-restricted antigen presentation to antigen-specific CD8 T cells. *PLoS Pathog.* 6, e1000805.
- Belair, C., Baud, J., Chabas, S., Sharma, C.M., Vogel, J., Staedel, C., and Darfeuille, F. (2011). *Helicobacter pylori* interferes with an embryonic stem cell micro RNA cluster to block cell cycle progression. *Silence* 2, 7.
- Benito, A., Feliu, J.X., and Villaverde, A. (1996). Beta-galactosidase enzymatic activity as a molecular probe to detect specific antibodies. *J. Biol. Chem.* 271, 21251–21256.
- Bhatnagar, S., Shinagawa, K., Castellino, F.J., and Schorey, J.S. (2007). Exosomes released from macrophages infected with intracellular pathogens stimulate a proinflammatory response in vitro and in vivo. *Blood* 110, 3234–3244.
- Bhowmick, S., Ravindran, R., and Ali, N. (2008). gp63 in stable cationic liposomes confers sustained vaccine immunity to susceptible BALB/c mice infected with *Leishmania donovani*. *Infect. Immun.* 76, 1003–1015.
- Brittingham, A., Morrison, C.J., McMaster, W.R., McGwire, B.S., Chang, K.P., and Mosser, D.M. (1995). Role of the *Leishmania* surface protease gp63 in complement fixation, cell adhesion, and resistance to complement-mediated lysis. *J. Immunol.* 155, 3102–3111.
- Cazalla, D., Yario, T., and Steitz, J.A. (2010). Down-regulation of a host microRNA by a Herpesvirus saimiri noncoding RNA. *Science* 328, 1563–1566.
- Chakraborty, D., Banerjee, S., Sen, A., Banerjee, K.K., Das, P., and Roy, S. (2005). *Leishmania donovani* affects antigen presentation of macrophage by disrupting lipid rafts. *J. Immunol.* 175, 3214–3224.
- Chang, J., Nicolas, E., Marks, D., Sander, C., Lerro, A., Buendia, M.A., Xu, C., Mason, W.S., Moloshok, T., Bort, R., et al. (2004). miR-122, a mammalian liver-specific microRNA, is processed from hcr mRNA and may downregulate the high affinity cationic amino acid transporter CAT-1. *RNA Biol.* 1, 106–113.
- Cooper, J.A., and King, C.S. (1986). Dephosphorylation or antibody binding to the carboxy terminus stimulates pp60c-src. *Mol. Cell. Biol.* 6, 4467–4477.
- Croft, S.L., Sundar, S., and Fairlamb, A.H. (2006). Drug resistance in leishmaniasis. *Clin. Microbiol. Rev.* 19, 111–126.
- Desjardins, M., and Descoteaux, A. (1998). Survival strategies of *Leishmania donovani* in mammalian host macrophages. *Res. Immunol.* 149, 689–692.
- Durieux, A.C., Vignaud, A., Prudhon, B., Viou, M.T., Beuvin, M., Vassilopoulos, S., Frayssé, B., Ferry, A., Lainé, J., Romero, N.B., et al. (2010). A centronuclear myopathy-dynamin 2 mutation impairs skeletal muscle structure and function in mice. *Hum. Mol. Genet.* 19, 4820–4836.
- Elmén, J., Lindow, M., Silahatoglu, A., Bak, M., Christensen, M., Lind-Thomsen, A., Hedtjörn, M., Hansen, J.B., Hansen, H.F., Straarup, E.M., et al. (2008). Antagonism of microRNA-122 in mice by systemically administered LNA-antimiR leads to up-regulation of a large set of predicted target mRNAs in the liver. *Nucleic Acids Res.* 36, 1153–1162.
- Engwerda, C.R., Ato, M., and Kaye, P.M. (2004). Macrophages, pathology and parasite persistence in experimental visceral leishmaniasis. *Trends Parasitol.* 20, 524–530.
- Esau, C., Davis, S., Murray, S.F., Yu, X.X., Pandey, S.K., Pear, M., Watts, L., Booten, S.L., Graham, M., McKay, R., et al. (2006). miR-122 regulation of lipid metabolism revealed by in vivo antisense targeting. *Cell Metab.* 3, 87–98.
- Filipowicz, W., Bhattacharyya, S.N., and Sonenberg, N. (2008). Mechanisms of post-transcriptional regulation by microRNAs: are the answers in sight? *Nat. Rev. Genet.* 9, 102–114.
- Ghosh, J., Lal, C.S., Pandey, K., Das, V.N., Das, P., Roychoudhury, K., and Roy, S. (2011). Human visceral leishmaniasis: decrease in serum cholesterol as a function of splenic parasite load. *Ann. Trop. Med. Parasitol.* 105, 267–271.
- Ghosh, J., Das, S., Guha, R., Ghosh, D., Naskar, K., Das, A., and Roy, S. (2012). Hyperlipidemia offers protection against *Leishmania donovani* infection: role of membrane cholesterol. *J. Lipid Res.* 53, 2560–2572.
- Girard, M., Jacquemin, E., Munnich, A., Lyonnet, S., and Henrion-Caude, A. (2008). miR-122, a paradigm for the role of microRNAs in the liver. *J. Hepatol.* 48, 648–656.
- Hallé, M., Gomez, M.A., Stuble, M., Shimizu, H., McMaster, W.R., Olivier, M., and Tremblay, M.L. (2009). The *Leishmania* surface protease GP63 cleaves multiple intracellular proteins and actively participates in p38 mitogen-activated protein kinase inactivation. *J. Biol. Chem.* 284, 6893–6908.
- Jaramillo, M., Gomez, M.A., Larsson, O., Shio, M.T., Topisirovic, I., Contreras, I., Luxenburg, R., Rosenfeld, A., Colina, R., McMaster, R.W., et al. (2011). *Leishmania* repression of host translation through mTOR cleavage is required for parasite survival and infection. *Cell Host Microbe* 9, 331–341.
- Krützfeldt, J., and Stoffel, M. (2006). MicroRNAs: a new class of regulatory genes affecting metabolism. *Cell Metab.* 4, 9–12.
- Lal, C.S., Kumar, A., Kumar, S., Pandey, K., Kumar, N., Bimal, S., Sinha, P.K., and Das, P. (2007). Hypocholesterolemia and increased triglyceride in pediatric visceral leishmaniasis. *Clin. Chim. Acta* 382, 151–153.
- Liberopoulos, E., Alexandridis, G., Bairaktari, E., and Elisaf, M. (2002). Severe hypocholesterolemia with reduced serum lipoprotein(a) in a patient with visceral leishmaniasis. *Ann. Clin. Lab. Sci.* 32, 305–308.
- Libri, V., Helwak, A., Miesen, P., Santhakumar, D., Borger, J.G., Kudla, G., Grey, F., Tollervey, D., and Buck, A.H. (2012). Murine cytomegalovirus encodes a miR-27 inhibitor disguised as a target. *Proc. Natl. Acad. Sci. USA* 109, 279–284.
- Murray, H.W., Berman, J.D., Davies, C.R., and Saravia, N.G. (2005). Advances in leishmaniasis. *Lancet* 366, 1561–1577.
- Olivier, M., Gregory, D.J., and Forget, G. (2005). Subversion mechanisms by which *Leishmania* parasites can escape the host immune response: a signaling point of view. *Clin. Microbiol. Rev.* 18, 293–305.
- Raposo, G., Nijman, H.W., Stoorvogel, W., Liejendekker, R., Harding, C.V., Melief, C.J., and Geuze, H.J. (1996). B lymphocytes secrete antigen-presenting vesicles. *J. Exp. Med.* 183, 1161–1172.
- Saha, B., Nanda-Roy, H., Pakrashi, A., Chakrabarti, R.N., and Roy, S. (1991). Immunobiological studies on experimental visceral leishmaniasis. I. Changes in lymphoid organs and their possible role in pathogenesis. *Eur. J. Immunol.* 21, 577–581.
- Silverman, J.M., Clos, J., de'Oliveira, C.C., Shirvani, O., Fang, Y., Wang, C., Foster, L.J., and Reiner, N.E. (2010). An exosome-based secretion pathway is responsible for protein export from *Leishmania* and communication with macrophages. *J. Cell Sci.* 123, 842–852.
- Tada, M., Hatano, E., Taura, K., Nitta, T., Koizumi, N., Ikai, I., and Shimahara, Y. (2006). High volume hydrodynamic injection of plasmid DNA via the hepatic artery results in a high level of gene expression in rat hepatocellular carcinoma induced by diethylnitrosamine. *J. Gene Med.* 8, 1018–1026.